United States Nuclear Regulatory Commission

Protecting People and the Environment

NUREG/CR-7249
ORNL/TM-2017/706

Overview of Nuclear Data Uncertainty in Scale and Application to Light Water Reactor Uncertainty Analysis

Office of Nuclear Regulatory Research

AVAILABILITY OF REFERENCE MATERIALS IN NRC PUBLICATIONS

NRC Reference Material

As of November 1999, you may electronically access NUREG-series publications and other NRC records at NRC's Library at www.nrc.gov/reading-rm.html. Publicly released records include, to name a few, NUREG-series publications; *Federal Register* notices; applicant, licensee, and vendor documents and correspondence; NRC correspondence and internal memoranda; bulletins and information notices; inspection and investigative reports; licensee event reports; and Commission papers and their attachments.

NRC publications in the NUREG series, NRC regulations, and Title 10, "Energy," in the *Code of Federal Regulations* may also be purchased from one of these two sources.

1. **The Superintendent of Documents**
   U.S. Government Publishing Office
   Washington, DC 20402-0001
   Internet: bookstore.gpo.gov
   Telephone: (202) 512-1800
   Fax: (202) 512-2104

2. **The National Technical Information Service**
   5301 Shawnee Road
   Alexandria, VA 22312-0002
   www.ntis.gov
   1-800-553-6847 or, locally, (703) 605-6000

A single copy of each NRC draft report for comment is available free, to the extent of supply, upon written request as follows:

Address: **U.S. Nuclear Regulatory Commission**
Office of Administration
Multimedia, Graphics, and Storage & Distribution Branch
Washington, DC 20555-0001
E-mail: distribution.resource@nrc.gov
Facsimile: (301) 415-2289

Some publications in the NUREG series that are posted at NRC's Web site address www.nrc.gov/reading-rm/doc-collections/nuregs are updated periodically and may differ from the last printed version. Although references to material found on a Web site bear the date the material was accessed, the material available on the date cited may subsequently be removed from the site.

Non-NRC Reference Material

Documents available from public and special technical libraries include all open literature items, such as books, journal articles, transactions, *Federal Register* notices, Federal and State legislation, and congressional reports. Such documents as theses, dissertations, foreign reports and translations, and non-NRC conference proceedings may be purchased from their sponsoring organization.

Copies of industry codes and standards used in a substantive manner in the NRC regulatory process are maintained at—

The NRC Technical Library
Two White Flint North
11545 Rockville Pike
Rockville, MD 20852-2738

These standards are available in the library for reference use by the public. Codes and standards are usually copyrighted and may be purchased from the originating organization or, if they are American National Standards, from—

American National Standards Institute
11 West 42nd Street
New York, NY 10036-8002
www.ansi.org
(212) 642-4900

Legally binding regulatory requirements are stated only in laws; NRC regulations; licenses, including technical specifications; or orders, not in NUREG-series publications. The views expressed in contractor prepared publications in this series are not necessarily those of the NRC.

The NUREG series comprises (1) technical and administrative reports and books prepared by the staff (NUREG–XXXX) or agency contractors (NUREG/CR–XXXX), (2) proceedings of conferences (NUREG/CP–XXXX), (3) reports resulting from international agreements (NUREG/IA–XXXX),(4) brochures (NUREG/BR–XXXX), and (5) compilations of legal decisions and orders of the Commission and Atomic and Safety Licensing Boards and of Directors' decisions under Section 2.206 of NRC's regulations (NUREG–0750).

DISCLAIMER: This report was prepared as an account of work sponsored by an agency of the U.S. Government. Neither the U.S. Government nor any agency thereof, nor any employee, makes any warranty, expressed or implied, or assumes any legal liability or responsibility for any third party's use, or the results of such use, of any information, apparatus, product, or process disclosed in this publication, or represents that its use by such third party would not infringe privately owned rights.

NUREG/CR-7249
ORNL/TM-2017/706

United States Nuclear Regulatory Commission

Protecting People and the Environment

Overview of Nuclear Data Uncertainty in Scale and Application to Light Water Reactor Uncertainty Analysis

Manuscript Completed: December 2017
Date Published: December 2018

Prepared by:
W. Wieselquist
M. Williams
D. Wiarda
M. Pigni
U. Mertyurek

Oak Ridge National Laboratory
Bethel Valley Road
Oak Ridge, TN 37831

Mourad Aissa, NRC Project Manager

Office of Nuclear Regulatory Research

ABSTRACT

This report presents the current state of the art in SCALE for nuclear data uncertainty analysis capability, and it provides an overview of the uncertainty in multigroup cross sections, fission product yields, and decay data. The effect of nuclear data uncertainty is demonstrated for a typical light water reactor (LWR) depletion analysis problem involving a Combustion Engineering 14 × 14 assembly irradiated in Calvert Cliffs Unit 1. A single fuel rod from assembly D047, designated as MKP109, has been subjected to destructive radiochemical assay to measure the isotopic contents.

The 95% range width (difference between the 97.5th and 2.5th percentiles) is used in this study to assess the calculation uncertainty. This approach uses the actual distribution of the data and does not make any assumptions about the normality of the distributions. If the distribution were normal, then the 95% range width would correspond to 4-sigma range, or +/- 2 sigma.

The calculation uncertainty determined in nuclide concentrations for the MKP109 rod ranges from a few percent to 50%. The power factor for this fuel rod shows a very low uncertainty of less than 0.5%.

Uncertainties in the macroscopic cross sections, reactivity, and power distributions are generally low, in the few percent range. The effective delayed neutron fraction, β_{eff}, shows higher uncertainty of 20–100%.

FOREWORD

Consideration of nuclear data uncertainty in calculations is an active area of research in data and software development. On the nuclear data side, uncertainty adds another dimension to an already complex database, and although the topic of uncertainty data is receiving attention—each subsequent ENDF/B release has additional data uncertainty—there is still not widespread usage of the uncertainty data due in part to lack of software tools, but also due to disagreements within the nuclear engineering analysis community on how exactly it can be used. This report demonstrates usage of the uncertainty data in one of the areas where many code developers and analysts spend a lot of time: code and model validation. This report recommends error metrics that use uncertainty, additional avenues for interpreting validation results when calculation uncertainty is included, and avenues for additional usage of the uncertainty data. Ideally, data uncertainty should become standard in validation, leading to new pathways for data improvement.

TABLE OF CONTENTS

ABSTRACT ..... **iii**

FOREWORD ..... **v**

LIST OF FIGURES ..... **ix**

LIST OF TABLES ..... **xi**

EXECUTIVE SUMMARY ..... **xiii**

ABBREVIATIONS AND ACRONYMS ..... **xv**

1 INTRODUCTION **1-1**

1.1 Model Equations 1-1
1.1.1 Transport Equation 1-2
1.1.2 Transmutation Equation 1-3
1.1.3 Multigroup Representation 1-4
1.2 Additional Models 1-5
1.2.1 Few-Group Macroscopic Cross Sections 1-5
1.2.2 Activity and Decay Heat 1-5
1.2.3 Reactivity Coefficients 1-5
1.2.4 Kinetics Parameters 1-6
1.2.5 Power Peaking Factors 1-6
1.3 Uncertainty Quantification Methods 1-7
1.3.1 Perturbation Theory 1-7
1.3.2 Sampling 1-7

2 DATA UNCERTAINTY **2-1**

2.1 Cross Section Uncertainty 2-1
2.1.1 Background 2-1
2.1.2 Implementation 2-1
2.1.3 Data Characteristics 2-1
2.2 Fission Product Yield Uncertainty 2-4
2.2.1 Background 2-4
2.2.2 Implementation 2-4
2.2.3 Characteristics 2-5
2.3 Decay Uncertainty 2-6
2.3.1 Background 2-6
2.3.2 Implementation 2-6
2.3.3 Characteristics 2-6

3 LWR APPLICATIONS WITH UNCERTAINTY **3-1**

3.1 Description 3-1
3.1.1 Operating History 3-1
3.1.2 Measurements 3-3

3.2 Calculation Results 3-6
3.2.1 Macroscopic Cross Section Uncertainty 3-7
3.2.2 Reactivity Uncertainty 3-13
3.2.3 Power Distribution Uncertainty 3-16
3.2.4 Isotopic Uncertainties 3-18
3.2.5 Source Terms 3-68

4 DISCUSSION 4-1

4.1 Importance of Non-Data Error 4-1
4.2 Calculation Uncertainty Is a Prediction 4-1
4.3 Data Assimilation 4-2
4.4 Significant Bias Identification 4-2

5 CONCLUSIONS 5-1

6 FUTURE WORK 6-1

7 REFERENCES 7-1

LIST OF FIGURES

Figure 1-1 SCALE/Sampler Work Flow 1-8

Figure 2-1 Uncertainty in Energy-Dependent ^{235}U Fission Cross Section, $\boldsymbol{\sigma\ 235U, fg}$, With Various Energy-Average Approximations 2-4

Figure 3-1 Configuration of Assembly D047 From CC-1 [7] 3-2

Figure 3-2 ^{137}Cs Gamma Scan Showing Sample S1 and S2 Locations [7] 3-3

Figure 3-3 Fast Macroscopic Absorption Cross Section 3-8

Figure 3-4 Thermal Macroscopic Absorption Cross Section 3-9

Figure 3-5 Fast Macroscopic Nu-Fission Cross Section 3-10

Figure 3-6 Thermal Macroscopic Nu-Fission Cross Section 3-11

Figure 3-7 Fast Macroscopic Scattering Cross Section 3-12

Figure 3-8 Thermal Macroscopic Scattering Cross Section 3-13

Figure 3-9 Eigenvalue Uncertainty 3-14

Figure 3-10 Delayed Neutron Fraction Uncertainty 3-15

Figure 3-11 Reactivity Coefficient Uncertainty 3-16

Figure 3-12 Irradiation Sample Power Factor Uncertainty 3-17

Figure 3-13 Flux Magnitude Uncertainty 3-18

Figure 3-14 ^{241}Am Isotopic Uncertainty 3-20

Figure 3-15 ^{243}Am Isotopic Uncertainty 3-21

Figure 3-16 ^{140}Ce Isotopic Uncertainty 3-22

Figure 3-17 ^{142}Ce Isotopic Uncertainty 3-23

Figure 3-18 ^{244}Cm Isotopic Uncertainty 3-24

Figure 3-19 ^{133}Cs Isotopic Uncertainty 3-25

Figure 3-20 ^{135}Cs Isotopic Uncertainty 3-26

Figure 3-21 ^{137}Cs Isotopic Uncertainty 3-27

Figure 3-22 ^{151}Eu Isotopic Uncertainty 3-28

Figure 3-23 ^{152}Eu Isotopic Uncertainty 3-29

Figure 3-24 ^{153}Eu Isotopic Uncertainty 3-30

Figure 3-25 ^{154}Eu Isotopic Uncertainty 3-31

Figure 3-26 ^{155}Eu Isotopic Uncertainty 3-32

Figure 3-27 ^{152}Gd Isotopics Uncertainty 3-33

Figure 3-28 ^{154}Gd Isotopic Uncertainty 3-34

Figure 3-29 ^{155}Gd Isotopic Uncertainty 3-35

Figure 3-30 ^{156}Gd Isotopic Uncertainty 3-36

Figure 3-31 ^{157}Gd Isotopic Uncertainty 3-37
Figure 3-32 ^{158}Gd Isotopic Uncertainty 3-38
Figure 3-33 ^{160}Gd Isotopic Uncertainty 3-39
Figure 3-34 ^{139}La Isotopic Uncertainty 3-40
Figure 3-35 ^{95}Mo Isotopic Uncertainty 3-41
Figure 3-36 ^{142}Nd Isotopic Uncertainty 3-42
Figure 3-37 ^{143}Nd Isotopic Uncertainty 3-43
Figure 3-38 ^{144}Nd Isotopic Uncertainty 3-44
Figure 3-39 ^{145}Nd Isotopic Uncertainty 3-45
Figure 3-40 ^{146}Nd Isotopic Uncertainty 3-46
Figure 3-41 ^{148}Nd Isotopic Uncertainty 3-47
Figure 3-42 ^{150}Nd Isotopic Uncertainty 3-48
Figure 3-43 ^{237}Np Isotopic Uncertainty 3-49
Figure 3-44 ^{238}Pu Isotopic Uncertainty 3-50
Figure 3-45 ^{239}Pu Isotopic Uncertainty 3-51
Figure 3-46 ^{240}Pu Isotopic Uncertainty 3-52
Figure 3-47 ^{241}P Isotopics Uncertainty 3-53
Figure 3-48 ^{242}Pu Isotopic Uncertainty 3-54
Figure 3-49 ^{103}Rh Isotopic Uncertainty 3-55
Figure 3-50 ^{101}Ru Isotopic Uncertainty 3-56
Figure 3-51 ^{147}Sm Isotopic Uncertainty 3-57
Figure 3-52 ^{148}Sm Isotopic Uncertainty 3-58
Figure 3-53 ^{149}Sm Isotopic Uncertainty 3-59
Figure 3-54 ^{150}Sm Isotopic Uncertainty 3-60
Figure 3-55 ^{151}Sm Isotopic Uncertainty 3-61
Figure 3-56 ^{152}Sm Isotopic Uncertainty 3-62
Figure 3-57 ^{154}Sm Isotopic Uncertainty 3-63
Figure 3-58 ^{90}Sr Isotopic Uncertainty 3-64
Figure 3-59 ^{234}U Isotopic Uncertainty 3-65
Figure 3-60 ^{235}U Isotopic Uncertainty 3-66
Figure 3-61 ^{236}U Isotopic Uncertainty 3-67
Figure 3-62 ^{238}U Isotopic Uncertainty 3-68
Figure 3-63 Activity Uncertainty 3-69

LIST OF TABLES

Table 2-1 Key Cross Section Uncertainty Data in SCALE 2-3
Table 2-2 Uncertainty in Key Fission Yield Data 2-5
Table 2-3 Uncertainty in Key Decay Data 2-7
Table 3-1 Measurement and Uncertainty Data for CC-1 MKP109 Samples S1 and S2 3-5

EXECUTIVE SUMMARY

This report presents the current state of the art in SCALE for nuclear data uncertainty analysis capability, and it provides an overview of the uncertainty in multigroup cross sections, fission product yields, and decay data.

The nuclear data used in a typical SCALE calculation are processed from evaluated nuclear data files (ENDF/B) produced by the National Nuclear Data Center [1] through the AMPX code system distributed with SCALE. The ENDF/B data are based on a large set of nuclear data measurements that have been evaluated by the world's top nuclear data experts and compiled into a cohesive, consistent database. Ideally, ENDF/B data should include an associated uncertainty (and correlations to other data) indicating the accuracy of the measurement, as well as any uncertainty introduced in the evaluation due to modeling fits, consistency adjustments, or other causes. This uncertainty in the nuclear data can be propagated to uncertainty in calculated quantities of interest for the nuclear analyst—whether it is k_{eff} for criticality safety applications or a void coefficient of reactivity for reactor physics applications. However, ENDF/B uncertainty information is not available for many nuclides or for some types of nuclear data relevant to nuclear engineering applications. To address this need, supplemental data have been developed within SCALE to provide complete uncertainty data sets for (1) fission yield data, (2) multigroup cross section data, and (3) decay data.

The effect of nuclear data uncertainty is demonstrated for a typical LWR depletion analysis problem involving a Combustion Engineering 14 × 14 assembly irradiated in Calvert Cliffs Unit 1. A single fuel rod from assembly D047, designated as MKP109, has been subjected to destructive radiochemical assay to measure the isotopic contents.

The 95% range width (difference between the 97.5th and 2.5th percentiles) is used in this study to assess the calculation uncertainty. This approach uses the actual distribution of the data and does not make any assumptions about the normality of the distributions. If the distribution were normal, then the 95% range width would correspond to 4-sigma range, or +/- 2 sigma.

The calculation uncertainty determined in nuclide concentrations for the MKP109 rod ranges from a few percent to 50%. The power factor for this fuel rod shows a very low uncertainty of less than 0.5%. There is also a low uncertainty of less than 2% in activity.

Uncertainties in the macroscopic cross sections, reactivity, and power distributions are generally low, in the few percent range. The effective delayed neutron fraction, β_{eff}, shows an unexpectedly high uncertainty of 20–100%.

The considered application of the MKP109 fuel rod enabled a bias estimation and comparisons of calculated uncertainty in the isotopic concentrations to measurements of samples S1 and S2. In this case, the relative bias range was calculated to include both the calculation and measurement uncertainty. A bias range (2.5^{th}–97.5^{th} percentile) that includes zero is within expectation, whereas a bias which does not include zero is unexpected. Identifying unexpected biases can lead to improvements in the model or in nuclear data.

Section 1 introduces the relevant model equations used to explicitly define the data parameters, discusses the background of uncertainty quantification (UQ), and describes the sampling-based propagation technique as implemented in SCALE. Section 2 describes the uncertainty data in SCALE. Section 3 presents an application uncertainty problem in light water reactor (LWR) analysis. Section 4 provides general recommendations for interpreting results with uncertainty.

ABBREVIATIONS AND ACRONYMS

AMPX	Automation of MUG, POPOP4, and XLACS
CC	Calvert Cliffs
CE	Combustion Engineering (company)
CE	continuous energy
COVERX	cross section covariance data format
ENDF	evaluated nuclear data file
GRS	Gesellschaft für Anlagen- und Reaktorsicherheit laboratory
JEFF	joint evaluated fission and fusion file
JENDL	Japanese evaluated nuclear data library
LWR	light water reactor
MEDUSA	software developed by GRS for random sampling of covariances in XSUSA
ORIGEN	Oak Ridge Isotope Generation code
ORNL	Oak Ridge National Laboratory
PIE	post-irradiation examination
PWR	pressurized water reactor
sEL	elastic scattering
sIN	inelastic scattering
TENDL	TALYS-based evaluated nuclear data library
TRITON	Transport Rigor Implemented with Time-Dependent Operation for Neutronic Depletion
TSUNAMI	Tools for Sensitivity and Uncertainty Analysis Methodology Implementation
UQ	uncertainty quantification
XSUSA	cross section software developed by GRS for uncertainty and sensitivity analyses

1 INTRODUCTION

This report summarizes the nuclear data uncertainty content available in version 6.2.2 of SCALE [2], presents the sampling-based uncertainty propagation methodology implemented in SCALE/Sampler which uses these data, and discusses some applications of the data.

The nuclear data used in a typical SCALE calculation are processed from evaluated nuclear data files (ENDF/B) produced by the National Nuclear Data Center [1] through the AMPX code system distributed with SCALE. The ENDF/B data are based on a large set of nuclear data measurements that have been evaluated by the world's top nuclear data experts and compiled into a cohesive, consistent database. Ideally, ENDF/B data should include an associated uncertainty (and correlations to other data) indicating the accuracy of the measurement, as well as any uncertainty introduced in the evaluation due to modeling fits, consistency adjustments, or other causes. This uncertainty in the nuclear data can be propagated to uncertainty in calculated quantities of interest for the nuclear analyst—whether it is k_{eff} for criticality safety applications or a void coefficient of reactivity for reactor physics applications. However, ENDF/B uncertainty information is not available for many nuclides or for some types of nuclear data relevant to nuclear engineering applications. To address this need, supplemental data have been developed within SCALE to provide complete uncertainty data sets for (1) fission yield data, (2) multigroup cross section data, and (3) decay data.

The remainder of this document is organized as follows. Section 1.1 introduces the relevant model equations used to explicitly define the data parameters, and Section 1.2 discusses some background of uncertainty quantification (UQ). The sampling-based propagation technique as implemented in SCALE/Sampler is discussed in Section 1.3. Section 2 describes the uncertainty data in SCALE, Section 3 presents an application uncertainty problem in light water reactor (LWR) analysis, and Section 4 provides general recommendations for interpreting results with uncertainty.

1.1 Model Equations

Although the average SCALE user does not need to know details of the equations solved in SCALE calculations, the easiest way to discuss data uncertainty is to first show the relevant models in which the data parameters occur. This will provide a common reference point and basic understanding of which data parameters can affect which quantities of interest. The fundamental unknowns (those from which all other quantities of interest can be calculated) in SCALE are:

- neutron angular flux, $\psi(\vec{r}, E, \vec{\Omega}, t)$, and
- nuclide distribution, $n(\vec{r}, t)$,

with the following independent variables:

- $\vec{r}$ for the location in space,
- E for the neutron energy,

- $\vec{\Omega}$ for the neutron direction, and

- t for time.

Throughout this section, one or more of the independent variables may be suppressed for brevity.

1.1.1 Transport Equation

The neutron transport equation is framed as an eigenvalue problem with quasistatic representation of the time-dependent neutron angular flux:

$$\vec{\Omega} \cdot \vec{\nabla}\psi_\ell + \Sigma_t(\vec{r}, E, t_\ell)\, \psi(\vec{r}, E, \vec{\Omega}, t_\ell) = \int_{4\pi} d\Omega' \int_0^\infty dE'\, \Sigma_s(\vec{r}, E' \to E, \vec{\Omega}' \to \vec{\Omega}, t_\ell)\ \psi(\vec{r}, E', \vec{\Omega}', t_\ell) + \frac{1}{k_{eff}} \int_0^\infty dE'\, \nu\Sigma_f(\vec{r}, E' \to E, t_\ell)\ \phi(\vec{r}, E', t_\ell), \tag{1}$$

where

- ℓ is a time index from 0 to L with $\psi_\ell = \psi(t_\ell)$;

- $\phi_\ell = \phi(t_\ell)$ is the scalar flux at time t_ℓ, defined as the angle-integrated angular flux, $\phi_\ell = \int_{4\pi} d\Omega'\ \psi_\ell(\vec{\Omega}')$;

- Σ_t, Σ_s, and $\nu\Sigma_f$ are macroscopic data corresponding to the total cross section, double-differential scattering cross section, multiple-neutron emission cross section, and fission production cross section, respectively; and

- k_{eff} is the eigenvalue.

The macroscopic data are defined in terms of the fundamental microscopic nuclear data and the nuclide distributions. The total cross section is defined as

$$\Sigma_t(\vec{r}, E, t_\ell) = \sum_j \sigma_{j,t}(E)\, n_j(\vec{r}, t_\ell), \tag{2}$$

where $\sigma_{j,t}(E)$ is the total cross section for nuclide j at energy E, and $n_j(\vec{r}, t_\ell)$ is the nuclide number density for nuclide j at location $\vec{r}$ at time t_ℓ. The macroscopic double differential scattering cross section is similarly defined:

$$\Sigma_s(\vec{r}, E' \to E, \vec{\Omega}' \to \vec{\Omega}, t_\ell) = \sum_j \left[\sigma_{j,s}(E' \to E, \vec{\Omega}' \to \vec{\Omega}) + \sum_{\nu=2,3} \nu\sigma_{j,\nu n}(E' \to E, \vec{\Omega}' \to \vec{\Omega}) \right] n_j(\vec{r}, t_\ell), \tag{3}$$

where $\sigma_{j,s}(E' \to E, \vec{\Omega}' \to \vec{\Omega})$ is the microscopic double differential scattering cross section of nuclide j, which describes scattering from energy E' to energy E and direction $\vec{\Omega}'$ to direction $\vec{\Omega}$; and $\sigma_{j,\nu n}(E' \to E, \vec{\Omega}' \to \vec{\Omega})$ are microscopic double differential cross sections describing reactions that emit an integer number of neutrons, ν. Typical nuclear engineering problems consider only $\nu = 2$ and $\nu = 3$. The microscopic scattering cross section is further divided into elastic and inelastic components,

$$\sigma_{j,s} = \sigma_{j,sEL} + \sigma_{j,sIN}, \tag{4}$$

where $\sigma_{j,sEL}$ is the elastic component and $\sigma_{j,sIN}$ is the inelastic component consisting of scattering from discrete inelastic levels and from the continuum range. The macroscopic fission production cross section is defined as

$$\upsilon\Sigma_f(\vec{r}, E' \to E, t_\ell) = \sum_j \bar{\chi}_{j,f}(E' \to \mathrm{E})\, \bar{\nu}_{j,f}(E')\, \sigma_{j,f}(E')\, n_j(\vec{r}, t_\ell), \tag{5}$$

where

- $\bar{\chi}_{j,f}(E' \to \mathrm{E})$ is the energy distribution of secondary neutrons emitted from fission at energy E',
- $\bar{\nu}_{j,f}(E')$ is the average number of neutrons emitted per fission, and
- $\sigma_{j,f}(E')$ is the fission cross section for nuclide j.

1.1.2 Transmutation Equation

The nuclide distribution $n_j(\vec{r}, t_\ell)$ is the solution of the transmutation equations for each nuclide j,

$$\begin{aligned} \frac{dn_j}{dt} = \sum_j \left[\left(\sum_x f_{i,x\to j}(\vec{r},t)\sigma_{i,x}(\vec{r},t) \right) \phi(\vec{r},t) + \sum_d f_{i,d\to j}\, \lambda_{i,d} \right] n_i(\vec{r},t) \\ - \left[\sigma_{j,tt}(\vec{r},t)\, \phi(\vec{r},t) + \lambda_j\right] n_j(\vec{r},t) \\ \text{for} \quad t_{\ell-1} \le t \le t_\ell \end{aligned} \tag{6}$$

where

- $f_{i,x\to j}(\vec{r},t)$ is the fractional yield of nuclide j from reaction type x with nuclide i;
- $\sigma_{i,x}(\vec{r},t)$ is the energy-averaged cross section, $\sigma_{i,x} = \frac{\int_\infty dE' \sigma_{i,x}(E')\ \phi(E')}{\int_\infty dE'\ \phi(E')}$, for reaction type x of nuclide i;
- $\phi(\vec{r},t)$ is the energy-integrated scalar flux, $\phi = \int_0^\infty dE' \phi(E')$;
- $f_{i,d\to j}$ is the branching ratio for creation of nuclide j from decay mode d of nuclide i;

- $\lambda_{i,d}$ is the decay constant for decay mode d of decay of nuclide i;
- $\sigma_{j,tt}(\vec{r},t)$ is the energy-averaged transmutation cross section (i.e., absorption plus discrete inelastic scatter to isomeric states) for nuclide j, $\sigma_{j,tt} = \sum_x \sigma_{j,x}$; and
- λ_j is the total decay constant, $\lambda_j = \sum_d \lambda_{j,d}$.

The fractional yield term $f_{i,x\to j}(\vec{r},t)$ represents yields due to isomeric branching or fission. The isomeric branching yield is defined as

$$f_{i,x\to j[m]} = \frac{\int_0^\infty dE'\, f_{i,x\to j[m]}(E')\, \sigma_{i,x}(E')\, \phi(E')}{\int_0^\infty dE'\, \sigma_{i,x}(E')\, \phi(E')}, \tag{7}$$

where $f_{i,x\to j[m]}(E')$ is the energy-dependent isomeric branching ratio to nuclide j with isomeric state m. For example, the (n,γ) reaction in ^{234}U can produce both ^{235}U and ^{235m}U, with the energy-average yield of ^{235m}U calculated as $f_{^{234}U,\gamma\to^{235m}U} = \frac{\int_\infty dE' f_{^{234}U,\gamma\to^{235m}U}(E')\, \sigma_{^{234}U,\gamma}(E')}{\int_\infty dE'\, \sigma_{^{234}U,\gamma}(E')}$.

The fractional yield of fission product j from fissioning nuclide i in a particular system is usually obtained from the energy-dependent yield distribution, evaluated at the average fission energy for the system,

$$f_{i,f\to j} = interp(f_{i,f\to j}(E), \bar{E}_{i,f}), \tag{8}$$

where $\bar{E}_{i,f}$ is the average energy of fission calculated as

$$\bar{E}_{i,f} = \frac{\int_\infty dE'\, E'\, \sigma_{i,f}(E')\phi(E')}{\int_\infty dE'\, \sigma_{i,f}(E')\phi(E')}. \tag{9}$$

The transmutation cross section differs from the conventional total cross section by the omission of elastic scatter and discrete inelastic scatter to non-isomeric states, which has no effect on production or loss of nuclides appearing in Eq. (6).

1.1.3 Multigroup Representation

One standard solution technique for the neutron transport equation is to assume a multigroup representation in energy, which leads to multigroup angular fluxes defined as

$$\psi^g = \int_{E^g}^{E^{g-1}} dE\, \psi(E), \tag{10}$$

and multigroup cross sections defined as

$$\sigma^g = \frac{\int_{E^g}^{E^{g-1}} dE\, \sigma(E) w(E)}{\int_{E^g}^{E^{g-1}} dE\, w(E)}, \tag{11}$$

where $w(E)$ is a weighting function, and energies E^0, E^1, E^g, and E^G are energy group boundaries in descending order. The energy group structure and number of groups are selected for a particular multigroup application. SCALE 6.2 includes two multigroup structures optimized for LWR applications: 56- and 252-groups.

1.2 Additional Models

1.2.1 Few-Group Macroscopic Cross Sections

SCALE is commonly used to generate data for nodal simulators such as the Purdue Advanced Reactor Core Simulator (PARCS). In this case, few-group macroscopic cross sections are one of the main outputs, with standard flux-volume weighting,

$$\Sigma_x^h(t) = \frac{\sum_{g\in h}\sum_m \phi_m^g(t)V_m \sum_j \sigma_{jm,x}^g(t)n_{jm}(t)}{\sum_{g\in h}\sum_m \phi_m^g(t)V_m}, \tag{12}$$

where h is the few-group energy index, m is a material index, V_m is the material volume, and ϕ_m^g is the material-average multigroup scalar flux.

1.2.2 Activity and Decay Heat

Activity and decay heat are key responses in spent fuel and source terms analysis. Activity is expressed as

$$A(t) = \sum_j \lambda_j\, n_j(t), \tag{13}$$

whereas decay heat is given as

$$H(t) = \sum_j Q_j\, \lambda_j\, n_j(t), \tag{14}$$

where Q_j is the nuclide-dependent energy release per decay. Decay heat responses are not addressed in this report.

1.2.3 Reactivity Coefficients

Reactivity coefficients are simple coefficients that relate state changes to changes in reactivity, defined here as

$$\alpha_B = \frac{\partial k_{eff}}{\partial B}, \tag{15}$$

where B is a given state parameter such as fuel temperature. Reactivity coefficients are typically calculated from discrete state changes called *branches*. For example, a fuel temperature branch could be used to calculate the reactivity coefficient for fuel temperature as

$$\alpha_{T_{fuel}} \approx \frac{k_{eff}\left(T_{fuel} + \Delta T_{fuel}\right) - k_{eff}(T_{fuel})}{\Delta T_{fuel}}, \tag{16}$$

where ΔT_{fuel} is the branch temperature change.

1.2.4 Kinetics Parameters

SCALE does not have a time-dependent kinetics capability, but it supports that capability in nodal simulators through lattice physics outputs of domain-average delayed neutron fractions, β_{eff}^{p}, and decay constants, λ^{p}, where $p = 1, 2, \ldots, 6$ in the traditional six-group precursor formalism. The six-group effective delayed neutron fractions are defined as

$$\beta_{eff}^{p} = \frac{\sum_j n_j \left[\int_0^\infty dE \bar{\nu}_{j,f}(E)\, \sigma_{j,f}(E)\, \phi(E)\right] \left[\int_0^\infty dE'\, \beta_j^p(E')\, \chi_j^p(E')\, \phi^*(E')\right]}{\sum_j n_j \left[\int_0^\infty dE \bar{\nu}_{j,f}(E)\, \sigma_{j,f}(E)\, \phi(E)\right] \left[\int_0^\infty dE'\, \bar{\chi}_j(E')\, \phi^*(E')\right]}, \tag{17}$$

and six-group precursor decay constants are defined as

$$\lambda^{p} = \frac{\sum_i \lambda_i^p\, n_i}{\sum_j n_i}, \tag{18}$$

where

- $\beta_j^p(E)$ is the energy-dependent fraction of delayed neutrons into precursor group p, from fission of nuclide i, emitted at energy E,
- λ_i^p is the decay constant corresponding to neutron emission in fission product nuclide i,
- $\chi_j^p(E')$ is the energy spectrum of delayed neutrons produced by precursor group p, and
- ϕ^* is the adjoint flux.

λ_i^p, $\chi_j^p(E')$, and $\beta_i^p(E)$ are the fundamental nuclear data. The total effective delayed neutron fraction is the sum over precursor groups

$$\beta_{eff} = \sum_p \beta_{eff}^{p}. \tag{19}$$

1.2.5 Power Peaking Factors

One of the principal measures of the power distribution in simulations of nuclear reactors is the fission distribution. For use as a power distribution metric, the fission distribution is usually normalized as a region-to-average factor

$$p_m = \frac{\int_0^\infty dE\ \Sigma_{m,f}(E)\ \phi_m(E)}{\frac{1}{V}\sum_m V_m \int_0^\infty dE\ \Sigma_{m,f}(E)\ \phi_m(E)}, \tag{20}$$

where m is a material region index, V_m is a material region volume, and the total volume $V = \sum_m V_m$. These factors are used in safety analysis to obtain the peak local power, $P_{peak} = \bar{P} \max_m p_m$, where $\bar{P}$ is the core-average specific power.

1.3 Uncertainty Quantification Methods

SCALE currently includes two UQ methods: a perturbation theory–based method called Tools for Sensitivity and Uncertainty Analysis Methodology Implementation (TSUNAMI), and the sampling-based method known as Sampler.

1.3.1 Perturbation Theory

TSUNAMI implements a perturbation theory–based sensitivity analysis methodology that can produce first-order uncertainty estimates according to

$$\boldsymbol{C}_y = \boldsymbol{S}_{y/x}^T\ \boldsymbol{C}_x\ \boldsymbol{S}_{y/x}, \tag{21}$$

where $\boldsymbol{C}_x$ is a covariance matrix for inputs x, and $\boldsymbol{S}_{y/x}$ is a sensitivity matrix, computed from first-order perturbation theory, containing sensitivity coefficients for each response y in columns with respect to each input x in rows.

Perturbation theory–based methods require solutions of adjoint equations specific to the forward equations and the desired response. In TSUNAMI, an adjoint scheme exists only for the eigenvalue transport equation.

TSUNAMI's original application in version 5 of SCALE was to determine appropriate criticality benchmarks for a particular user system, with the fundamental assumption being that cross section uncertainty is the primary uncertainty in a criticality benchmark. Therefore, the sensitivity matrix was originally for a k_{eff} response with respect to input cross sections. With SCALE 6.0, additional outputs were added for reaction rates, thus extending the applicability into reactor physics applications, but with the same limitation on the inputs that could be considered uncertain (only cross sections) and the types of problems which could be analyzed (only transport problems without depletion). With SCALE 6.2, TSUNAMI is available with continuous energy KENO, whereas before it was available only for multigroup transport methods.

1.3.2 Sampling

Sampler implements sampling-based uncertainty quantification, assuming that every input may have a probability distribution, $pdf(x)$, which is propagated to determine the output probability distribution, $pdf(y)$,

$$pdf(y) = \boldsymbol{\Theta}[\ pdf(x)], \tag{22}$$

where $\boldsymbol{\Theta}$ is an operator the effect of which can be approximated by sampling N realizations of x from $pdf(x)$, performing N realization calculations, and reconstructing $pdf(y)$ from N realizations of y. The perturbation theory approach calculates sensitivities for a single response per run and then approximates the uncertainties. The sampling-based approach calculates uncertainties directly and can only provide very limited sensitivity information. The SCALE/Sampler workflow is shown in Figure 1-1.

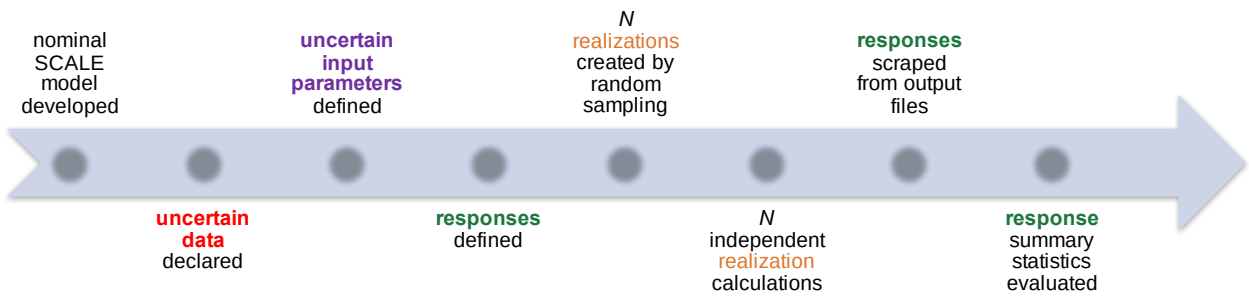

Figure 1-1 SCALE/Sampler Work Flow

Data uncertainty can be particularly complex because of the large amount of data and the potentially correlated nature. For this reason, SCALE/Sampler provides precalculated data samples. Sampler was initially released in SCALE 6.2.

2 DATA UNCERTAINTY

The following sections discuss the data uncertainty available in SCALE 6.2.

2.1 Cross Section Uncertainty

Uncertainty in cross sections $\sigma_{i,x}(E)$ for nuclide i, reaction type x, and energy E impacts all aspects of an analysis with SCALE, affecting both transport and depletion calculations.

2.1.1 Background

Cross section uncertainty has been a consideration in SCALE since the introduction of the TSUNAMI tools and their application to criticality safety in SCALE 5.0. Cross section data uncertainty is historically referred to as *covariance data*. The ENDF6 data format currently used by all evaluated data files (ENDF/B, joint evaluated fission and fusion file [JEFF], Japanese evaluated nuclear data library [JENDL], TALYS-based evaluated nuclear data library [TENDL]), imposes a normal distribution representation for the cross section probability distribution, and thus the uncertainty data are stored as a covariance matrix. The SCALE 6.2 covariance library is based on ENDF/B-VII.1 data for 187 nuclides, combined with previous SCALE 6.1 covariances from other sources for ~215 nuclides not available in ENDF/B-VII.1. Thus, SCALE-6.2 has a complete set of uncertainties for important data of all nuclides in the multigroup cross sections [2].

2.1.2 Implementation

In SCALE 6.2, cross section covariance matrices are distributed in the COVERX multigroup format in both the 56- and 252-group structures that are processed through AMPX. The perturbation theory–based approach (TSUNAMI) operates directly on the covariance matrices, folding them with calculated sensitivity coefficients to arrive at uncertainty. In the sampling-based approach (Sampler), the multigroup covariance matrices are sampled using the XSUSA/MEDUSA [3] random sampling code developed by GRS (Gesellschaft für Anlagen- und Reaktorsicherheit) to produce 1,000 perturbed multigroup cross sections for each datum in the library,[1] ${\sigma'}^{g}_{i,x}$. A perturbed cross section is converted to a perturbation factor,

$$p^{g}_{i,x} = \frac{{\sigma'}^{g}_{i,x}}{\sigma^{g}_{i,x}}. \tag{23}$$

The perturbation factors are applied before the transport calculation to each self-shielded region in a multigroup problem [3].

2.1.3 Data Characteristics

Table 2-1 shows cross section uncertainty from the SCALE 6.2 library for some key nuclides in typical LWR analyses, with data condensed to approximate one-group cross sections,

[1] The number of samples (1,000) to ship with SCALE was chosen to exceed the needs of most analyses, for which 100–300 samples have been deemed sufficient.

$$\sigma_{i,x} = \sum_g \sigma_{i,x}^g w^g, \quad \textbf{(24)}$$

where w^g is an LWR weighting spectra. Three different uncertainty measures are shown in the table.

The first, denoted by the phrase *with correlation*, is the most accurate and uses the uncertainty propagation rule on the one-group cross section to approximate the variance in the one-group cross section as

$$var(\sigma_{i,x}) \approx \sum_{g'} \sum_g w^{g'} cov^{gg'}(\sigma_{i,x})\, w^g, \quad \textbf{(25)}$$

where $cov^{gg'}(\sigma_{i,x})$ is the covariance matrix for the group-wise data.

This is in contrast with the *without correlation* approach, which is simply

$$var(\sigma_{i,x}) \approx \sum_{g'} \sum_g w^{g'} var(\sigma_{i,x}^g)\, w^g, \quad \textbf{(26)}$$

where $var(\sigma_{i,x}^g)$ is the variance term on the diagonal of the covariance matrix. Comparing the first two approaches from Eqs. (25) and (26) allows one to estimate the importance of energy correlation, which is significant in most instances, with a *higher uncertainty when correlation is included* by a factor of two or three. This can be understood in the limit of a uniform cross section and weighting function. Without correlation, the result is an averaging procedure in which the uncertainty in the average will be a factor of $\frac{1}{\sqrt{N}}$ smaller than the uncertainty in the components, where N is the number of parameters or energy groups in this example. Introducing correlation basically limits the number of *effective* components to $\widetilde{N} < N$, with perfect correlation resulting in $\widetilde{N} = 1$ component, and the average having the same uncertainty as the components.

The third weighted average is an *erroneous approach* that applies flux weighting to the standard deviations,

$$std(\sigma_{i,x}) \approx \sum_g std(\sigma_{i,x}^g)\, w^g, \quad \textbf{(27)}$$

where $std(\sigma_{i,x}^g) = \sqrt{var(\sigma_{i,x}^g)}$. This form is not valid since the total standard deviation is obtained from the square root of the summed of squares of the uncorrelated standard deviations; however, it is possibly what would be estimated by examining a plot of the standard deviation versus energy, as shown in the fission cross section uncertainty plot in Figure 2-1. In this plot, the energy-dependent relative uncertainty is shown, along with the three one-group estimates. Note that the incorrect weighted average is the only one that appears to represent an average of the data shown—it effectively multiplies the relative uncertainty times flux and cross section shapes and determines the average of that function. Due to the thermal spectrum and thermal cross section, the left-most region is by far the most important (note the shape functions are in a log scale), so the weighted average appears slightly above the left-most portion of the energy-

dependent curve. Comparing the *with correlation* (best) to *without correlation* shows that neglecting correlations is especially severe for this reaction, with an uncertainty that is lower by a factor of three.

Table 2-1 Key Cross Section Uncertainty Data in SCALE

Nuclide, *i*	Neutron reaction type, *x*	Cross section, $\sigma_{i,x}$ (barns)	Uncertainty with correlation (%)	Uncertainty without correlation (%)	Uncertainty weighted average (%)
^{235}U	fission (f)	3.73E+01	0.32	0.10	0.40
	gamma (γ)	8.68E+00	1.26	0.48	2.15
	$\bar{\nu}$	2.54E+00	0.11	0.05	0.26
^{238}U	fission (f)	1.27E-01	0.52	0.29	0.64
	gamma (γ)	2.12E+00	1.17	0.72	2.50
	scattering (sIN)	1.24E+00	14.08	6.49	16.10
^{239}Pu	fission (f)	8.20E+01	0.77	0.31	1.10
	gamma (γ)	4.42E+01	1.13	0.49	1.53
	$\bar{\nu}$	3.01E+00	0.07	0.05	0.22
^{240}Pu	gamma (γ)	2.16E+02	0.25	0.08	0.27
^{135}I	gamma (γ)	5.16E+00	3.65	3.65	13.24
^{135}Xe	gamma (γ)	1.63E+05	4.15	1.48	4.15
^{149}Pm	gamma (γ)	1.13E+02	16.14	5.53	21.43
^{149}Sm	gamma (γ)	4.44E+03	1.47	0.59	1.58
^{10}B	alpha (α)	2.50E+02	0.08	0.02	0.08
^{155}Gd	gamma (γ)	2.14E+03	3.27	1.76	4.95
^{90}Zr	gamma (γ)	9.53E-03	11.72	5.25	16.97
^{1}H	scattering (sEL)	1.21E+01	0.20	0.04	0.20
	gamma (γ)	2.16E-02	1.07	0.29	1.08
^{2}H	scattering (sEL)	3.03E+00	1.67	0.40	1.97
	gamma (γ)	3.63E-05	5.66	2.41	8.10
^{16}O	scattering (sEL)	3.41E+00	1.91	0.42	1.97
	gamma (γ)	7.62E-05	32.22	10.70	34.84
^{232}Th	gamma (γ)	2.80E+00	1.64	1.59	4.07

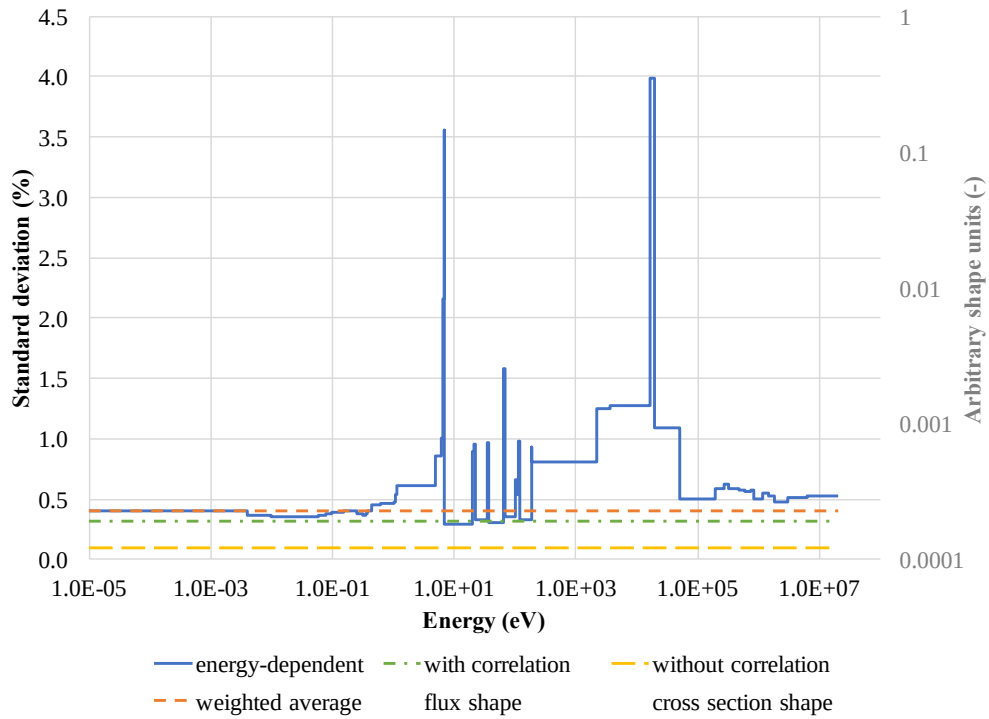

Figure 2-1 Uncertainty in Energy-Dependent ^{235}U Fission Cross Section, $\sigma^{g}_{^{235}U,f}$, With Various Energy-Average Approximations

2.2 Fission Product Yield Uncertainty

Uncertainty in fission product yields $f_{i,f\rightarrow j}(E)$—which is the number of atoms of fission product j produced from fission of nuclide i by a neutron energy with E—impacts only simulations of depletion.

2.2.1 Background

SCALE 6.2 is the first version which includes uncertainties in yield data. SCALE 6.2 uses ENDF/B-VII.1 yields with approximately 30 fissionable nuclides i, 1,100 fission products j, with dependence on incident neutron energy causing fission, as represented by tabulation of the data at different energies. For important fissile nuclides, three energies are typically available: fast (14 MeV), intermediate (500 keV), and thermal (0.025 eV). For some fissionable nuclides, only a single yield energy may be available. Assuming a normal distribution, ENDF/B-VII.1 does contain standard deviations for the yield data, but it does not contain the inherent correlations of these data.

2.2.2 Implementation

Fission yield covariance matrices are constructed using a Bayesian update procedure described by Pigni et al. [5] based on knowledge of independent and cumulative yields and decay methods along a mass chain. In SCALE 6.2, these covariance matrices are available for ^{235}U, ^{238}U, ^{239}Pu, and ^{241}Pu at energies relevant for LWR systems. One thousand random samples are drawn from these distributions and converted to yield perturbation factors, just as in the case of cross section perturbation factors. When Sampler is directed to consider uncertainty in

fission yield data, then the yield perturbation factors are applied to the nominal data and then renormalized. A particular nuclide with at least one energy set of yield perturbation factors will have those perturbation factors applied to all energy data of that nuclide. Yield data are not used by the TSUNAMI tools, which only support calculations with static nuclide compositions.

2.2.3 Characteristics

Table 2-2 shows the uncertainty in fission product yields from fissionable nuclides ^{235}U, ^{238}U, and ^{239}Pu, for several key fission products in LWR systems: ^{135}Te, ^{135}I, ^{135}Xe, ^{149}Nd, ^{149}Pm, and ^{149}Sm. The first three fission products are members of the A=135 mass chain, the main pathway for generating the most important neutron absorber for LWR reactor dynamics, ^{135}Xe. The next three fission products are members of the A=149 mass chain, which includes stable ^{149}Sm, an important neutron absorber in LWR systems. The buildup of ^{149}Sm after a shutdown requires overcoming that negative reactivity penalty to return to power.

It is important to note that a fission product may have a high uncertainty (e.g., ^{149}Sm yield has ~50% uncertainty) in its yield, but the production of that isotope may be driven by different means, such as decay of precursors. Therefore, the effect of the cumulative uncertainty of actual isotopics predictions is significantly smaller than the yield uncertainty would indicate.

Table 2-2 Uncertainty in Key Fission Yield Data

Fission-able nuclide *i*	Fission product *j*	Thermal incident neutron energy		Intermediate incident neutron energy		Fast incident neutron energy	
		Mean (-)	Standard deviation (%)	Mean (-)	Standard deviation (%)	Mean (-)	Standard deviation (%)
^{235}U	^{135}Te	3.23E-02	2.11	2.48E-02	9.93	1.05E-02	18.05
	^{135}I	2.92E-02	2.28	3.59E-02	6.58	3.13E-02	6.14
	^{135}Xe	7.97E-04	1.11	1.20E-03	10.86	4.54E-03	6.17
	^{149}Nd	6.87E-05	48.53	3.50E-05	48.39	6.98E-04	48.36
	^{149}Pm	3.93E-08	47.81	1.63E-08	49.60	1.31E-05	50.00
	^{149}Sm	1.75E-12	48.07	5.68E-13	48.57	2.67E-08	47.72
^{238}U	^{135}Te	-	-	4.61E-02	9.01	2.65E-02	9.18
	^{135}I	-	-	1.36E-02	28.92	2.59E-02	28.78
	^{135}Xe	-	-	1.23E-04	2.45	1.33E-03	2.54
	^{149}Nd	-	-	4.99E-06	47.71	6.30E-05	47.71
	^{149}Pm	-	-	1.19E-09	46.92	1.57E-07	46.92
	^{149}Sm	-	-	1.55E-14	50.35	2.27E-11	50.41
^{239}Pu	^{135}Te	2.19E-02	9.62	2.12E-02	28.11	6.87E-03	45.20
	^{135}I	4.28E-02	4.94	3.92E-02	9.97	3.25E-02	24.16
	^{135}Xe	3.14E-03	3.43	6.11E-03	6.14	8.54E-03	47.60
	^{149}Nd	4.99E-04	48.45	5.89E-04	49.10	2.37E-03	46.64
	^{149}Pm	2.38E-06	50.82	2.55E-06	48.70	1.39E-04	47.55
	^{149}Sm	8.22E-10	48.13	9.57E-10	48.52	9.81E-07	49.94

2.3 Decay Uncertainty

Uncertainty in decay constants $\lambda_{i,d}$ and branch ratios $f_{i,d\rightarrow j}$ impact isotopic evolution in depletion or decay calculations. However, uncertainty in decay constants and decay heat Q_i impact any activity or decay heat response. This report only addresses activity responses.

An analysis of decay heat uncertainty in this study identified errors in the uncertainties assigned to the Q_i values in the uncertainty libraries used by Sampler, resulting in unrealistically large estimates of decay heat uncertainty. This error impacts versions up to and including SCALE 6.2.2. Corrected libraries are being developed for distribution in parallel with the release of SCALE 6.2.3 through a separate distribution. This problem only impacts decay heat calculations.

2.3.1 Background

The SCALE decay data have only included uncertainties since the release of Sampler with SCALE 6.2. The decay data use ENDF/B VII.1 uncertainties and approximate correlations, which are described in the 2013 paper by Williams et al. [3].

2.3.2 Implementation

Decay constant $\lambda_{i,d}$ values are sampled according to independent normal probability distributions, with standard deviations given in ENDF/B-VII.1. The branch ratios $f_{i,d\rightarrow j}$ are sampled from ENDF/B-VII.1 data, assuming that the largest two branching fractions are anti-correlated. Any smaller branch ratios are assumed to be independent.

One thousand random samples of decay data are pre-generated and written to Oak Ridge Isotope Generation (ORIGEN)-formatted decay data files. When Sampler is directed to consider uncertainty in decay data, it substitutes one of these perturbed decay files in place of the nominal. Decay data are not used by the TSUNAMI tools, which only support calculations with fixed isotopics.

2.3.3 Characteristics

Table 2-3 shows uncertainty in total decay constants, λ_d, for nuclides that contribute to LWR fuel activity for decay times up to 40 years.

Table 2-3 Uncertainty in Key Decay Data

Radioactive nuclide i	λ_i Mean (1/s)	λ_i Standard deviation (%)
^{238}Pu	2.51E-10	0.11
^{106}Rh	2.31E-02	1.14
^{140}La	4.78E-06	0.01
^{144}Pr	6.69E-04	0.29
^{90}Sr	7.63E-10	0.21
^{137}Cs	7.30E-10	0.30
^{95}Zr	1.25E-07	0.01
^{137m}Ba	4.53E-03	0.04
^{134}Cs	1.06E-08	0.02
^{90}Y	3.01E-06	0.34
^{95}Nb	2.29E-07	0.02
^{89}Sr	1.59E-07	0.14
^{154}Eu	2.55E-09	0.12
^{241}Pu	1.54E-09	0.04
^{106}Ru	2.16E-08	0.48
^{144}Ce	2.82E-08	0.02
^{147}Pm	8.37E-09	0.01
^{118m}Ag	3.50E-01	10.24
^{103m}Rh	2.06E-04	0.04
^{103}Ru	2.04E-07	0.01
^{242}Cm	4.92E-08	0.04
^{244}Cm	1.21E-09	0.16
^{139}I	3.04E-01	0.46
^{3}H	1.78E-09	0.16
^{99}Tc	1.04E-13	0.57
^{91}Y	1.37E-07	0.10
^{243}Cm	7.55E-10	0.35
^{240}Pu	3.35E-12	0.10
^{243}Am	2.98E-12	0.20
^{14}C	3.85E-12	0.53
^{135}Te	3.65E-02	1.07
^{135}I	2.93E-05	0.31
^{135}Xe	2.11E-05	0.22
^{149}Nd	1.11E-04	0.06
^{149}Pm	3.63E-06	0.09

3 LWR APPLICATIONS WITH UNCERTAINTY

This section demonstrates the impact of nuclear data uncertainty on quantities of interest in typical LWR applications with SCALE, including

- few-group macroscopic cross sections for nodal core simulators,
- reactivity coefficients,
- power distributions,
- spent fuel isotopic concentrations, and
- source terms.

This section also compares calculated isotopic concentrations to measurements, including uncertainty in both calculation and measurement, as seen in Williams et al. [3], but with expanded results. A significant portion of the following discussion is focused on the interpretation of these comparisons.

3.1 Description

The analysis case for this purpose is the Calvert Cliffs Unit 1 (CC-1) reactor assembly D047, a Combustion Engineering (CE) 14 ×14 design with known operating history and high-precision radiochemical assay data available for multiple axial locations of rod MKP109 in this assembly [6]. The assembly configuration and location of measured rod MKP109 are shown in Figure 1.]. Two samples analyzed by Oak Ridge National Laboratory (ORNL) in 2011 [7], identified as samples S1 and S2, are of particular interest. These samples were extracted from adjacent axial locations, as shown in Figure 2. High-precision measurements were made for 50 different isotopes. The similarity of the two samples provides a measurement cross check that allows an opportunity to investigate the reported measurement uncertainty in terms of the reproducibility of the measurement process.

3.1.1 Operating History

A simplified operating history was assumed to achieve the measured sample-average burnup of 43.5 GWd/tU of the 3.038 wt% ^{235}U fuel sample. The operating history assumptions are as follows:

- constant material properties for soluble boron, temperatures, densities, etc.;
- 4 cycles with 15 days of intermittent decay and sample-average powers of
    - 34.21 MW/tU for 306 days,
    - 29.69 MW/tU for 382 days,
    - 24.61 MW/tU for 466 days, and
    - 22.28 MW/tU for 461 days; and

- a final decay to 28.69 years when the measurements of samples S1 and S2 were performed.

See Hu et al. [7] for additional details.

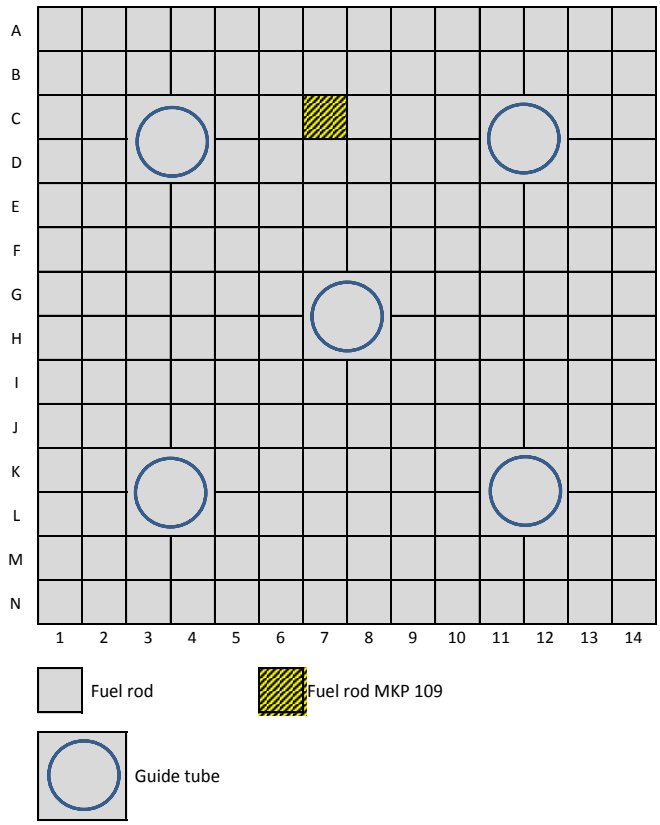

Figure 3-1 Configuration of Assembly D047 From CC-1 [7]

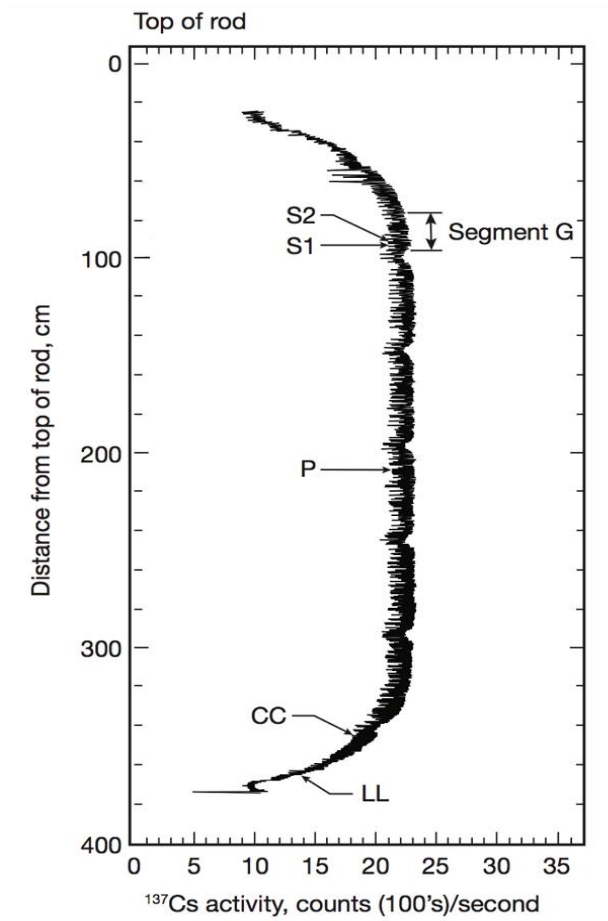

Figure 3-2 ^{137}Cs Gamma Scan Showing Sample S1 and S2 Locations [7]

3.1.2 Measurements

The measured isotopic concentrations for samples S1 and S2 are shown in Table 3-1, along with four different measures of the uncertainty which are labeled *Declared measurement uncertainty*, *Mean measurement uncertainty*, *Mean measurement standard error*, and *Effective measurement uncertainty*.

Declared measurement uncertainty

The *declared measurement uncertainty* is the measurement standard deviation $u(S)$ as reported for each isotope and sample [7], which is dependent on the measurement technique.

Mean measurement uncertainty

The *Mean measurement uncertainty* is calculated by applying uncertainty propagation to the sample mean of the two samples,

$$\bar{S} = \frac{1}{2}(S1 + S2), \tag{28}$$

resulting in standard deviation of the mean,

$$u(\bar{S}) = \frac{1}{2}\sqrt{v(S1) + v(S2)} = \frac{1}{\sqrt{2}}u(S), \tag{29}$$

where the variance is $v(S) = [u(S)]^2$.

Mean measurement standard error

The *Mean measurement standard error* is the standard error of the mean for two samples, $se(\bar{S})$,

$$se(\bar{S}) = \frac{1}{\sqrt{2}}std(S). \tag{30}$$

where $std(S)$ is calculated from the sample standard deviation for two samples as

$$std(S) = \sqrt{(S1 - \bar{S})^2 + (S2 - \bar{S})^2}. \tag{31}$$

The true uncertainty is given by the standard error $se(\bar{S})$, which is only applicable when there are multiple equivalent measurements. These equivalent measurements allow for verification of the experimentalist's uncertainty prediction. The only issue is when the standard error shows a lower uncertainty. In some cases, the two samples agree to the available three digits. In these cases, instead of using a very small standard error, the original uncertainty prediction is used.

Effective measurement uncertainty

The far right column shows this as the *Effective measurement uncertainty*, given as

$$u_{eff}(\bar{S}) = \max[u(\bar{S}), se(\bar{S})]. \tag{32}$$

Table 3-1 Measurement and Uncertainty Data for CC-1 MKP109 Samples S1 and S2

Nuclide	S1 measure-ment (g/gFuel)	S2 measure-ment (g/gFuel)	Declared measure-ment uncertainty, $u(S)$ (%)	Mean measure-ment uncertainty, $u(\bar{S})$ (%)	Mean measure-ment standard error, $se(\bar{S})$ (%)	Effective measure-ment uncertainty, $u_{eff}(\bar{S})$ (%)
^{241}Am	8.47E-04	9.24E-04	5.0	3.5	4.3	4.3
^{243}Am	1.69E-04	1.75E-04	5.0	3.5	1.7	3.5
^{140}Ce	1.36E-03	1.35E-03	1.0	0.7	0.4	0.7
^{142}Ce	1.23E-03	1.21E-03	1.0	0.7	0.8	0.8
^{244}Cm	2.88E-05	2.99E-05	5.0	3.5	1.9	3.5
^{133}Cs	1.20E-03	1.19E-03	1.0	0.7	0.4	0.7
^{135}Cs	4.19E-04	4.17E-04	1.0	0.7	0.2	0.7
^{137}Cs	6.70E-04	6.67E-04	1.0	0.7	0.2	0.7
^{151}Eu	2.76E-06	2.26E-06	2.7	1.9	10.0	10.0
^{152}Eu	2.64E-08	1.50E-07	15.0	10.6	70.1	70.1
^{153}Eu	1.32E-04	1.32E-04	1.0	0.7	0.0	0.7
^{154}Eu	2.58E-06	2.51E-06	2.7	1.9	1.4	1.9
^{155}Eu	1.47E-07	1.63E-07	15.0	10.6	5.2	10.6
^{152}Gd	4.92E-08	1.09E-07	15.0	10.6	37.8	37.8
^{154}Gd	2.89E-05	2.88E-05	1.0	0.7	0.2	0.7
^{155}Gd	1.02E-05	1.01E-05	1.0	0.7	0.5	0.7
^{156}Gd	1.42E-04	1.43E-04	1.0	0.7	0.4	0.7
^{157}Gd	3.55E-07	2.04E-07	15.0	10.6	27.0	27.0
^{158}Gd	2.25E-05	2.21E-05	1.0	0.7	0.9	0.9
^{160}Gd	1.78E-06	1.55E-06	2.7	1.9	6.9	6.9
^{139}La	1.45E-03	1.52E-03	5.0	3.5	2.4	3.5
^{95}Mo	8.35E-04	8.14E-04	5.0	3.5	1.3	3.5
^{142}Nd	3.14E-05	3.24E-05	1.4	1.0	1.6	1.6
^{143}Nd	7.81E-04	7.82E-04	1.0	0.7	0.1	0.7
^{144}Nd	1.63E-03	1.62E-03	1.0	0.7	0.3	0.7
^{145}Nd	7.30E-04	7.31E-04	1.0	0.7	0.1	0.7
^{146}Nd	8.21E-04	8.21E-04	1.0	0.7	0.0	0.7
^{148}Nd	4.28E-04	4.26E-04	1.0	0.7	0.2	0.7
^{150}Nd	2.07E-04	2.06E-04	1.0	0.7	0.2	0.7
^{237}Np	5.09E-04	5.40E-04	5.0	3.5	3.0	3.5
^{238}Pu	1.94E-04	2.11E-04	1.0	0.7	4.2	4.2
^{239}Pu	4.39E-03	4.57E-03	1.0	0.7	2.4	2.4
^{240}Pu	2.49E-03	2.62E-03	1.0	0.7	2.5	2.5
^{241}Pu	3.18E-04	3.38E-04	1.4	1.0	3.0	3.0
^{242}Pu	7.82E-04	8.22E-04	1.4	1.0	2.5	2.5
^{103}Rh	4.70E-04	4.85E-04	5.0	3.5	1.6	3.5
^{101}Rh	8.25E-04	8.18E-04	5.0	3.5	0.4	3.5
^{147}Sm	2.62E-04	2.60E-04	1.0	0.7	0.4	0.7
^{148}Sm	1.91E-04	1.91E-04	1.0	0.7	0.0	0.7
^{149}Sm	2.44E-06	2.34E-06	2.7	1.9	2.1	2.1
^{150}Sm	3.16E-04	3.17E-04	1.0	0.7	0.2	0.7
^{151}Sm	7.74E-06	7.72E-06	2.5	1.8	0.1	1.8

Nuclide	S1 measure-ment (g/gFuel)	S2 measure-ment (g/gFuel)	Declared measure-ment uncertainty, $u(S)$ (%)	Mean measure-ment uncertainty, $u(\bar{S})$ (%)	Mean measure-ment standard error, $se(\bar{S})$ (%)	Effective measure-ment uncertainty, $u_{eff}(\bar{S})$ (%)
^{152}Sm	1.10E-04	1.09E-04	1.0	0.7	0.5	0.7
^{154}Sm	4.43E-05	4.40E-05	1.0	0.7	0.3	0.7
^{90}Sr	2.54E-04	2.30E-04	5.0	3.5	5.0	5.0
^{234}U	1.64E-04	1.65E-04	5.0	3.5	0.3	3.5
^{235}U	3.85E-03	3.79E-03	1.4	1.0	0.8	1.0
^{236}U	3.64E-03	3.65E-03	1.4	1.0	0.1	1.0
^{238}U	8.23E-01	8.23E-01	1.0	0.7	0.0	0.7

3.2 Calculation Results

The results in this section demonstrate the uncertainty propagation capabilities of SCALE/Sampler, and they also provide a reference point for discussions on the implications or conclusions. The following results are provided:

- two-group macroscopic cross sections, including
    - absorption,
    - nu-fission, and
    - scattering;
- reactivity data, including
    - eigenvalue,
    - delayed neutron fraction, and
    - fuel temperature coefficient of reactivity;
- power distribution data, including
    - rod power fraction and
    - flux magnitude uncertainty;
- isotopic concentrations for all measured nuclides; and
- source activity

In Figures 3–8, the quantity of interest is shown on the left y-axis in terms of mean—*calc. mean*—with bands for the standard deviation—*calc. std. dev.*—calculated according to standard sample statistics:

$$std(C) = \sqrt{\frac{1}{N-1}\sum_{n}(C_n - \bar{C})^2}, \tag{33}$$

where $\bar{C}$ is the calculation mean and C_n is the n-th sample.

Through histograms, the 2.5th, 16th, 84th, 97.5th percentiles have also been estimated. These specific percentiles were chosen because if the distribution were normal, then the 84th and 16th percentiles would coincide with the mean plus and minus one standard deviation (1-sigma), respectively, and the 97.5th and 2.5th percentiles would coincide plus and minus 2-sigma.

Various error metrics are displayed in blue on the right y-axis. The calculation 95% range width (*calc. 95% range width*) and calculation 4-sigma (*4 × calc. std. dev.*) are provided for all results. The 95% range width is the 97.5th percentile minus the 2.5th percentile, and if the distribution were normal, then the 95% range width would be equivalent to four standard deviations (4-sigma). Thus, comparing these range widths indicates the normality of the distribution.

Measurements are available for many nuclides considered in this study. On the left y-axis, the measurement is shown as a black circle (*meas.*) with 2-sigma error bars given by the measurement effective uncertainty defined in Eq. (32). The bias (*bias*) is also shown as a blue *x*, defined as

$$bias = \frac{\bar{C}}{\bar{S}} - 1, \tag{34}$$

with 2-sigma error bars shown, calculated as the (relative) standard deviation,

$$rel.std(bias) = \sqrt{u_{eff}(\bar{S})^2 + std(C)^2/\bar{C}^2}. \tag{35}$$

It is convenient in the following sections to refer to the uncertainty using a single number; we have chosen the 95% range width. The 95% probability range is a standard range of interest in engineering safety analysis, is valid for any distribution, and can be described by the 2.5th percentile and 97.5th percentile values. To condense these two values to a single number that represents the uncertainty, the 95% range width is used here. In several instances, another measure has been used (e.g., 1-sigma measurement uncertainty). These instances are clearly marked.

Across the different outputs of interest, uncertainty magnitudes were observed from fractions of a percent to 50% or more. Each set is discussed individually in the following subsections.

3.2.1 Macroscopic Cross Section Uncertainty

The uncertainties in scattering, absorption, and nu-fission macroscopic cross sections in the thermal energy range all show similar behavior with irradiation time (burnup), with values of

approximately 2–4% over the course of the irradiation simulation. In the fast energy range, uncertainty for scattering and absorption ranges from 3–4%, and for fast nu-fission, it ranges from 2–7% with burnup.

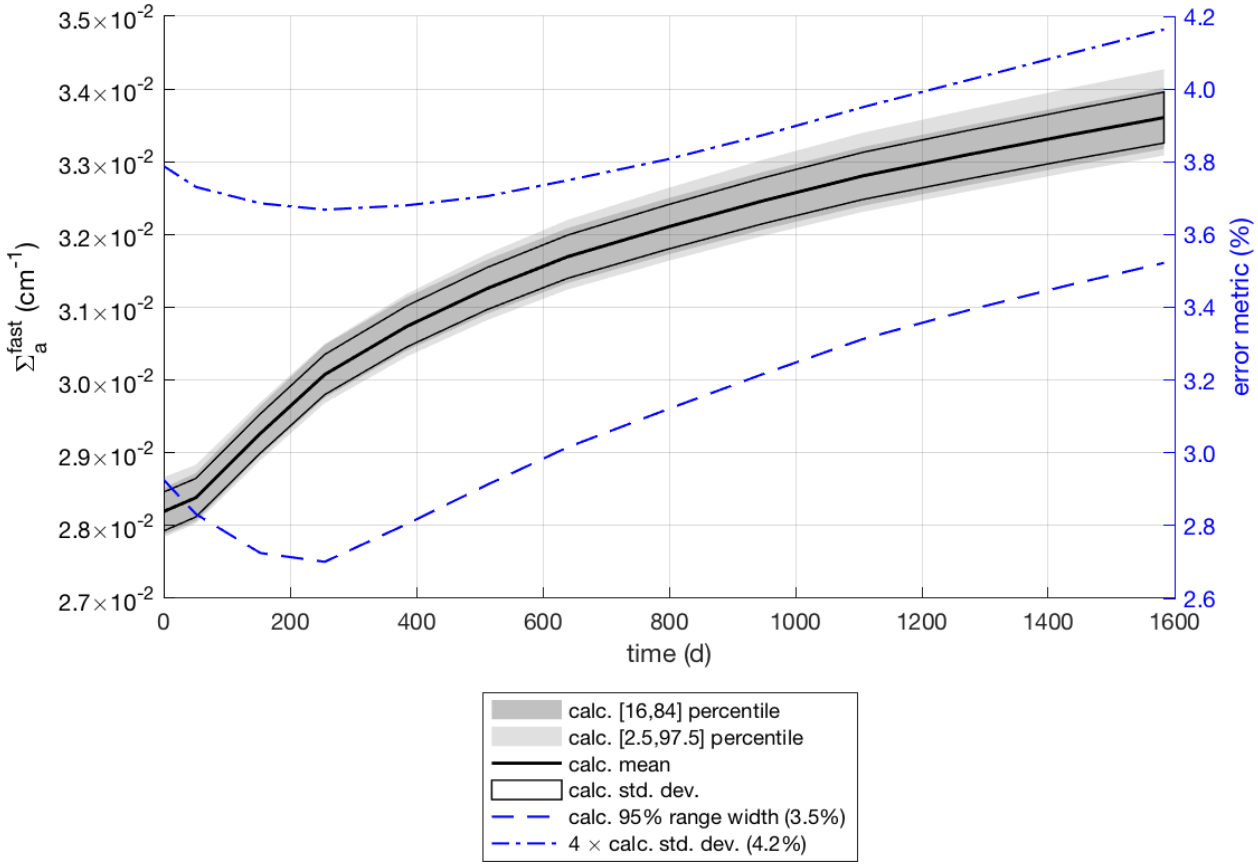

Figure 3-3 Fast Macroscopic Absorption Cross Section

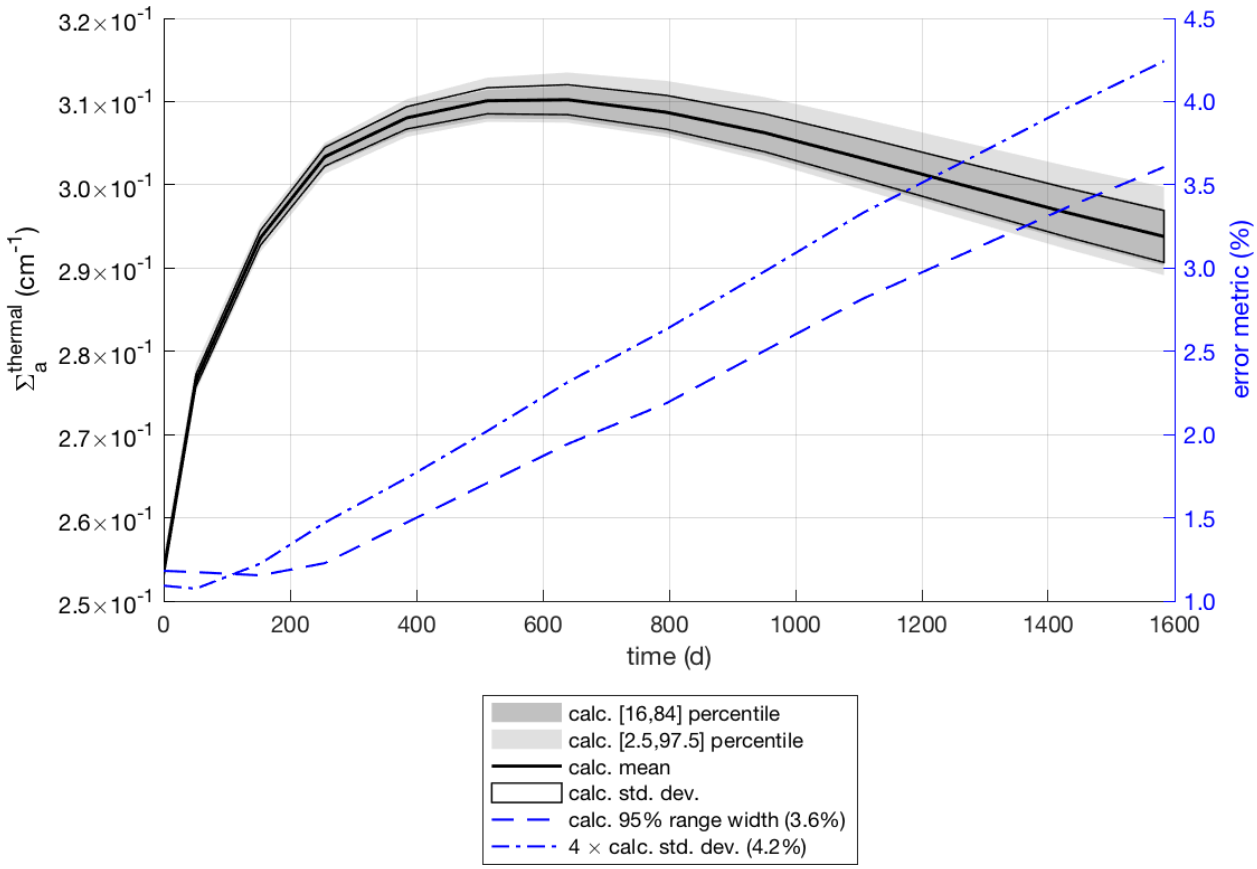

Figure 3-4 Thermal Macroscopic Absorption Cross Section

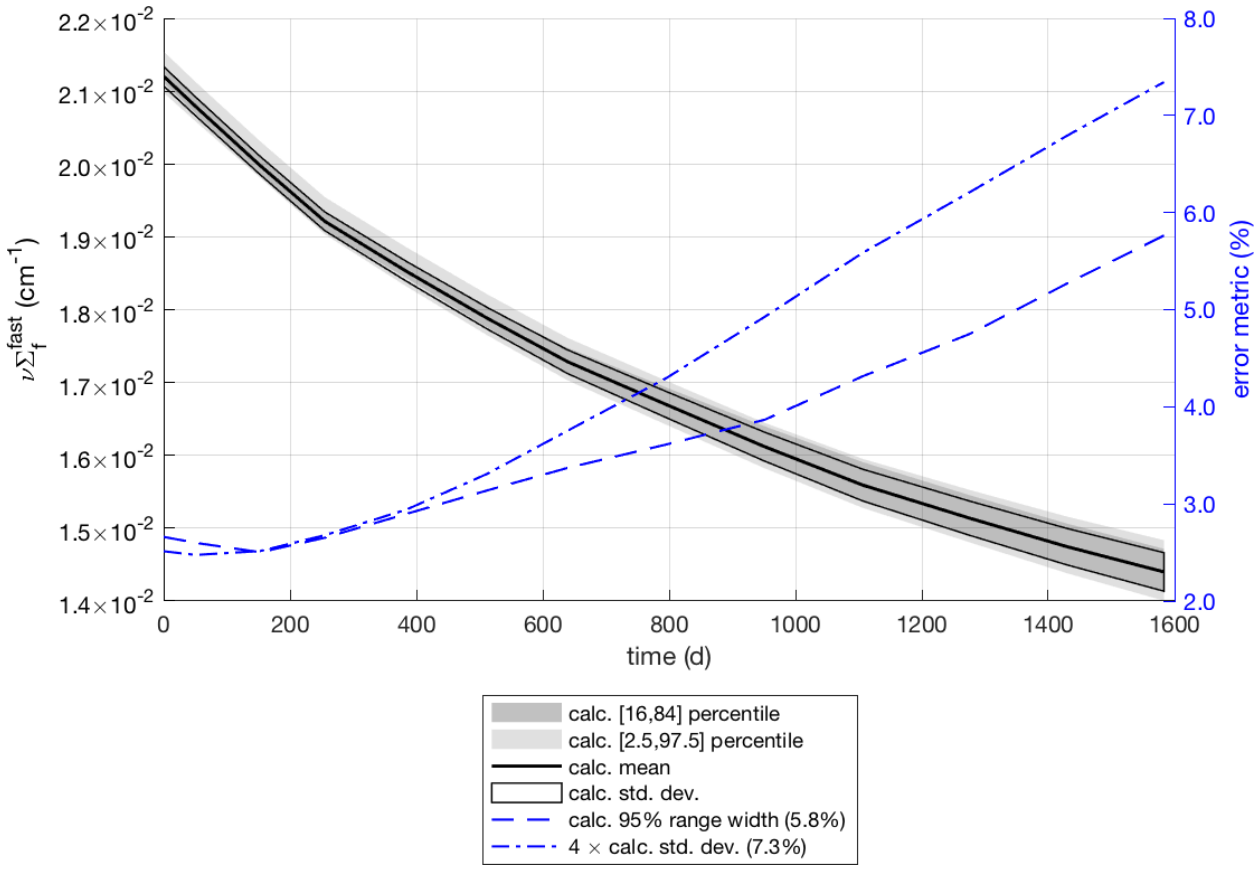

Figure 3-5 Fast Macroscopic Nu-Fission Cross Section

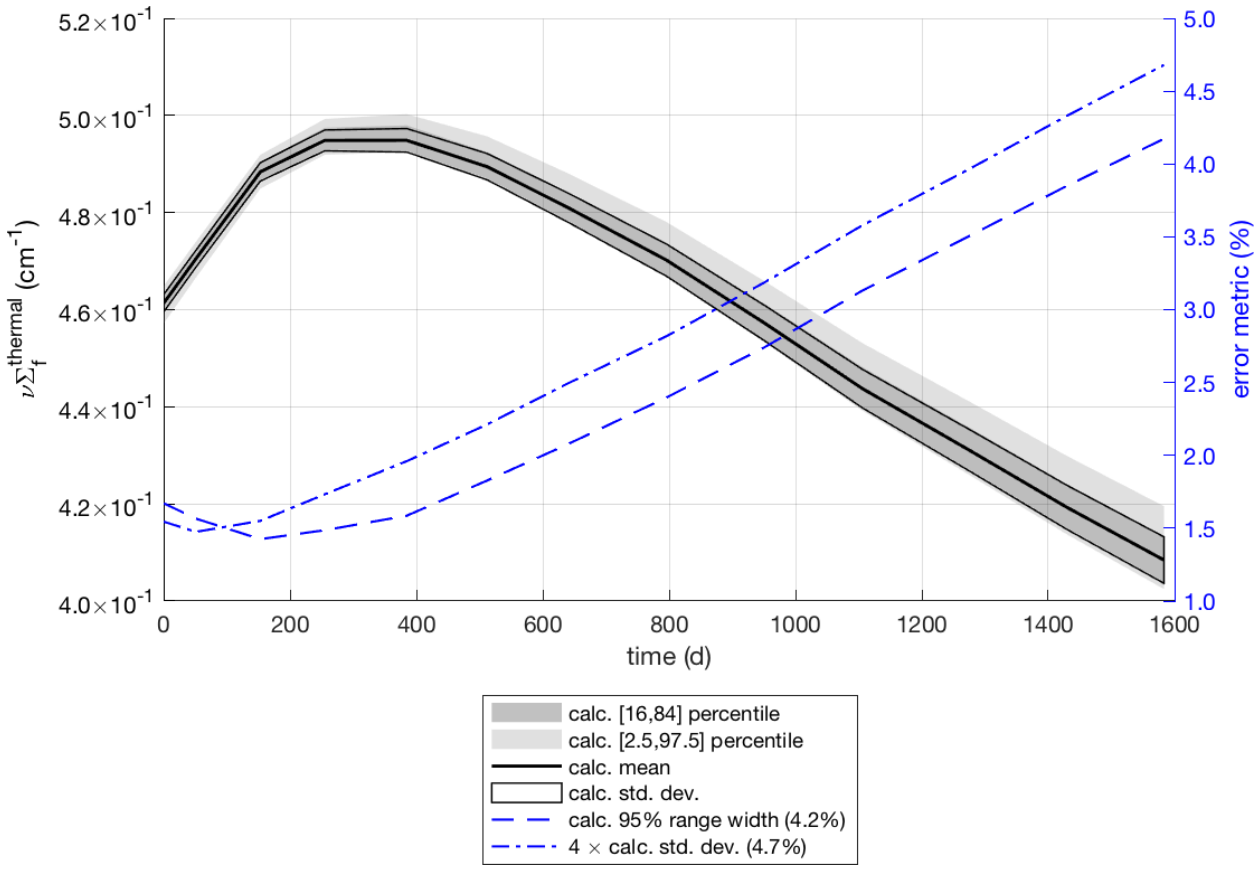

Figure 3-6 Thermal Macroscopic Nu-Fission Cross Section

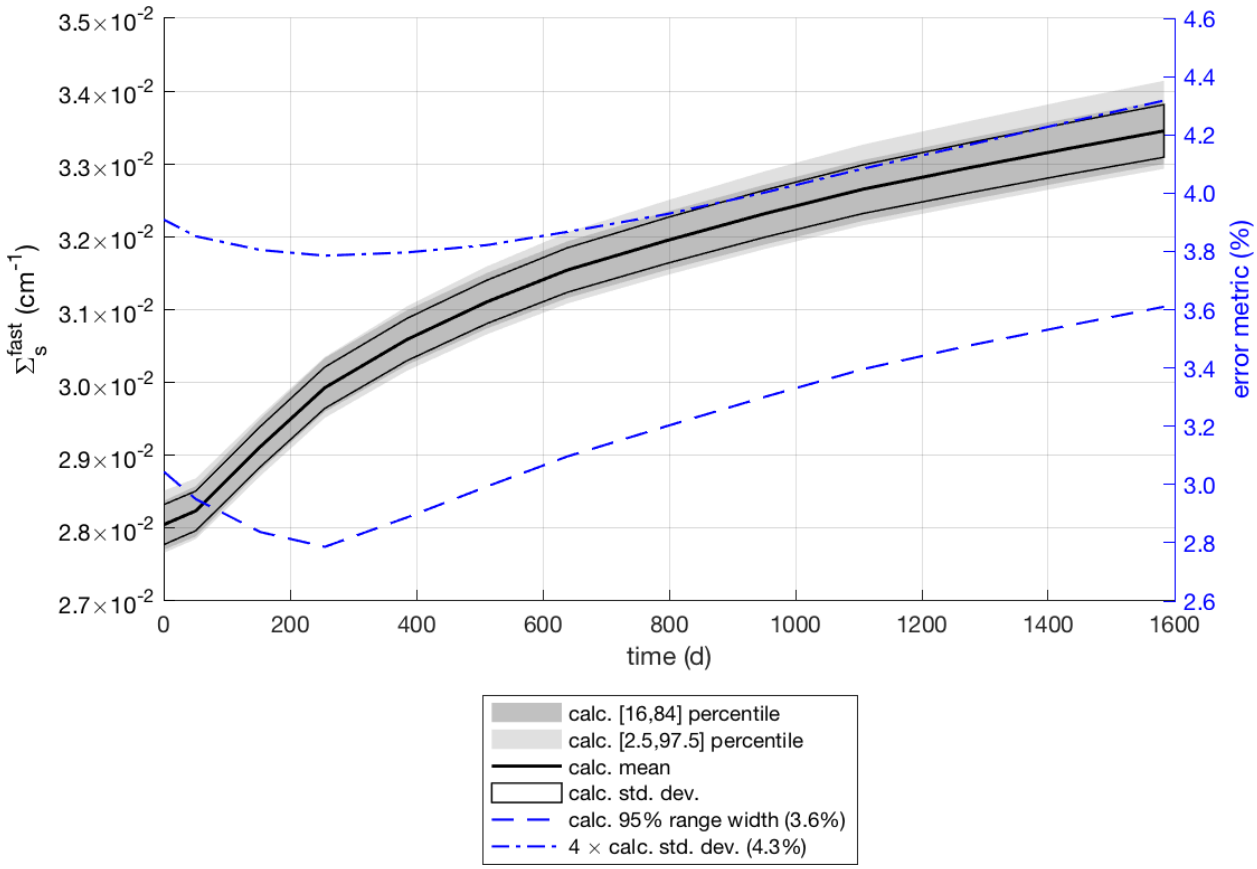

Figure 3-7 Fast Macroscopic Scattering Cross Section

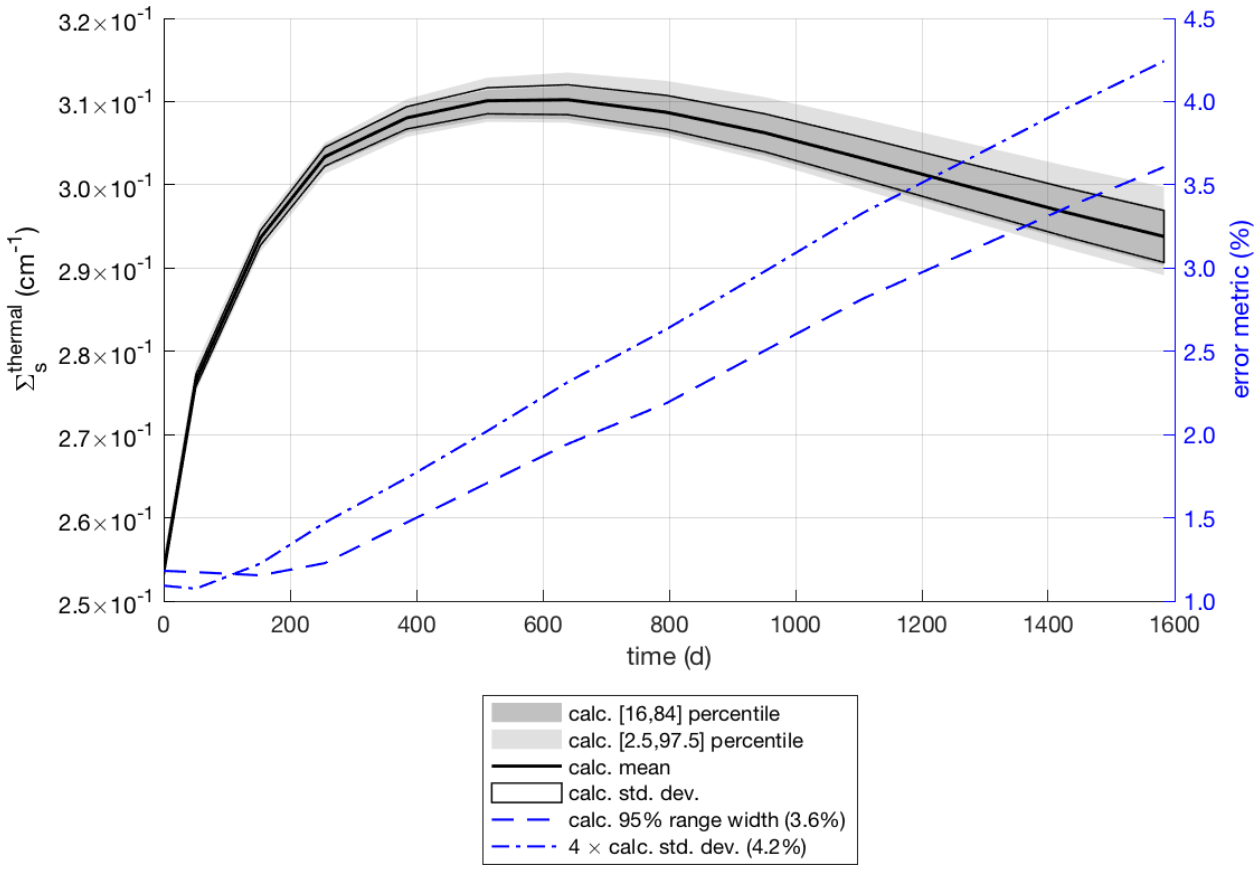

Figure 3-8 Thermal Macroscopic Scattering Cross Section

3.2.2 Reactivity Uncertainty

All reactivity parameters examined show increasing uncertainty with burnup, as illustrated in Figures 9 to 11. The eigenvalue, k_{eff}, shows 1.5–2% uncertainty. The total delayed neutron fraction, β_{eff}, shows a remarkably high uncertainty, initially 20%, increasing with burnup to 100%*. The temperature reactivity coefficient shows 5–7% uncertainty.

* Initial investigations have shown that this is due to the delayed chi uncertainty.

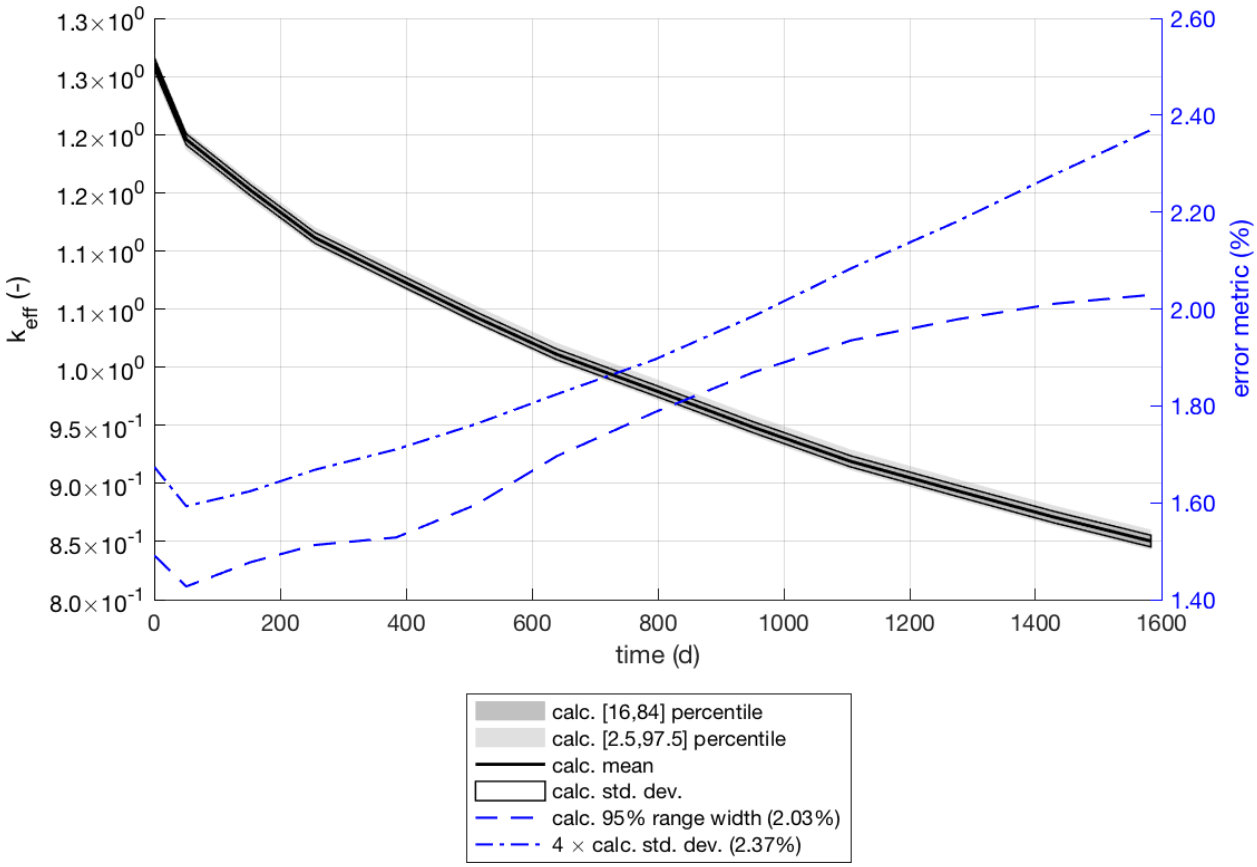

Figure 3-9 Eigenvalue Uncertainty

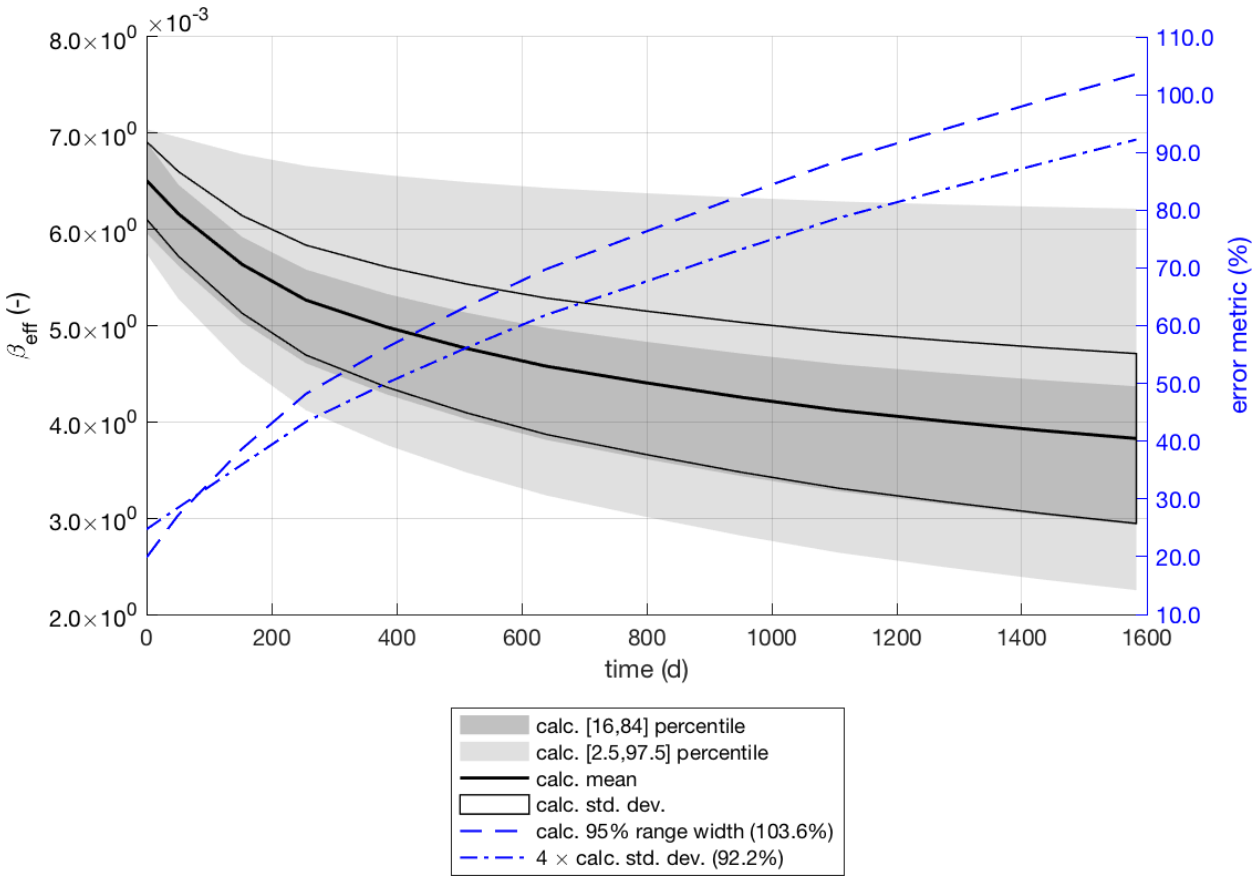

Figure 3-10 Delayed Neutron Fraction Uncertainty

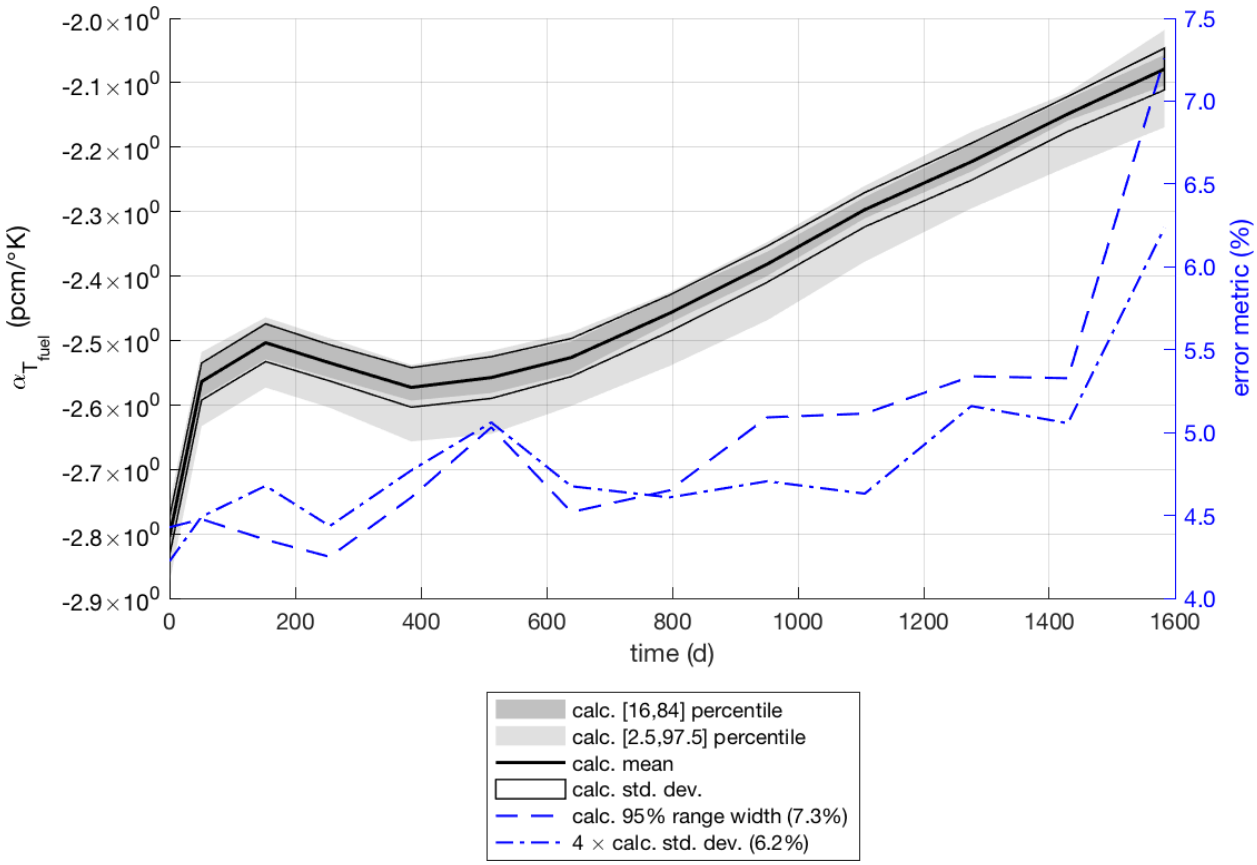

Figure 3-11 Reactivity Coefficient Uncertainty

3.2.3 Power Distribution Uncertainty

As illustrated in Figure 12, the power factor for the MKP109 rod shows a low uncertainty, with a maximum value of only 0.25%. This is likely to the result of power normalization methods. For example, the uncertainty in an average power factor of 1.0 is by definition zero. The power of the MKP109 rod is slightly below the assembly average power, with a power factor ranging from 0.93–0.97, which is very close to 1.0. As shown in Figure 13, the uncertainty in the flux is one of the few parameters where the uncertainty decreases with burnup, from an initial level of 3% down to 2%. The flux levels exhibit oscillations that occur when the flux distributions are recalculated by the transport calculation. This is performed in the middle of each depletion step corresponding to a reactor cycle in the Transport Rigor Implemented with Time-Dependent Operation for Neutronic Depletion (TRITON) depletion calculation. The flux decrease is caused by decreasing power in each subsequent cycle. During each cycle, power is assumed to be constant, and an expected gradual increase in flux is observed as the fissionable material is depleted.

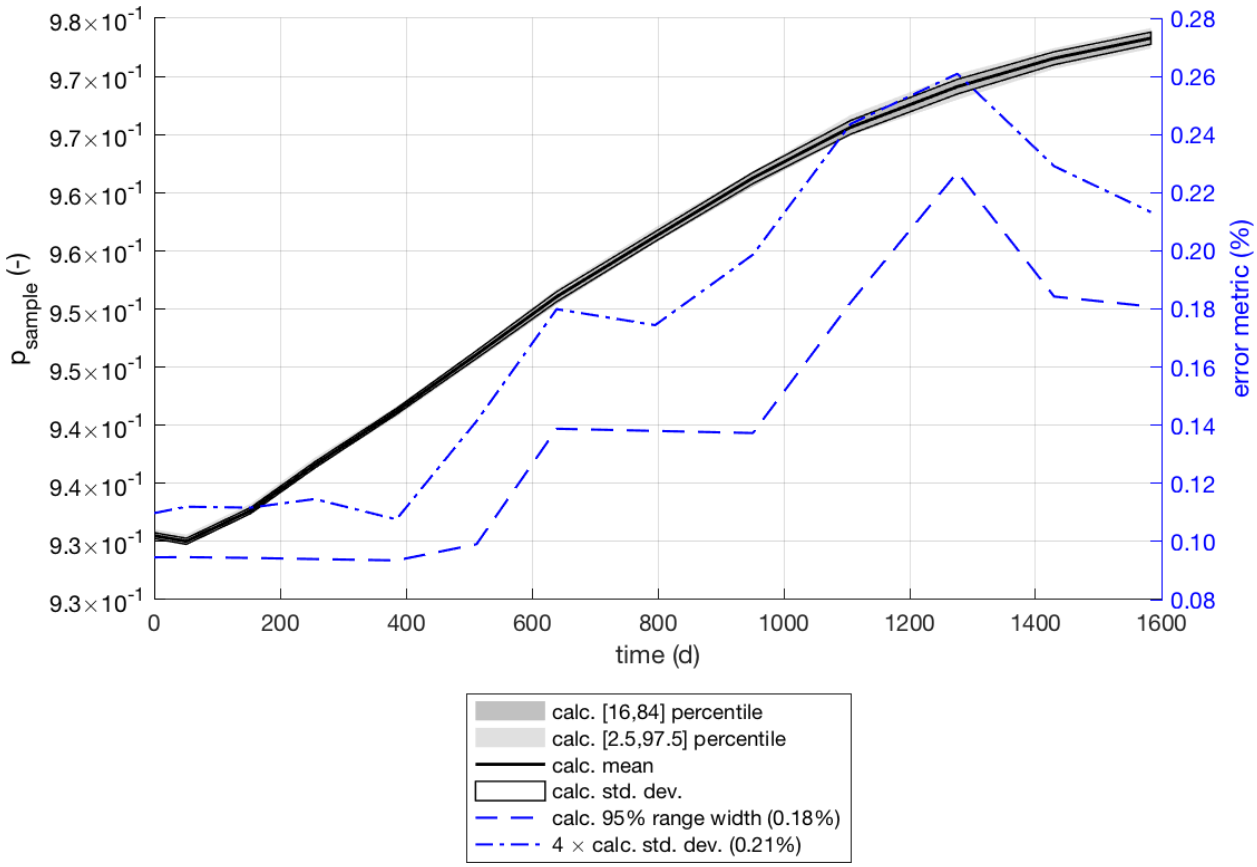

Figure 3-12 Irradiation Sample Power Factor Uncertainty

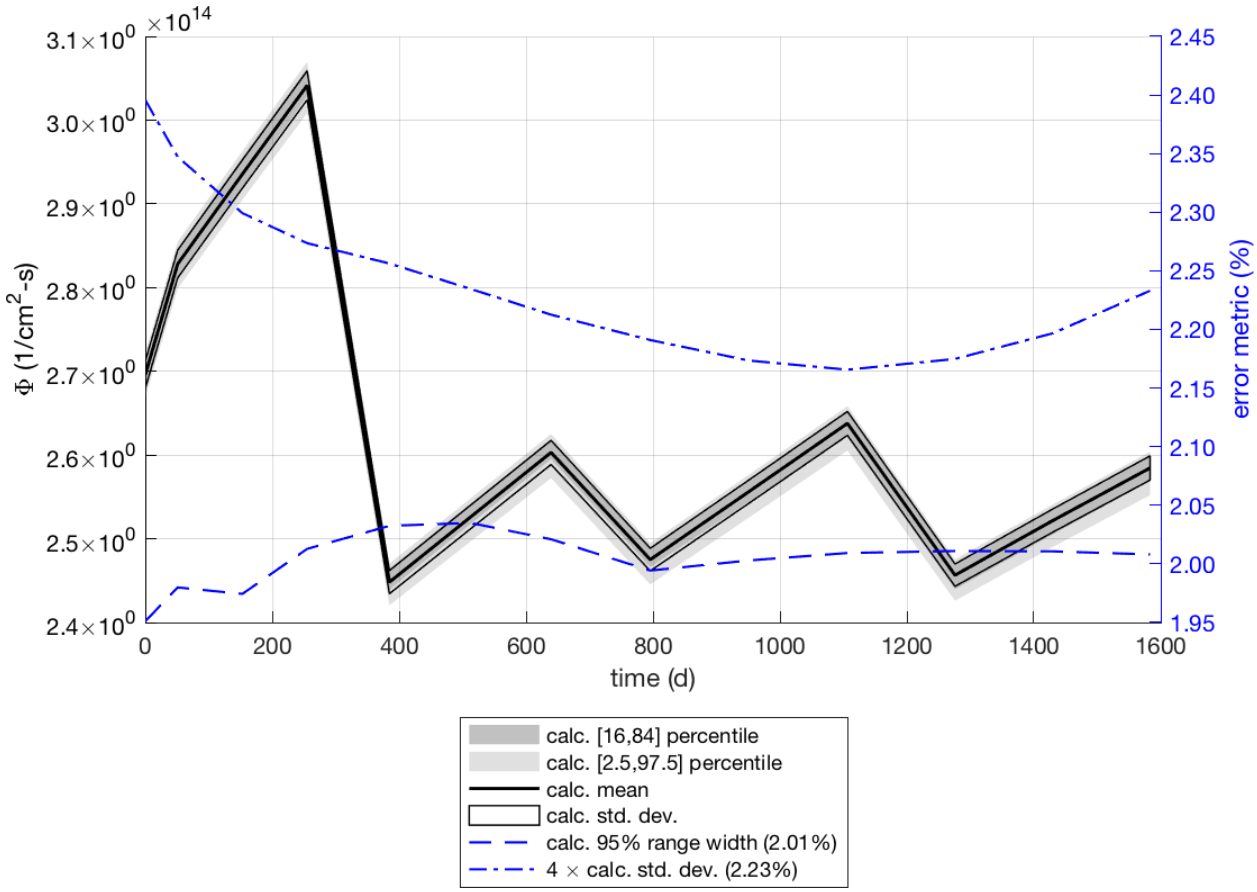

Figure 3-13 Flux Magnitude Uncertainty

3.2.4 Isotopic Uncertainties

Figures 13–63 illustrate isotopic uncertainties. The isotopic calculations include the irradiation time and the decay time before measurement of the nuclide compositions. The calculated content and uncertainty in many isotopes change in behavior, moving from irradiation to decay. The calculation uncertainties range from a few percent to 50% or more. The availability of measurements gives an additional aspect to the analysis which will be used to organize the discussion into four groups representing the various combinations of large or small calculation, uncertainty, and expected or unexpected bias. Here, a 95% range width uncertainty of less than 10% is considered small, and an unexpected bias is assumed when the bias 95% range does not include zero. For simplicity, the bias is assumed to be normally distributed.

3.2.4.1 Small Calculation Uncertainty / Expected Bias

These nuclides have less than 10% calculation uncertainty and an expected bias range that includes zero. It could be concluded that these nuclides are predicted accurately, within the expected uncertainties, and precisely, as the uncertainties are small. Nuclides in this category are ^{139}La, ^{95}Mo, ^{143,144,145,146}Nd, ^{239,240,241}Pu, ^{147,148,149,152}Sm, and ^{234,238}U, and they exhibit a wide range of notable behaviors.

The uranium isotope ^{234}U, present in the initial fuel, is observed to deplete during irradiation, and then it builds during decay due to production from ^{238}Pu decay. ^{149}Sm is an important neutron

absorber; it builds to a maximum shortly after discharge from the decay of precursor ^{149}Pm (53 hours), depending on the power level reached during prior operation. It is well predicted, with a bias range of -0.6 to 10.6%, including a calculated uncertainty of ~6% and a measured uncertainty of ~8%. It can be reasonably concluded that, based on this bias, the amount of ^{149}Sm may be predicted within 10% of the actual value.

Plutonium isotopes ^{239}Pu, Pu^{240}, and ^{241}Pu are predicted well within error bounds, with observed biases of only ~1%, while calculation uncertainties of ~5% are estimated from the data.

Neodymium isotopes ^{143}Nd, ^{144}Nd, ^{145} Nd, and ^{146}Nd are predicted to within ~3%.

3.2.4.2 Large Calculation Uncertainty / Expected Bias

These nuclides have 10% or greater calculation uncertainty and an expected bias range that includes zero. In contrast to the previous group of nuclides with small calculation uncertainty, it can be concluded that these nuclides are predicted within the expected uncertainty range, but the range exceeds a threshold of 10%. These nuclides are ^{243}Am, ^{244}Cm, ^{135}Cs, ^{151,153,155}Eu, ^{154,155,160}Gd, ^{142}Nd, ^{237}Np, and ^{151}Sm, and they are candidates for data improvements. One possible reason for the large uncertainty is that the evaluation process has overestimated the uncertainty.

^{244}Cm has a very large calculation uncertainty of ~40%, but it only has an observed bias of 2% and an effective measurement uncertainty of ~14%. This is another candidate for improvement, as the uncertainties in the data significantly overestimate the biases observed when comparing calculations with measurements.

^{151}Eu has linear buildup during decay, with an uncertainty of ~20% during irradiation, rising to ~40% at time of measurement. The effective measurement uncertainty in this case is also approximately 40%, based on observed differences in the two samples, although the reported measurement uncertainty for each sample was only 10%.

^{155}Gd, an important neutron absorber, is often added to fuel as a neutron-absorbing dopant, but here it is added as a fission product. The calculation uncertainty is ~60%, yet a bias of ~1% with a measurement uncertainty of ~1% was achieved. There may be overestimated data uncertainty that could be targeted for correction.

3.2.4.3 Small Calculation Uncertainty / Unexpected Bias

These nuclides have less than 10% calculation uncertainty and an unexpected bias range that does not include zero. In this group, the calculation is indicated to be precise, which implies that it should be accurate, but according to the comparison to measurement, it is actually inaccurate. Nuclides in this category are ^{241}Am, ^{140}Ce, ^{142}Ce, ^{133,137}Cs, ^{152,156,158}Gd, ^{148,150}Nd, ^{103}Rh, ^{101}Ru, ^{154}Sm, ^{90}Sr, and ^{235,236}U. Each of these nuclides contains an error that has not been taken into account. These errors could be due to issues in the model, the data, or the actual measurements.

Consider ^{137}Cs, an important radiological gamma-emitting nuclide used for determining axial and radial burnup profiles through gamma scanning. This nuclide is measured with an effective uncertainty of only ~1.4%, has an expected calculation uncertainty of only ~1.4%, and yet has a bias in the range of 7–9%.

^{235}U has a calculation uncertainty of 7% in this case, with 3% measurement uncertainty, but with a bias of 14%. According to Hu et al. [7], the observed bias in the amount of ^{235}U was found to be only ~1%. The most likely cause is the simplified model used here for the depletion calculations. For example, the soluble boron variations were not modeled explicitly, and a simplified operating history was used. Because ^{235}U is initially the main fissile nuclide in the system, and because the power is fixed in this type of model, there is a correlation between the major fissile isotopes of ^{235}U and ^{239}Pu. Thus, any changes made to the model which would impact ^{239}Pu production would also influence the amount of ^{235}U depleted.

3.2.4.4 Large Calculation Uncertainty / Unexpected Bias

The nuclides in this list include those with 10% or greater calculation uncertainty and an unexpected bias range that does not include zero. In this group, the calculation indicates significant uncertainty, but the result is still less accurate than expected. Nuclides in this category are ^{107}Ag, ^{152,154}Eu, ^{157}Gd, and ^{238,242}Pu. Historically, ^{238}Pu has been difficult to predict, but recent updates in ENDF/B-VII.1 cross sections available with SCALE 6.2 indicate reduced bias in other comparisons to measurement [7]. Here, the calculation uncertainty in ^{238}Pu is 16%, with an effective measurement uncertainty of 8%, but with a bias of 16%. In Hu et al. [7], a bias of 29% is reported, which indicates that the simplified model used here similarly predicts ^{238}Pu. However, the same study found a bias of only 1.5% for a different, similar sample P that was measured at a different laboratory. This indicates that there may be a systematic measurement error in samples S1 and S2.

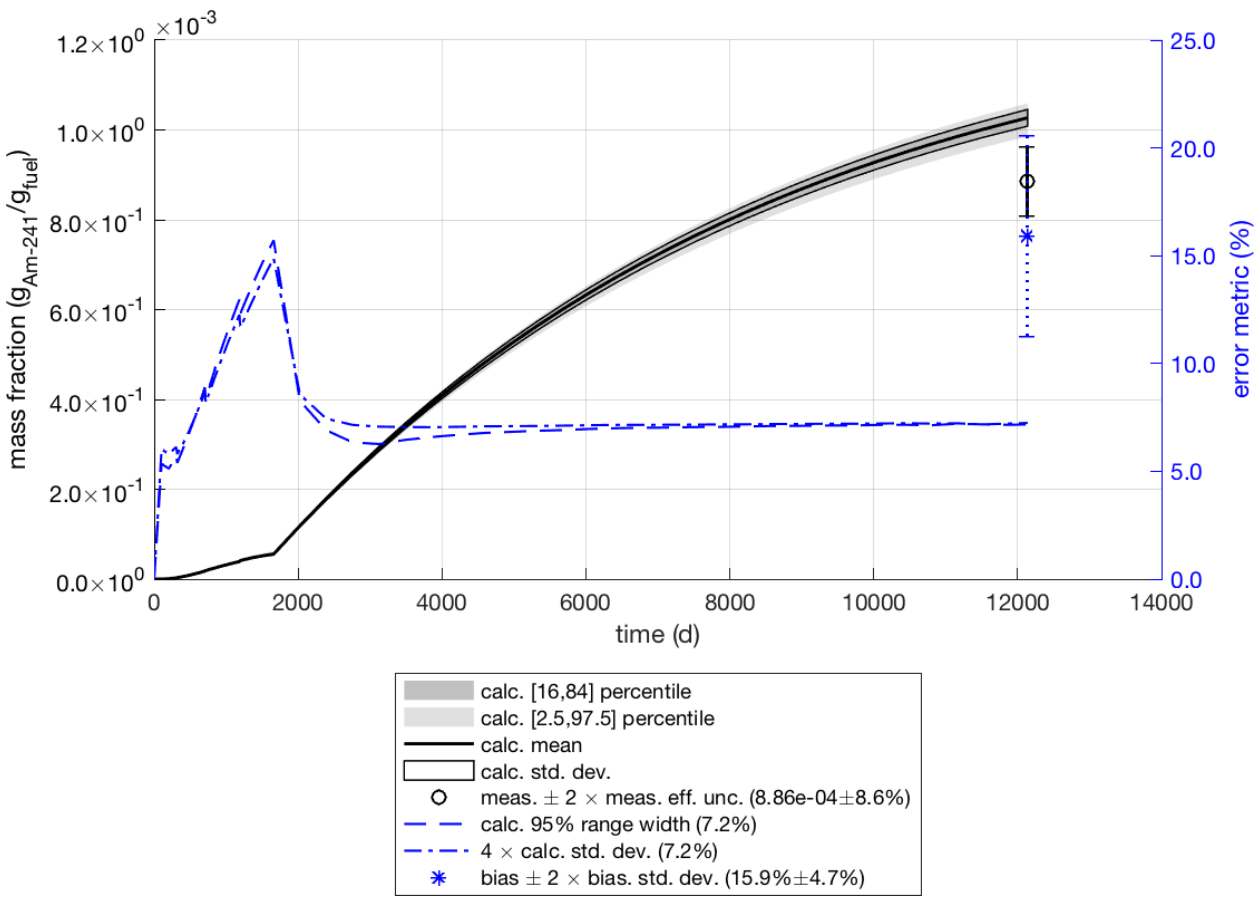

Figure 3-14 ^{241}Am Isotopic Uncertainty

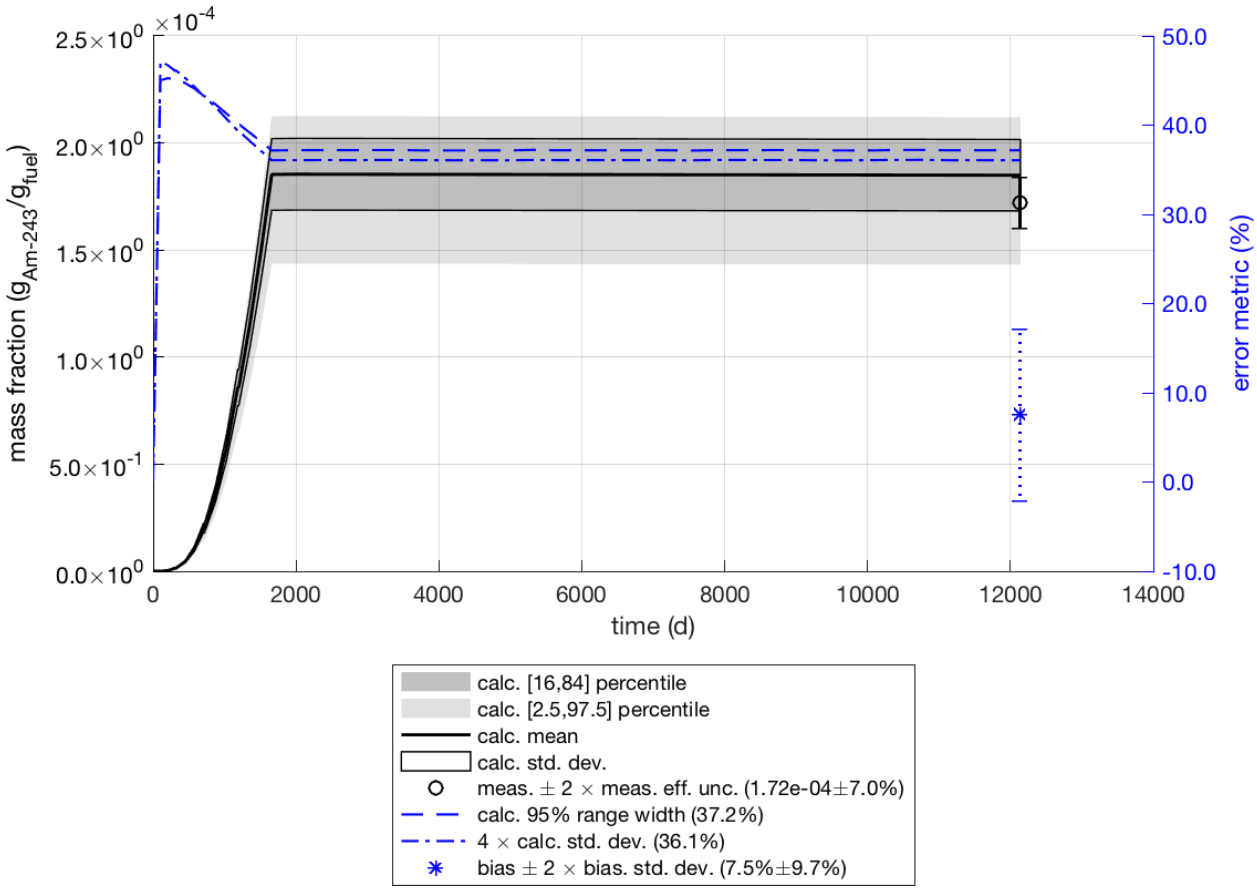

Figure 3-15 ^{243}Am Isotopic Uncertainty

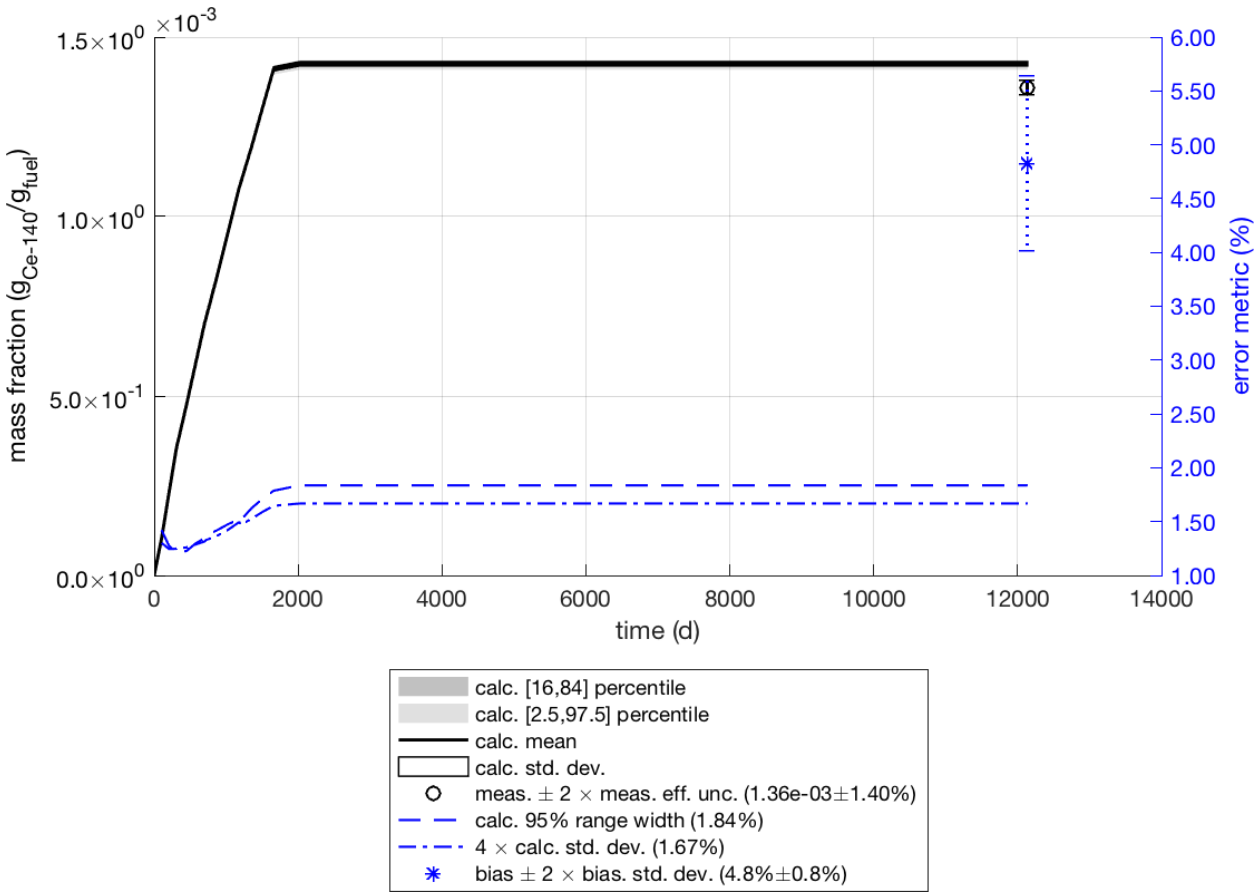

Figure 3-16 ^{140}Ce Isotopic Uncertainty

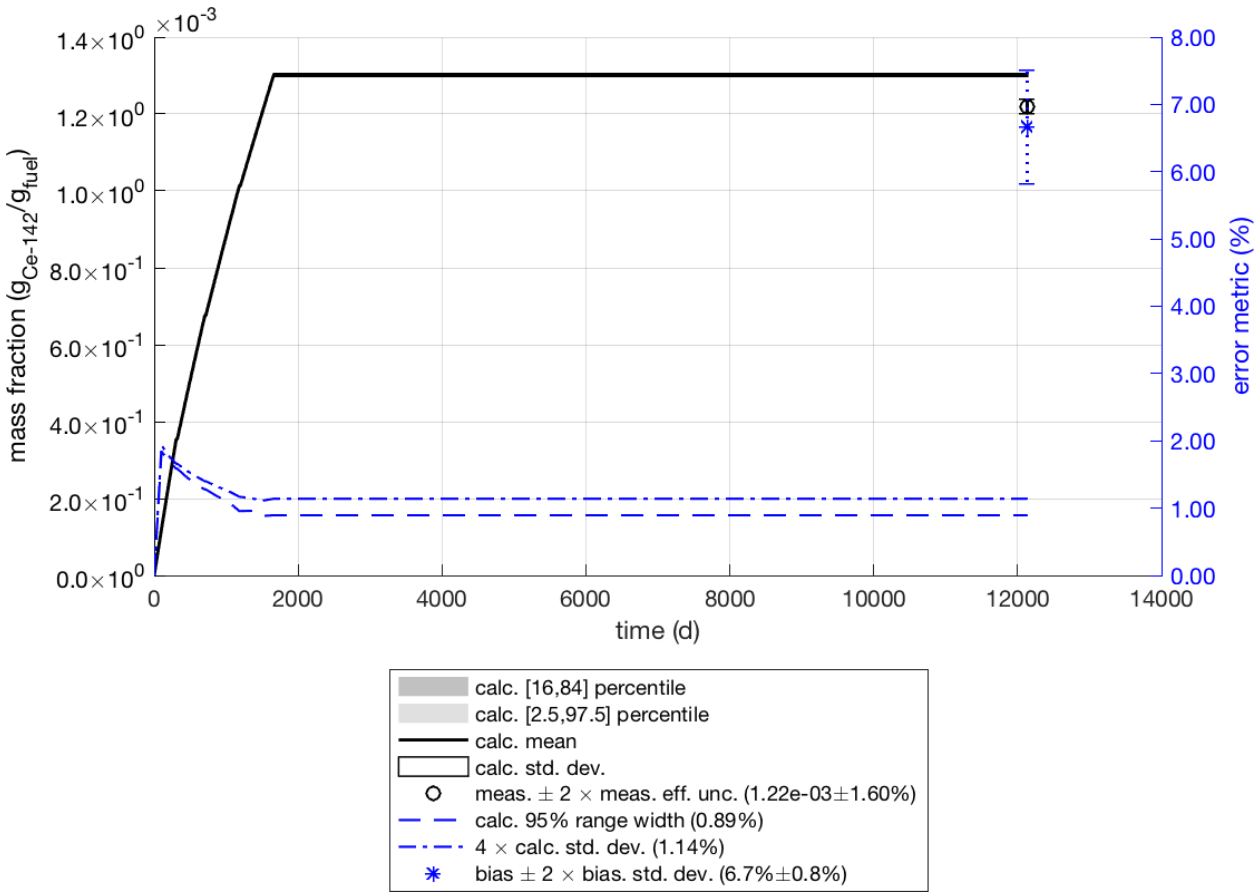

Figure 3-17 ^{142}Ce Isotopic Uncertainty

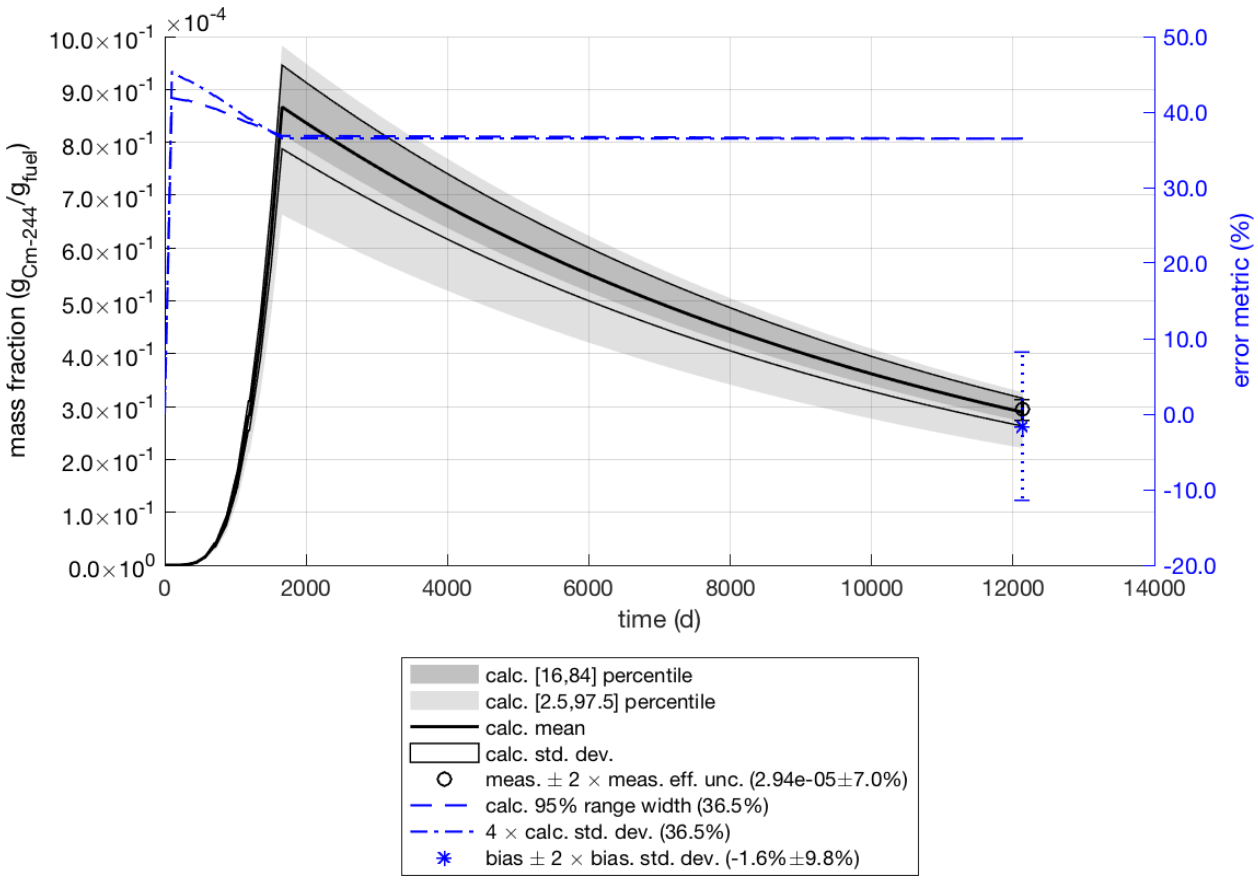

Figure 3-18 ^{244}Cm Isotopic Uncertainty

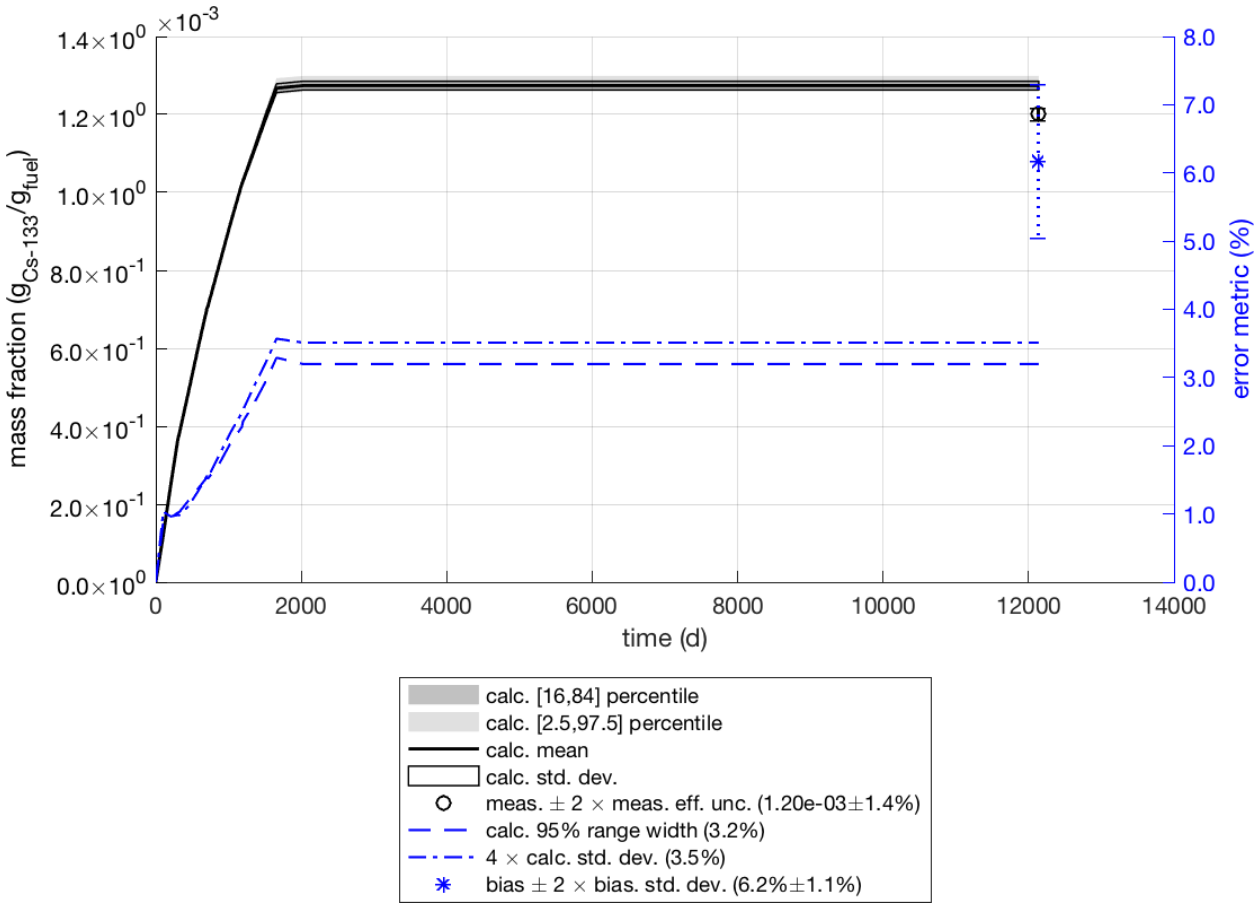

Figure 3-19 ^{133}Cs Isotopic Uncertainty

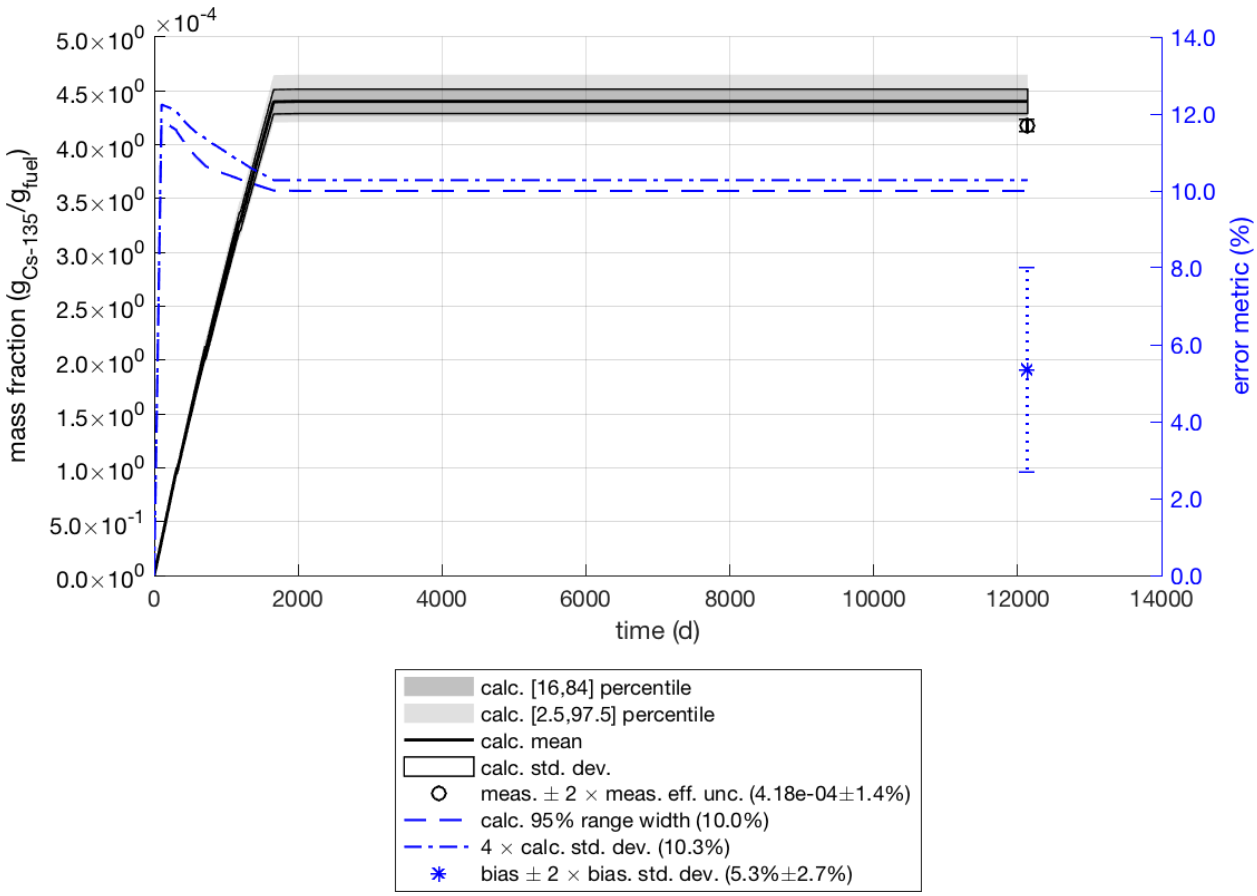

Figure 3-20 ^{135}Cs Isotopic Uncertainty

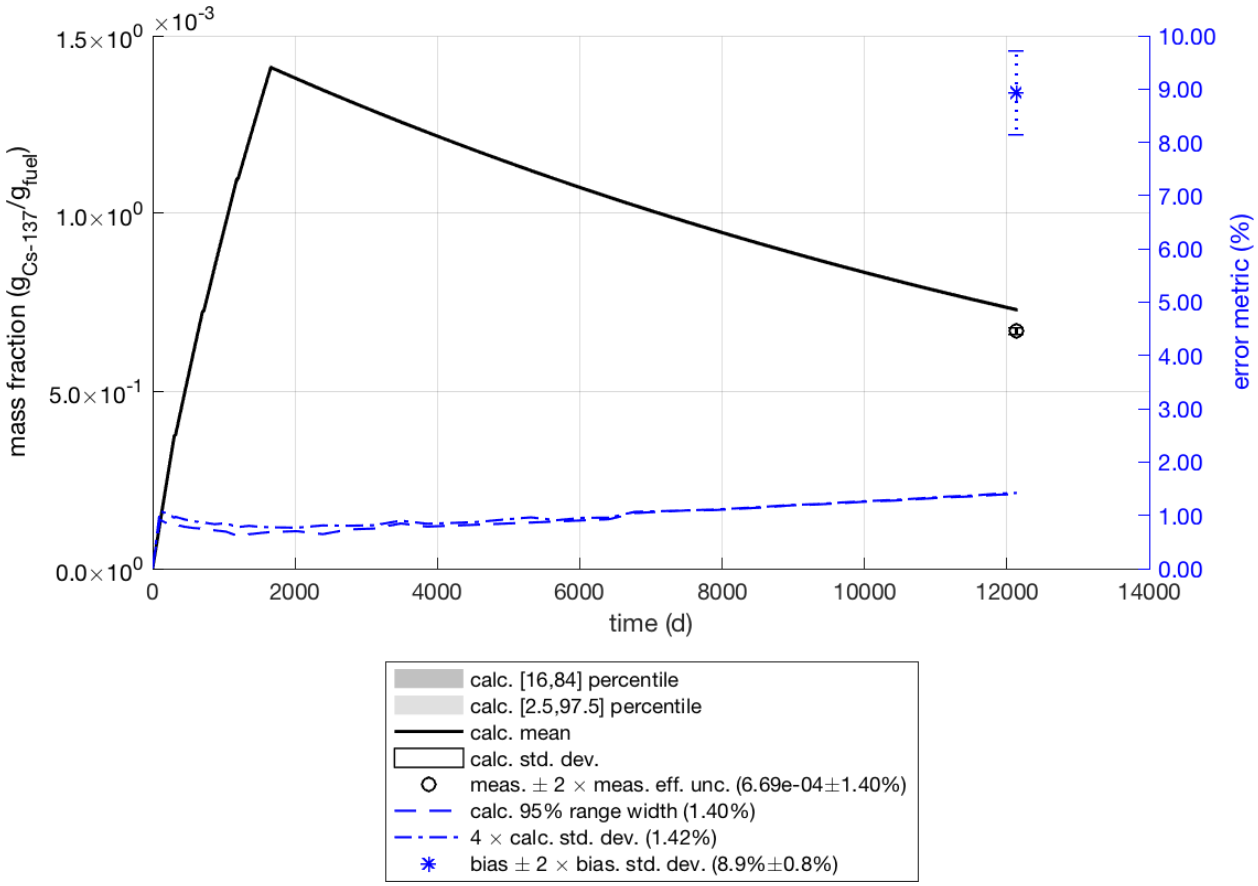

Figure 3-21 ^{137}Cs Isotopic Uncertainty

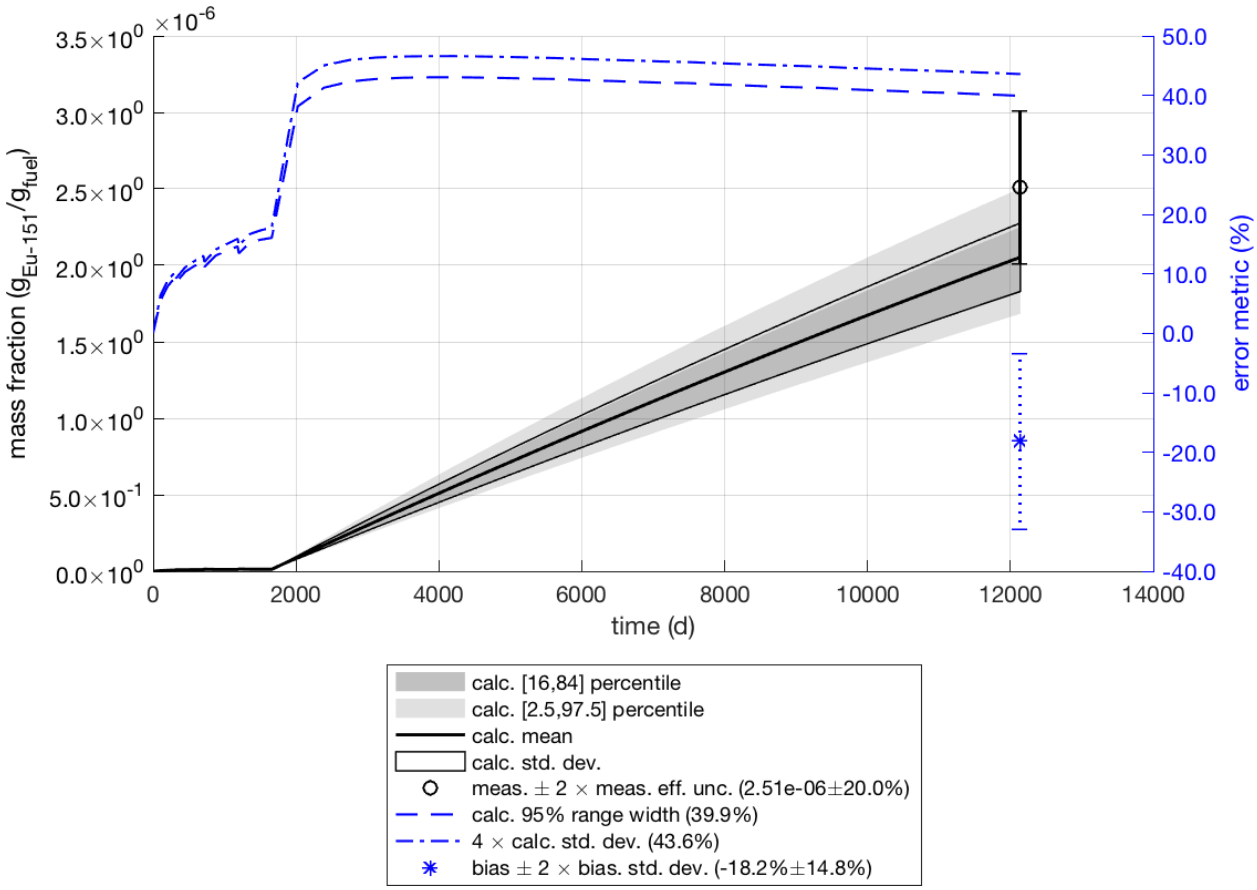

Figure 3-22 ^{151}Eu Isotopic Uncertainty

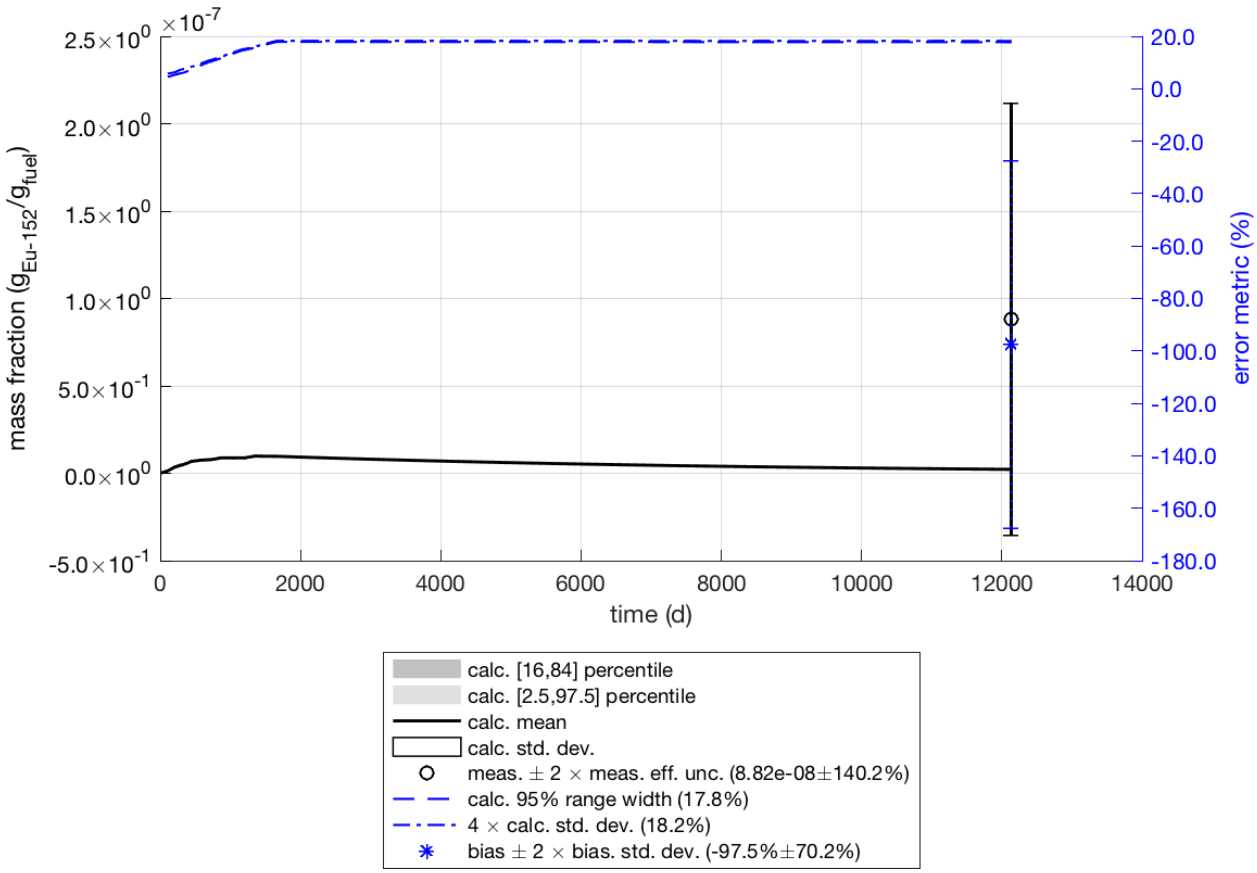

Figure 3-23 ^{152}Eu Isotopic Uncertainty

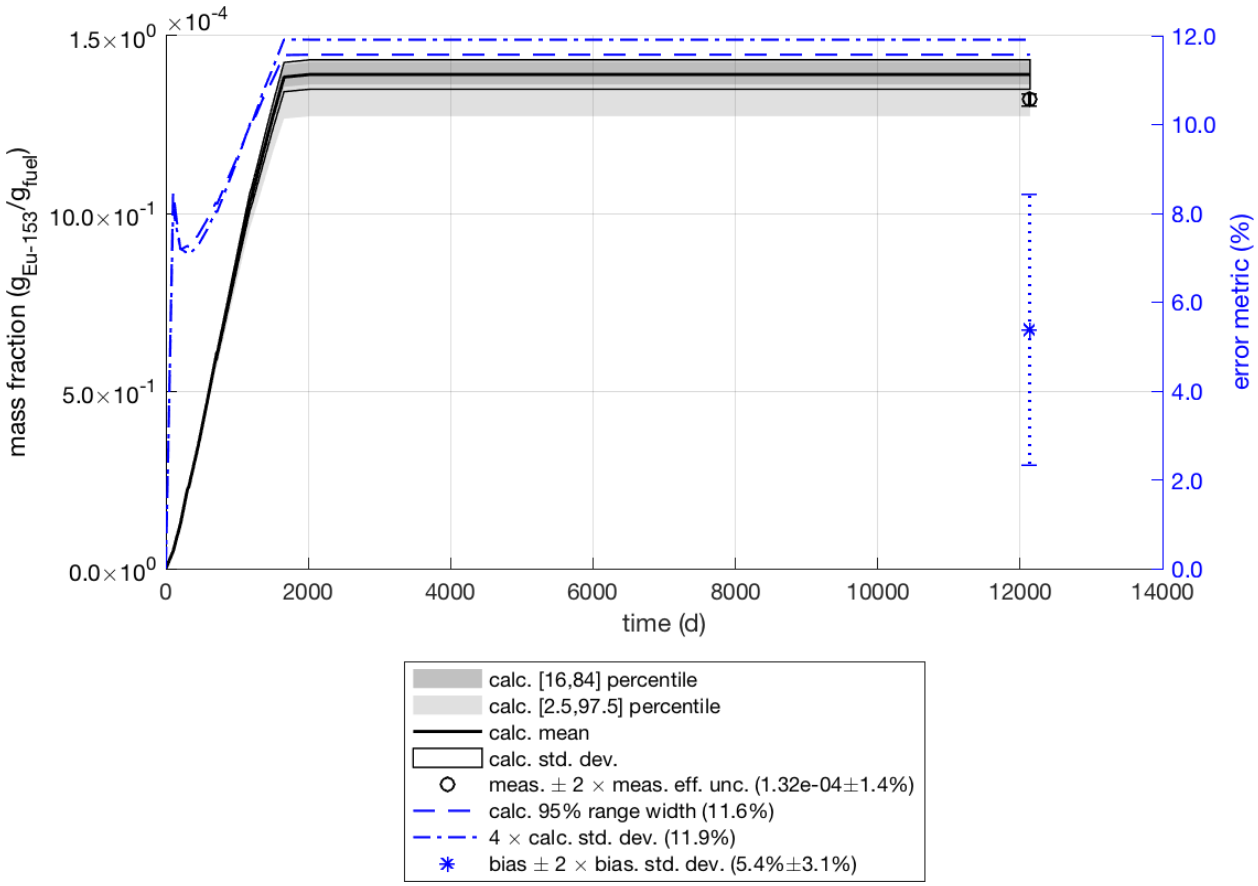

Figure 3-24 ^{153}Eu Isotopic Uncertainty

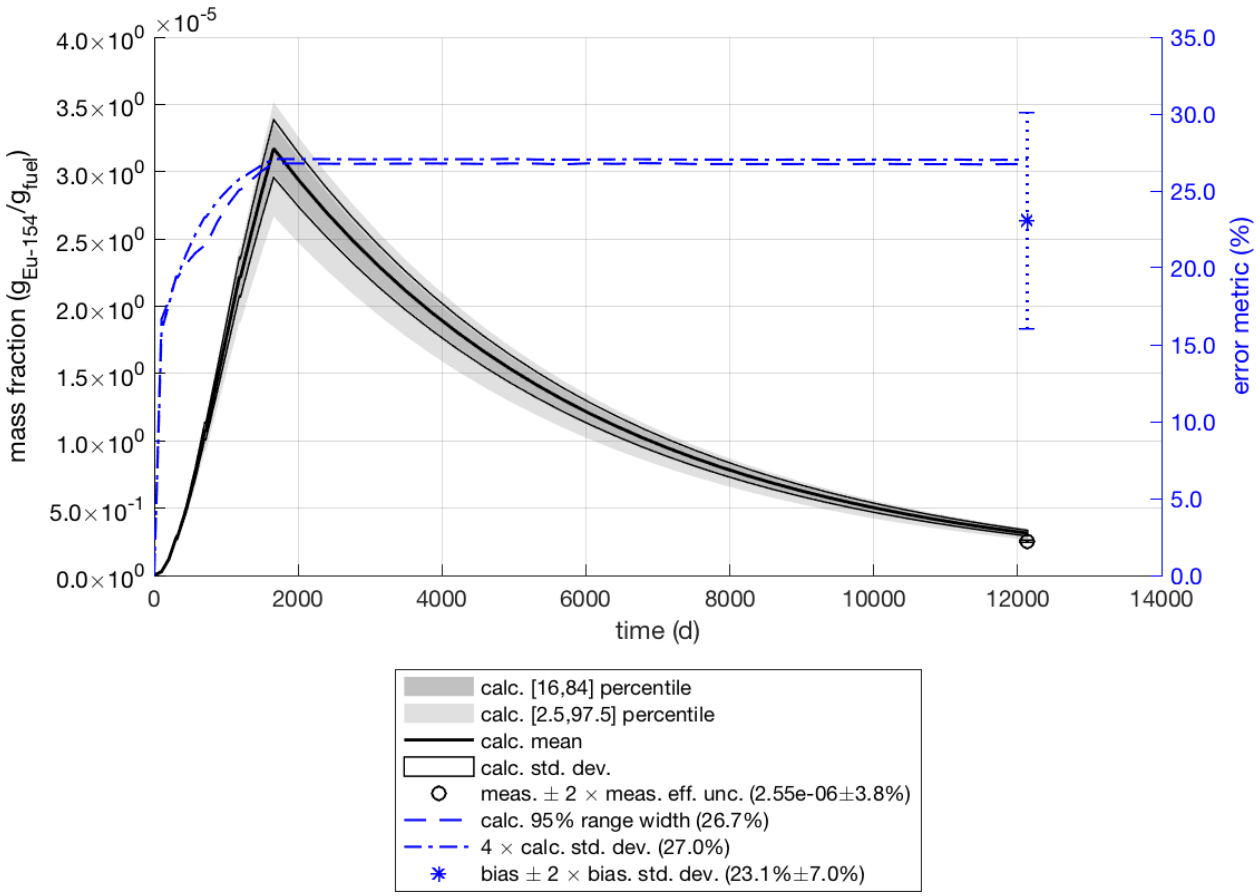

Figure 3-25 ^{154}Eu Isotopic Uncertainty

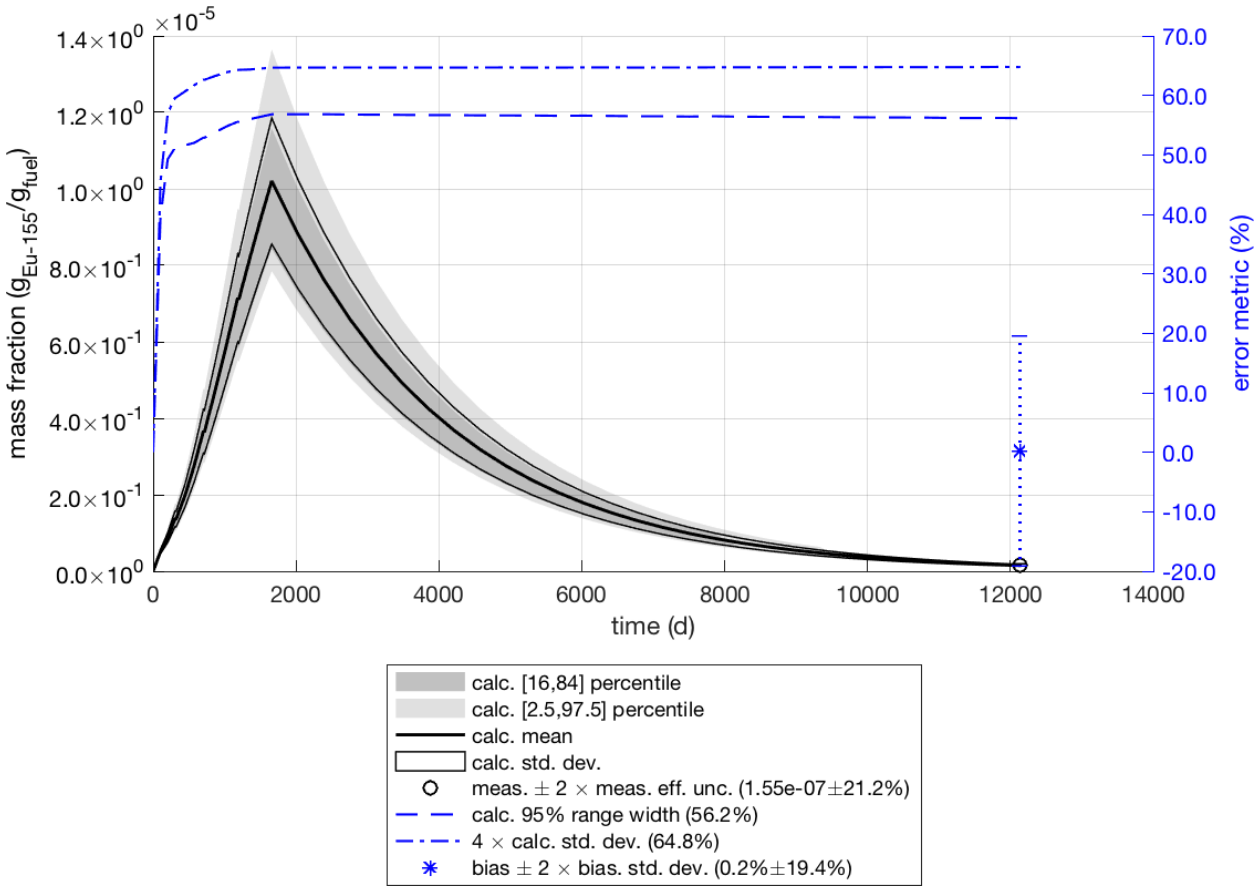

Figure 3-26 ^{155}Eu Isotopic Uncertainty

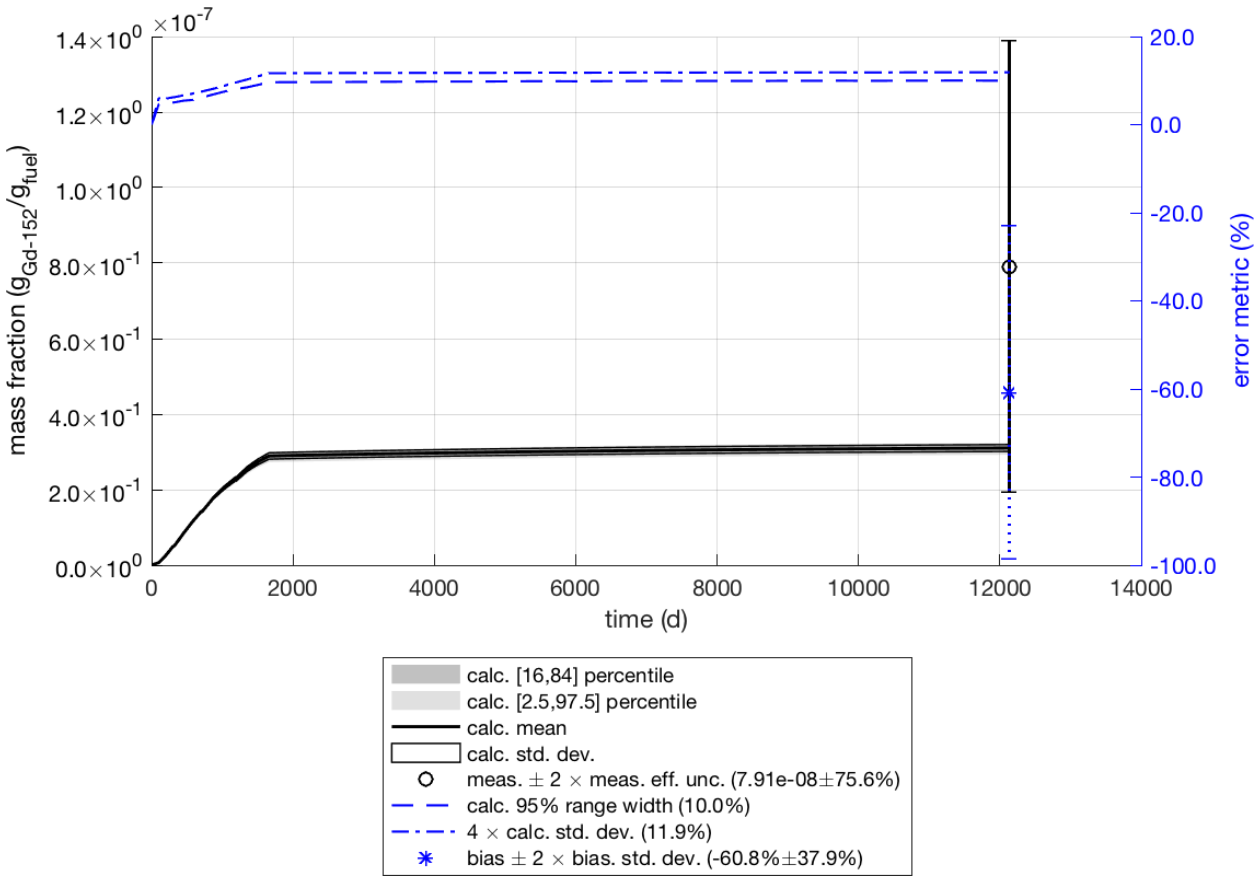

Figure 3-27 ^{152}Gd Isotopics Uncertainty

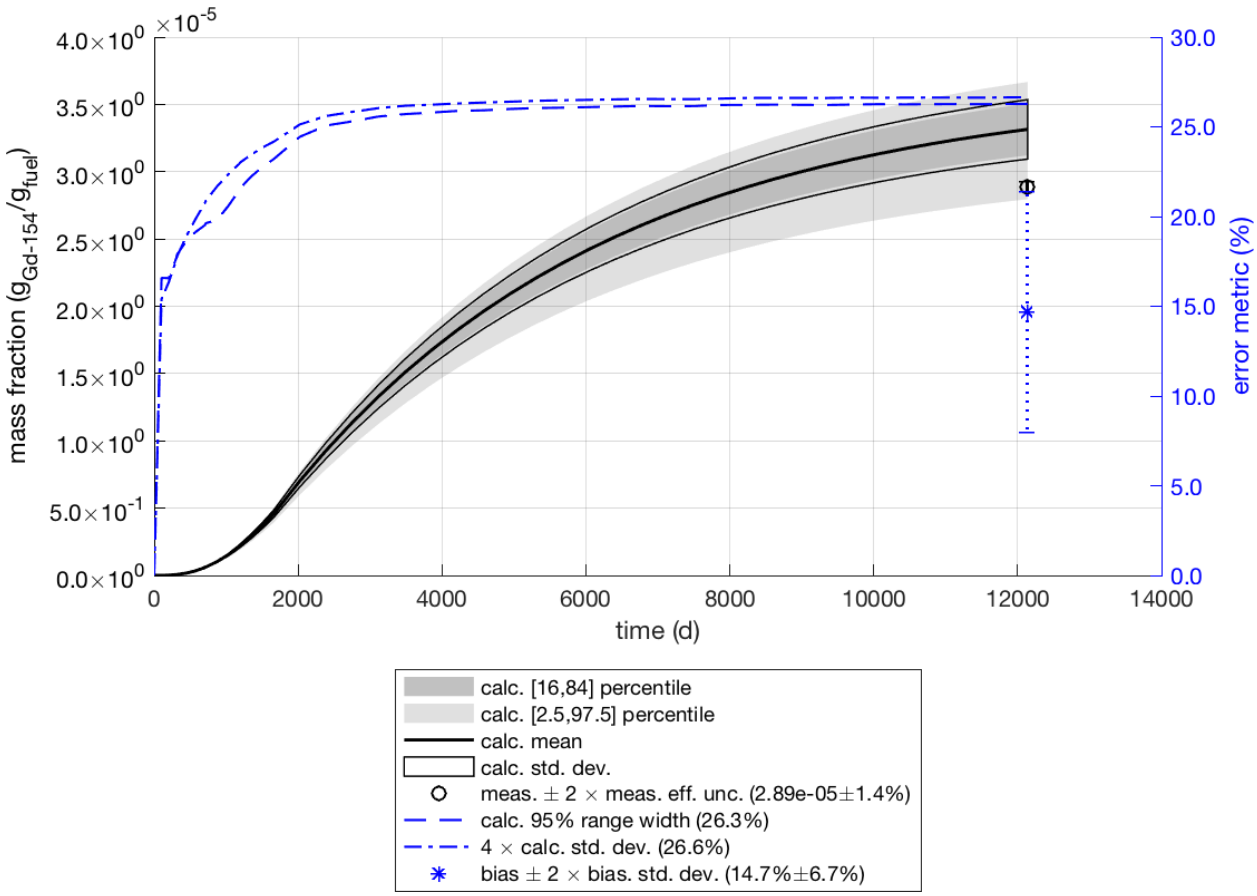

Figure 3-28 ^{154}Gd Isotopic Uncertainty

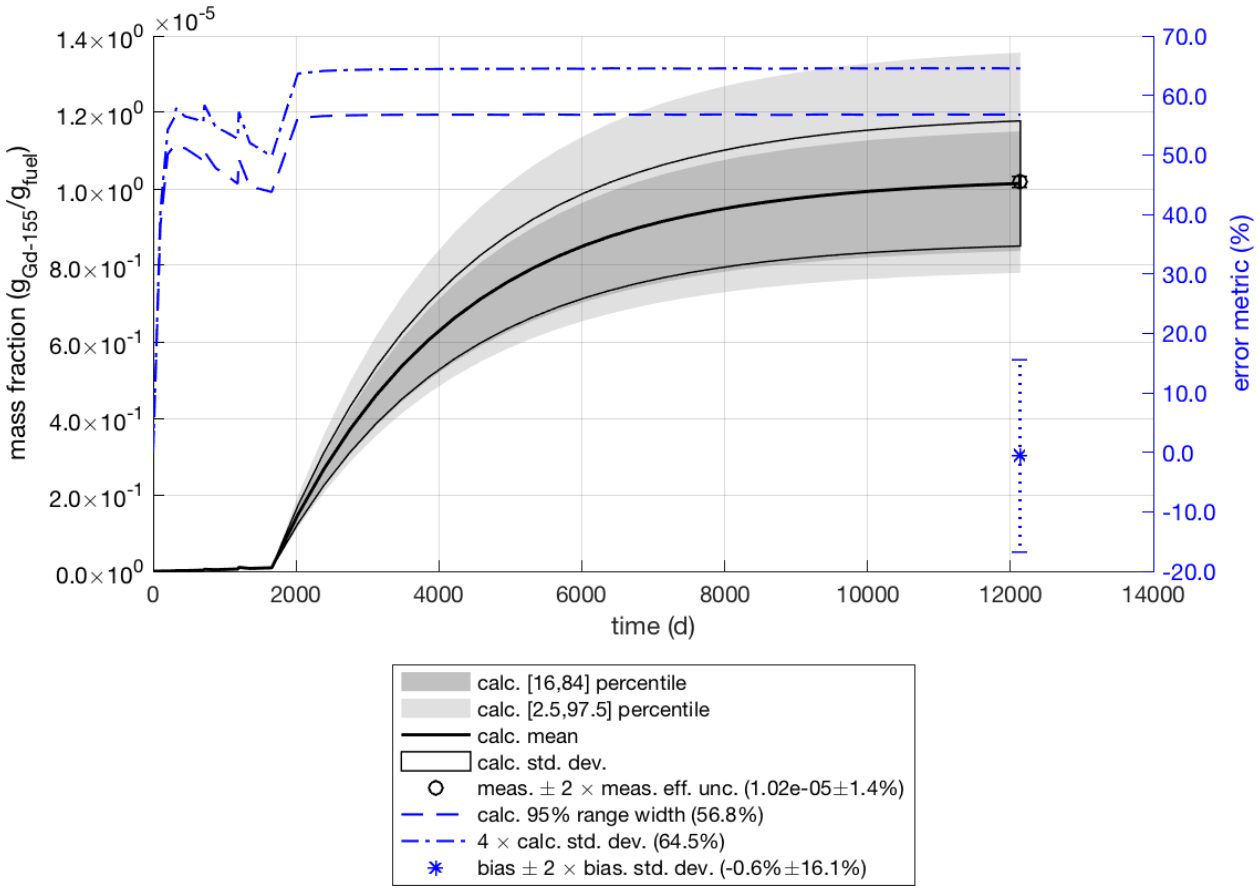

Figure 3-29 ^{155}Gd Isotopic Uncertainty

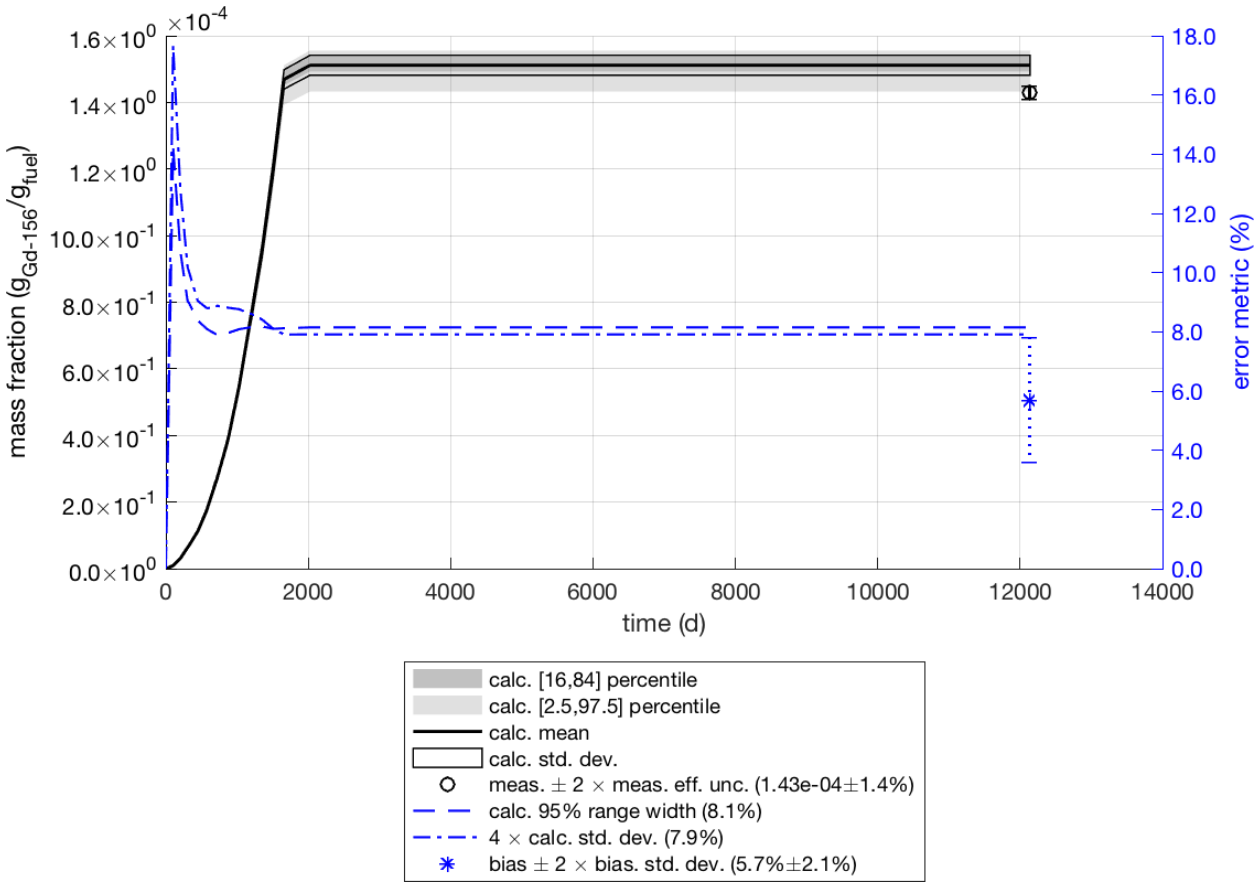

Figure 3-30 ^{156}Gd Isotopic Uncertainty

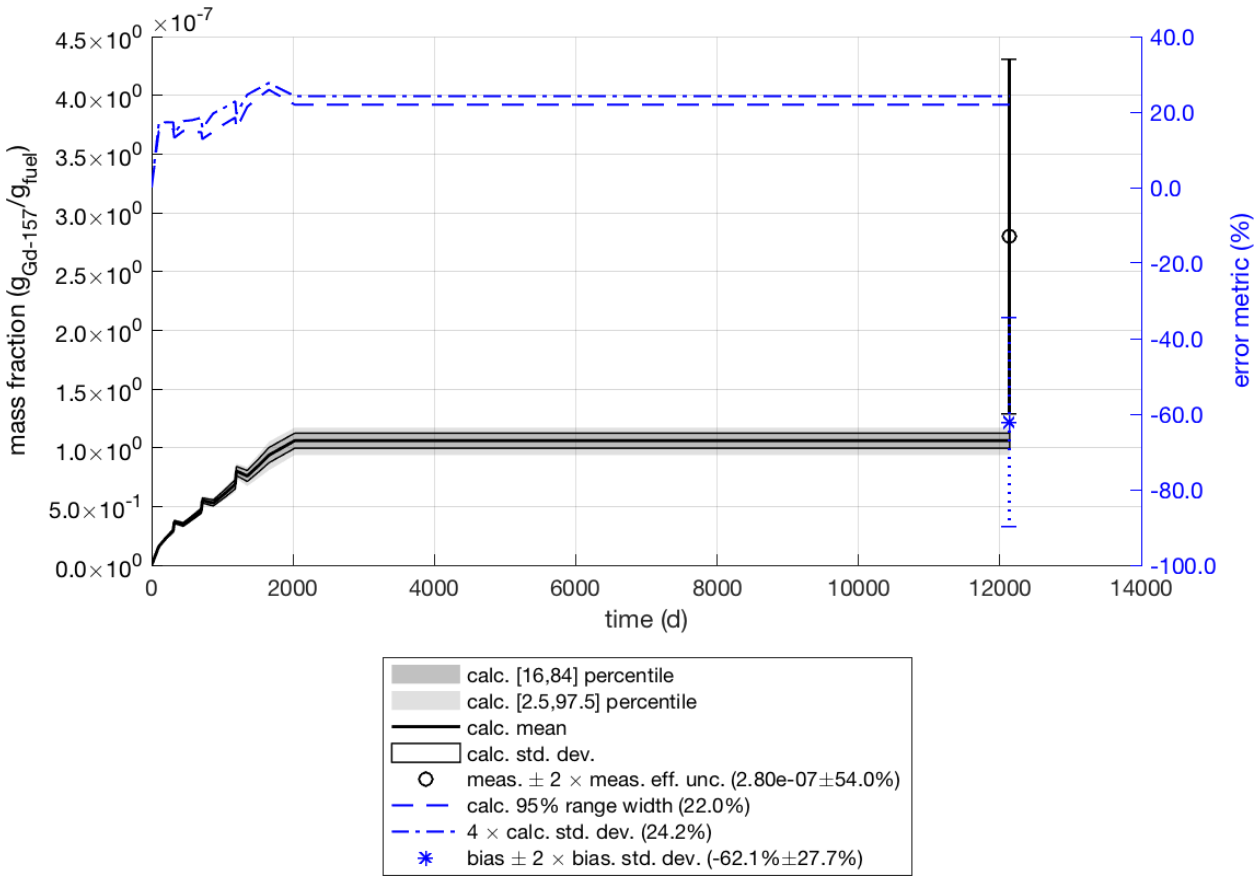

Figure 3-31 ^{157}Gd Isotopic Uncertainty

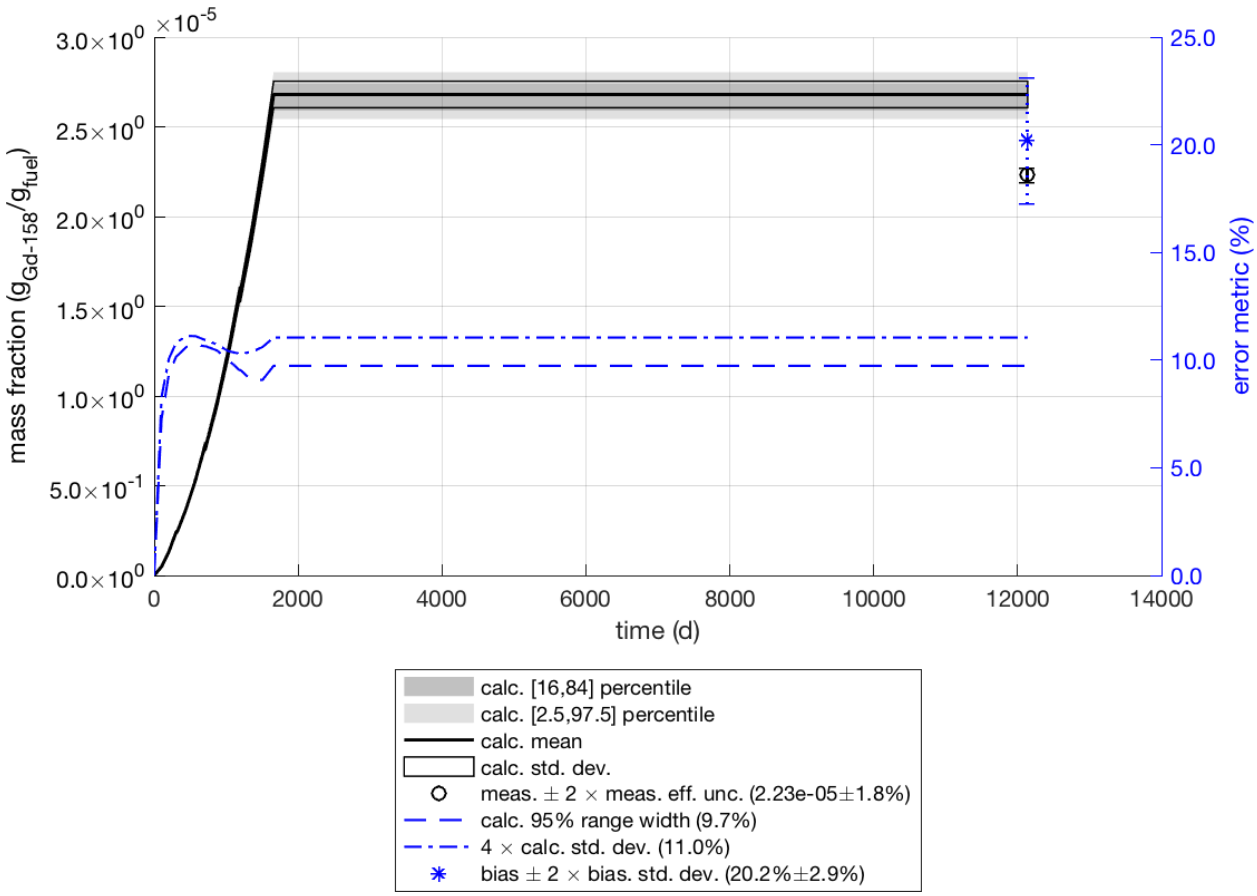

Figure 3-32 ^{158}Gd Isotopic Uncertainty

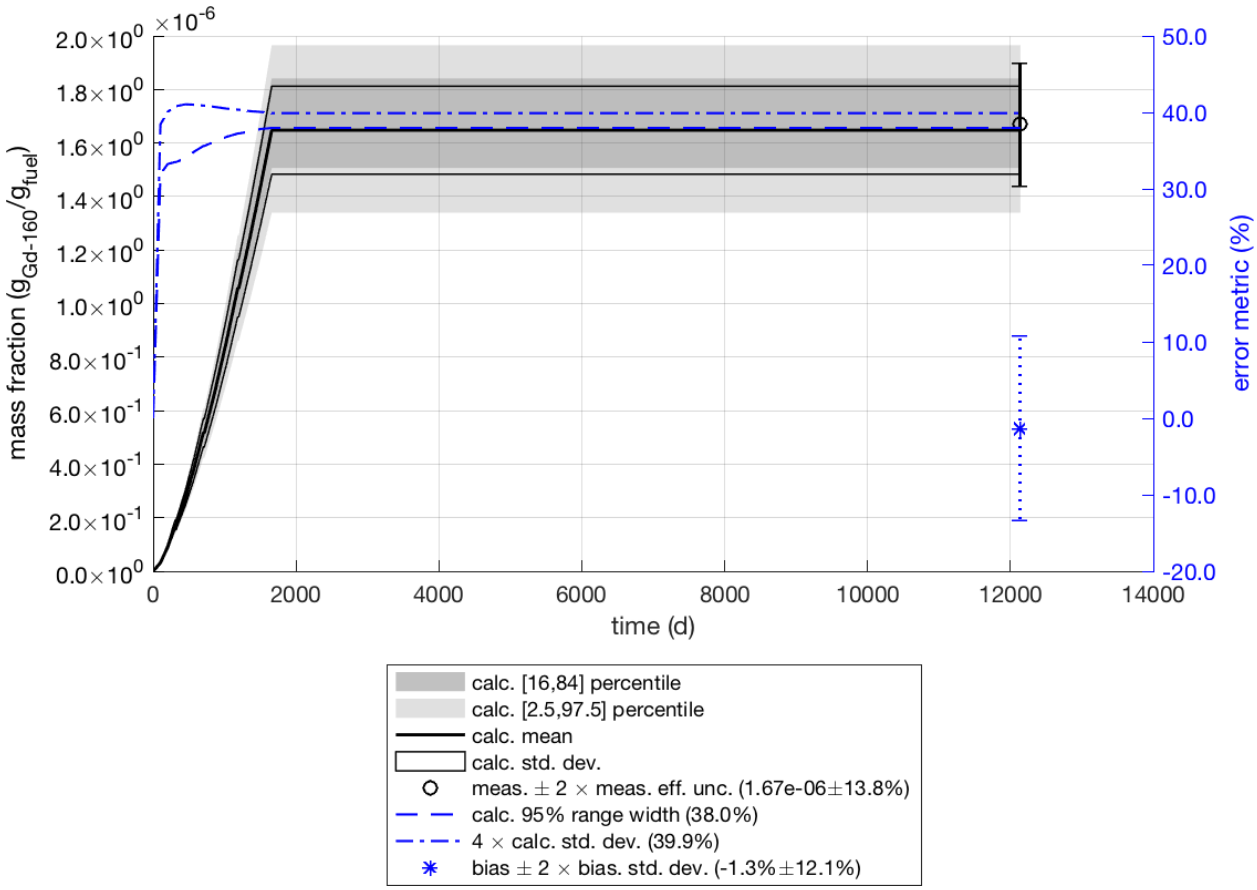

Figure 3-33 ^{160}Gd Isotopic Uncertainty

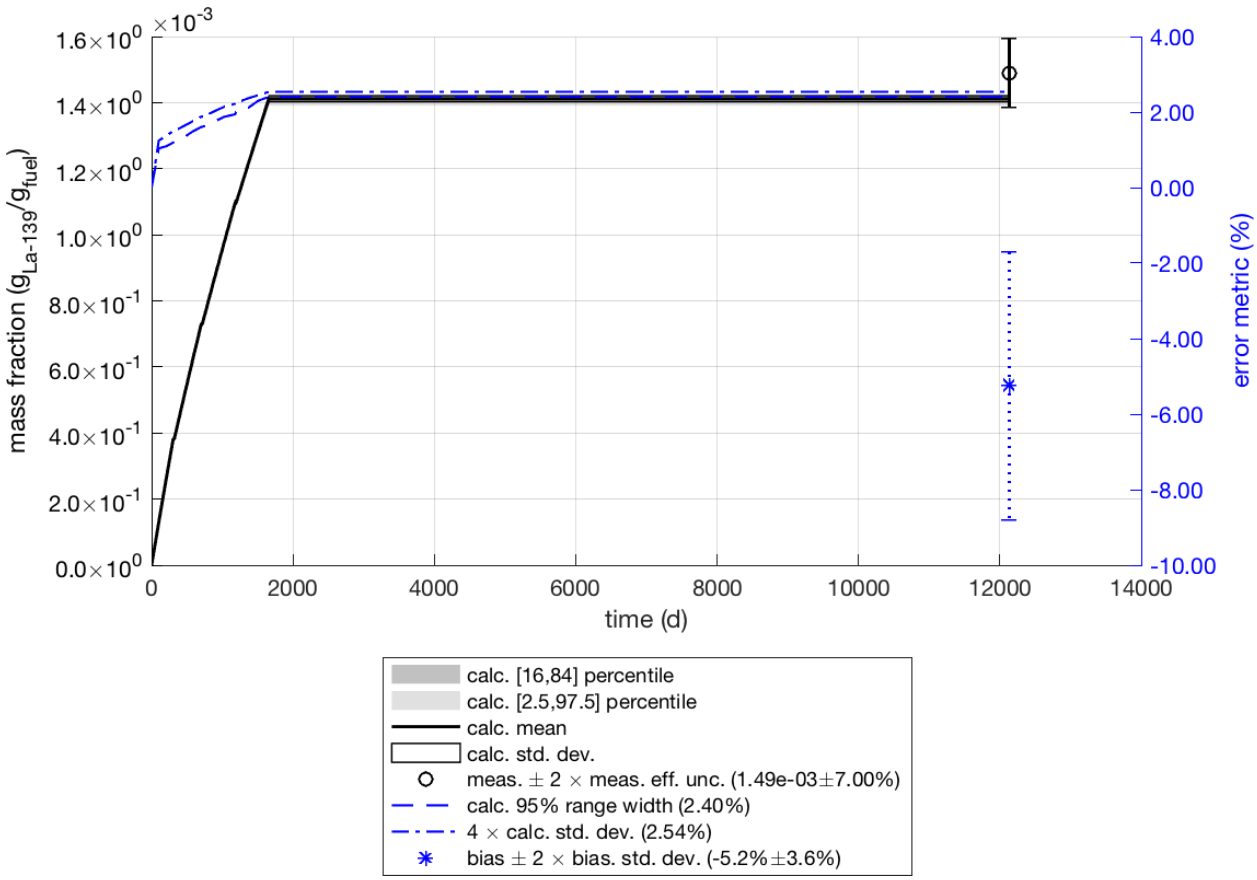

Figure 3-34 ^{139}La Isotopic Uncertainty

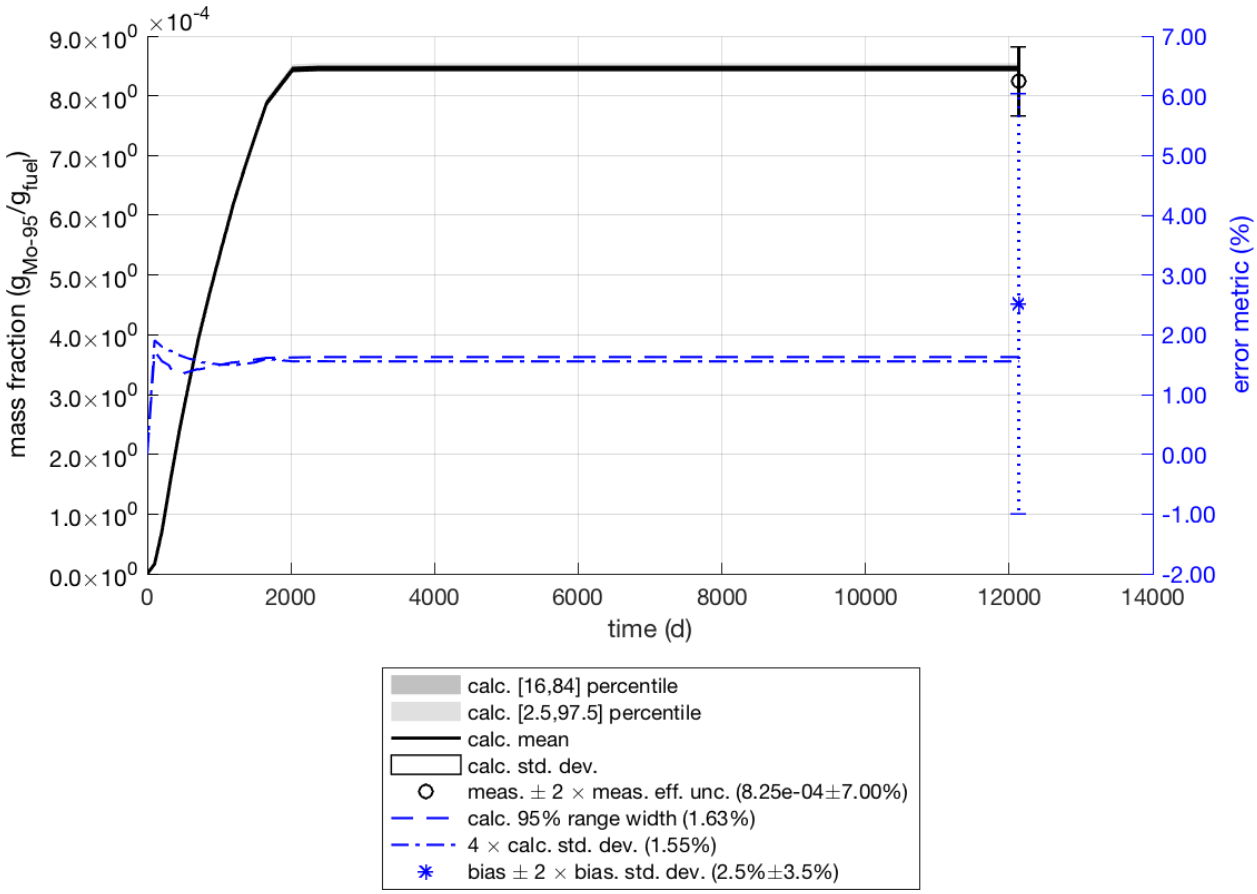

Figure 3-35 ^{95}Mo Isotopic Uncertainty

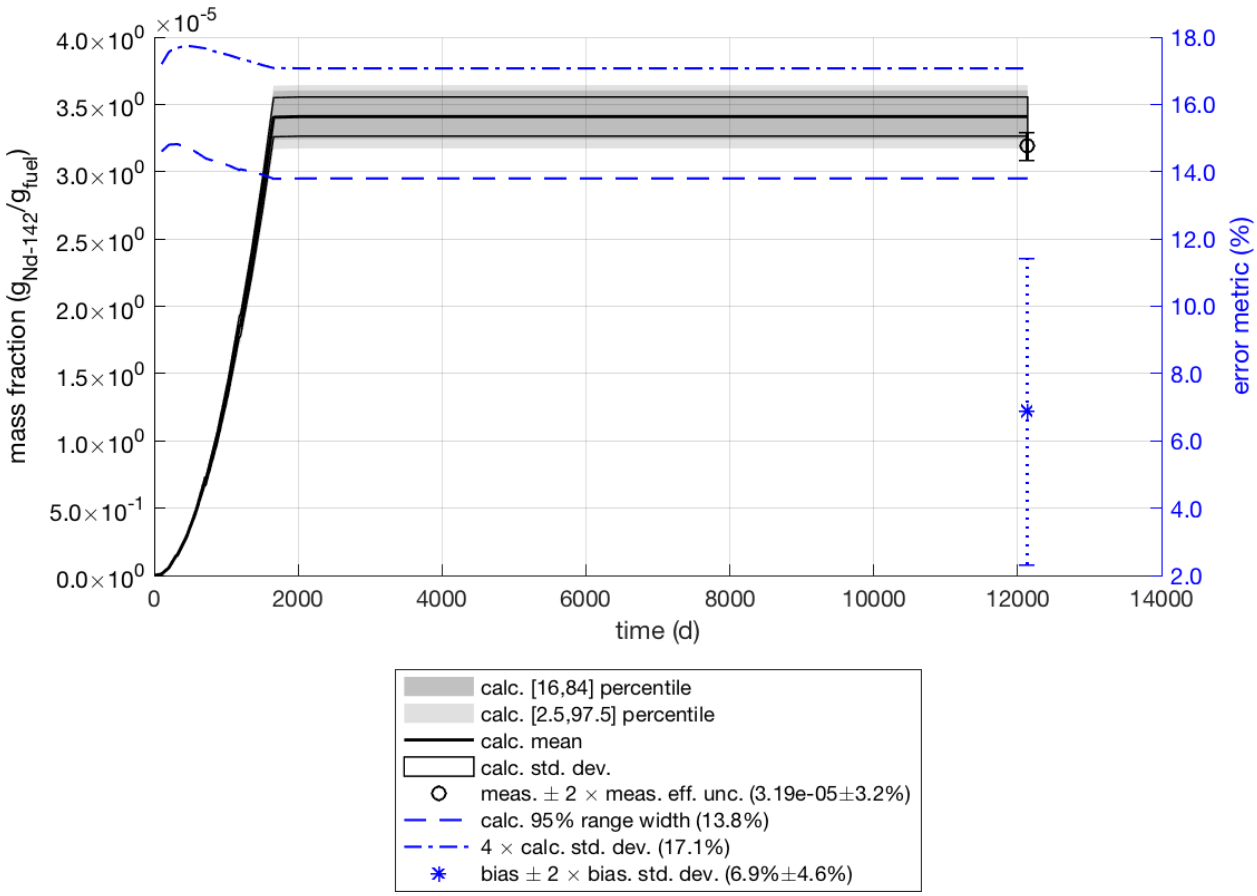

Figure 3-36 ^{142}Nd Isotopic Uncertainty

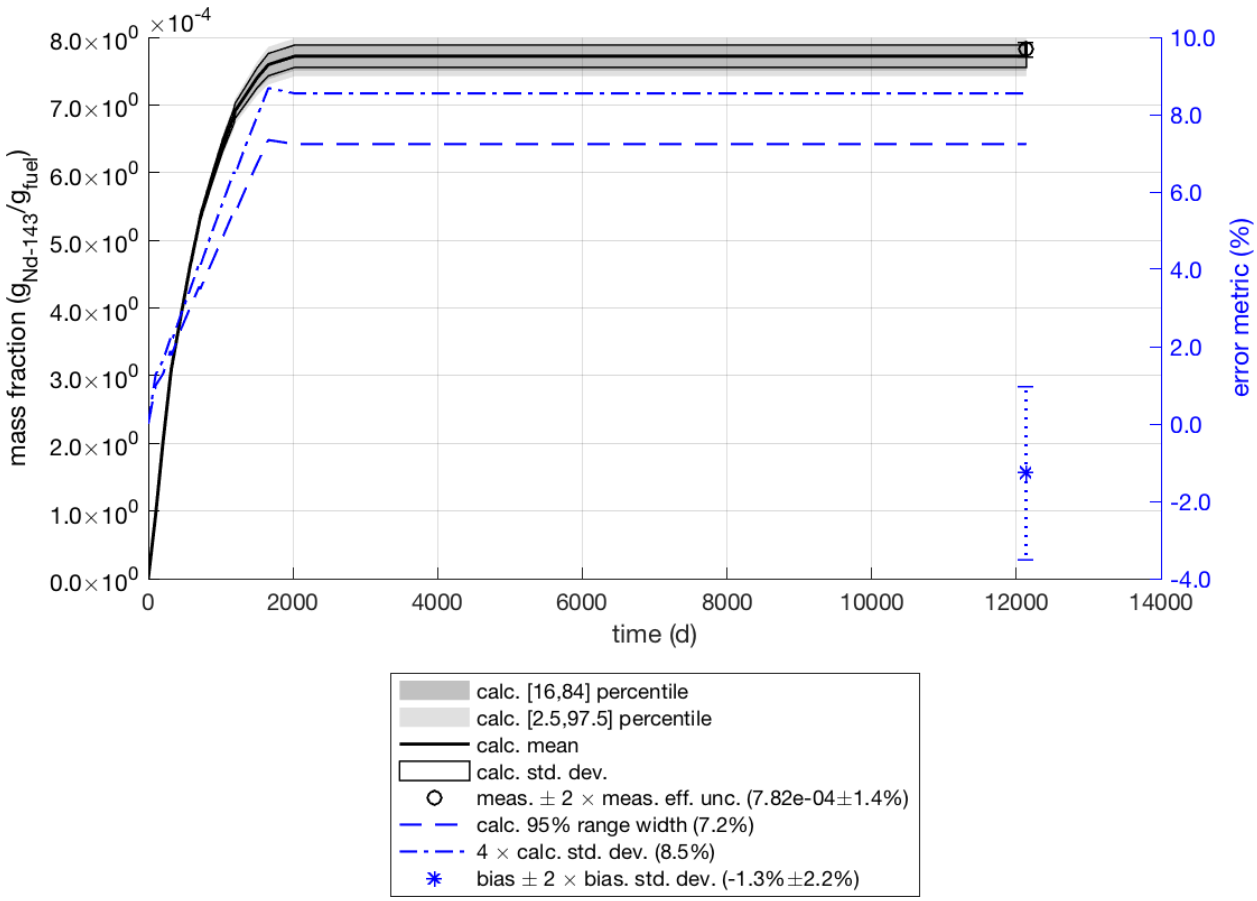

Figure 3-37 ^{143}Nd Isotopic Uncertainty

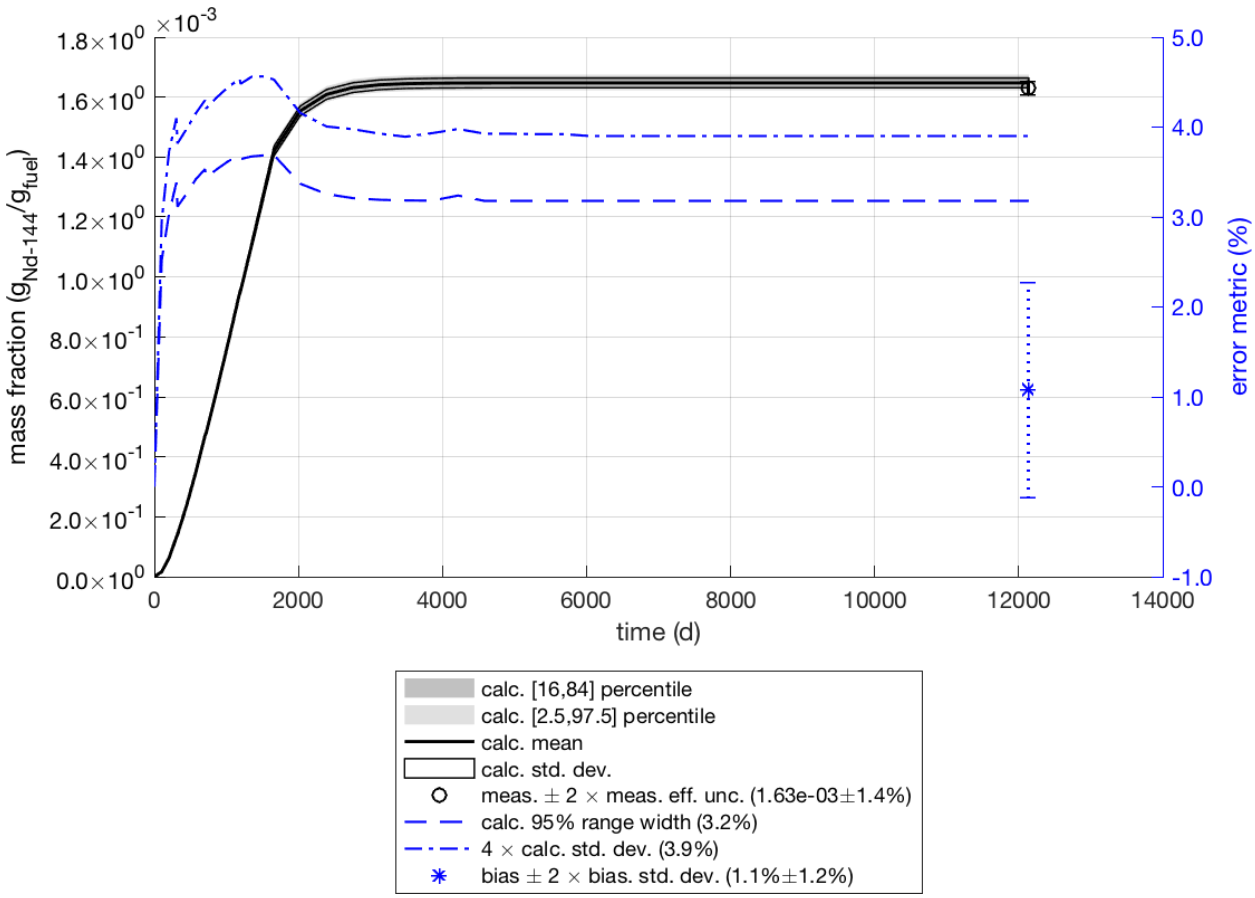

Figure 3-38 ^{144}Nd Isotopic Uncertainty

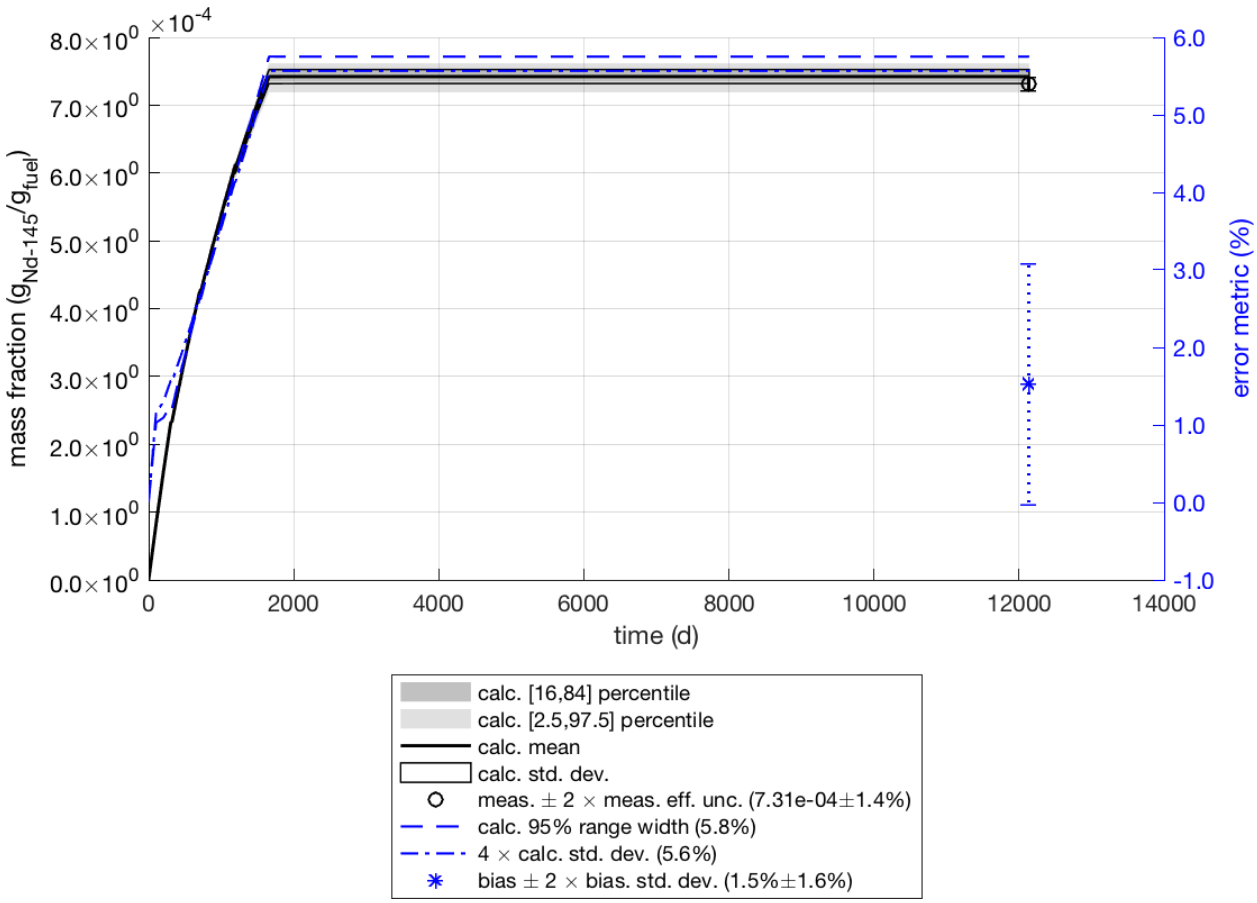

Figure 3-39 ^{145}Nd Isotopic Uncertainty

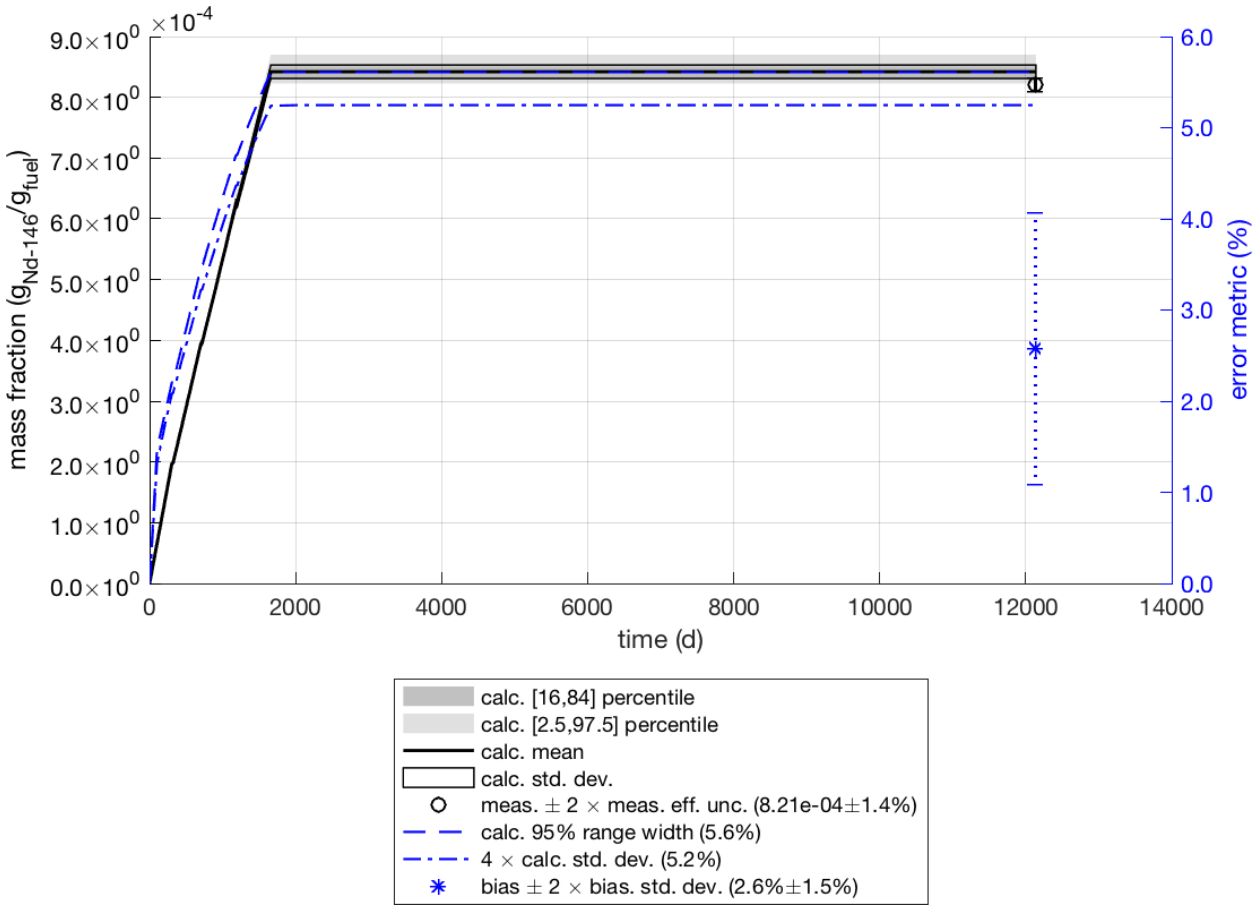

Figure 3-40 ^{146}Nd Isotopic Uncertainty

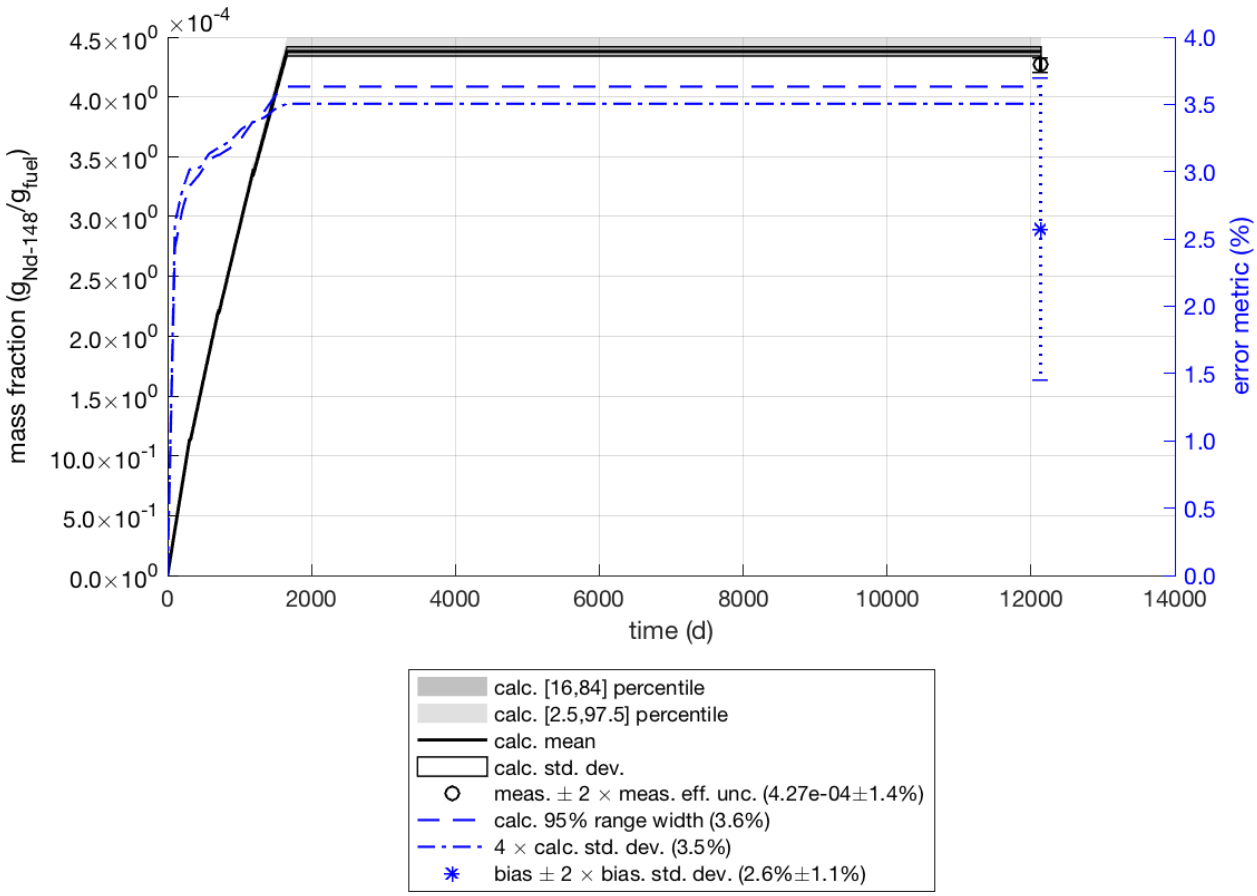

Figure 3-41 ^{148}Nd Isotopic Uncertainty

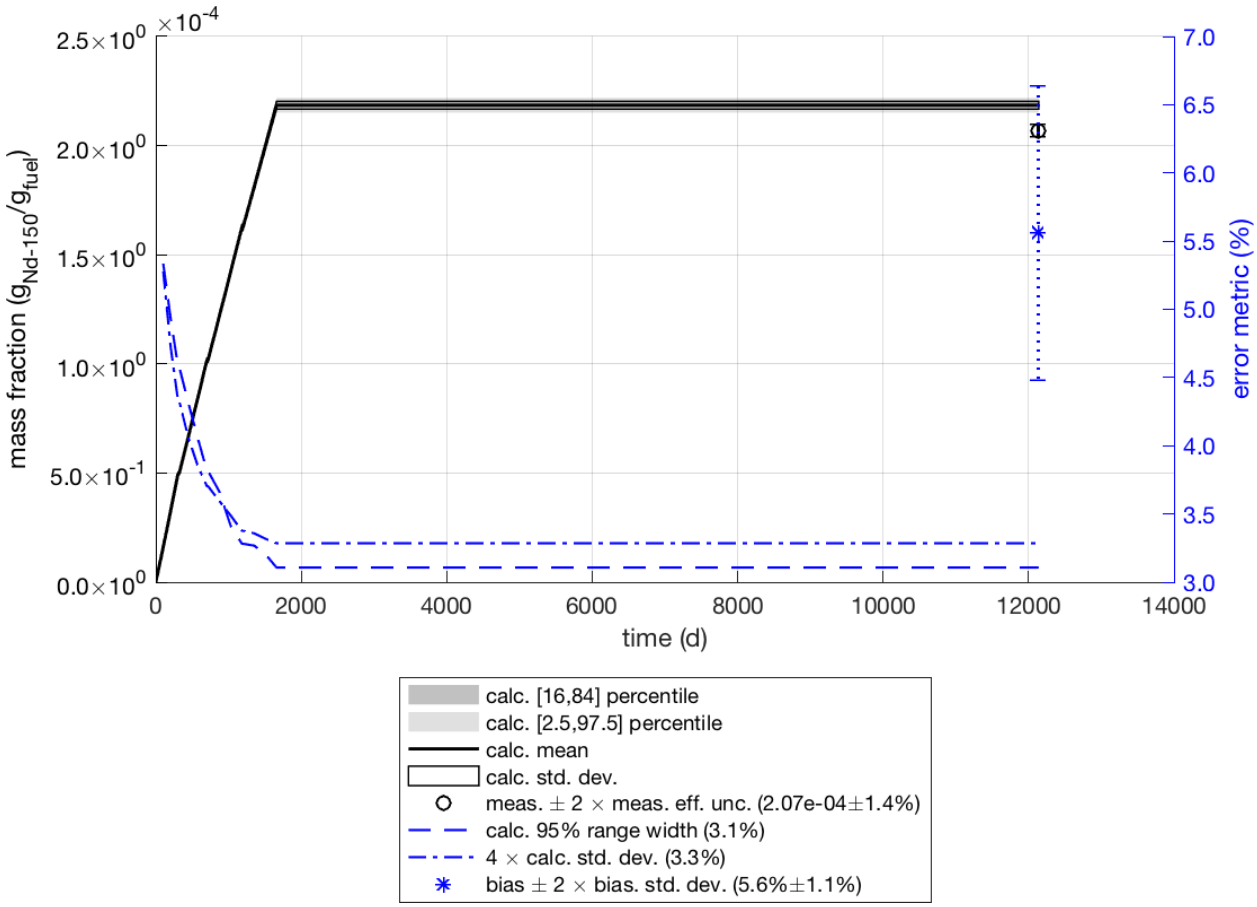

Figure 3-42 ^{150}Nd Isotopic Uncertainty

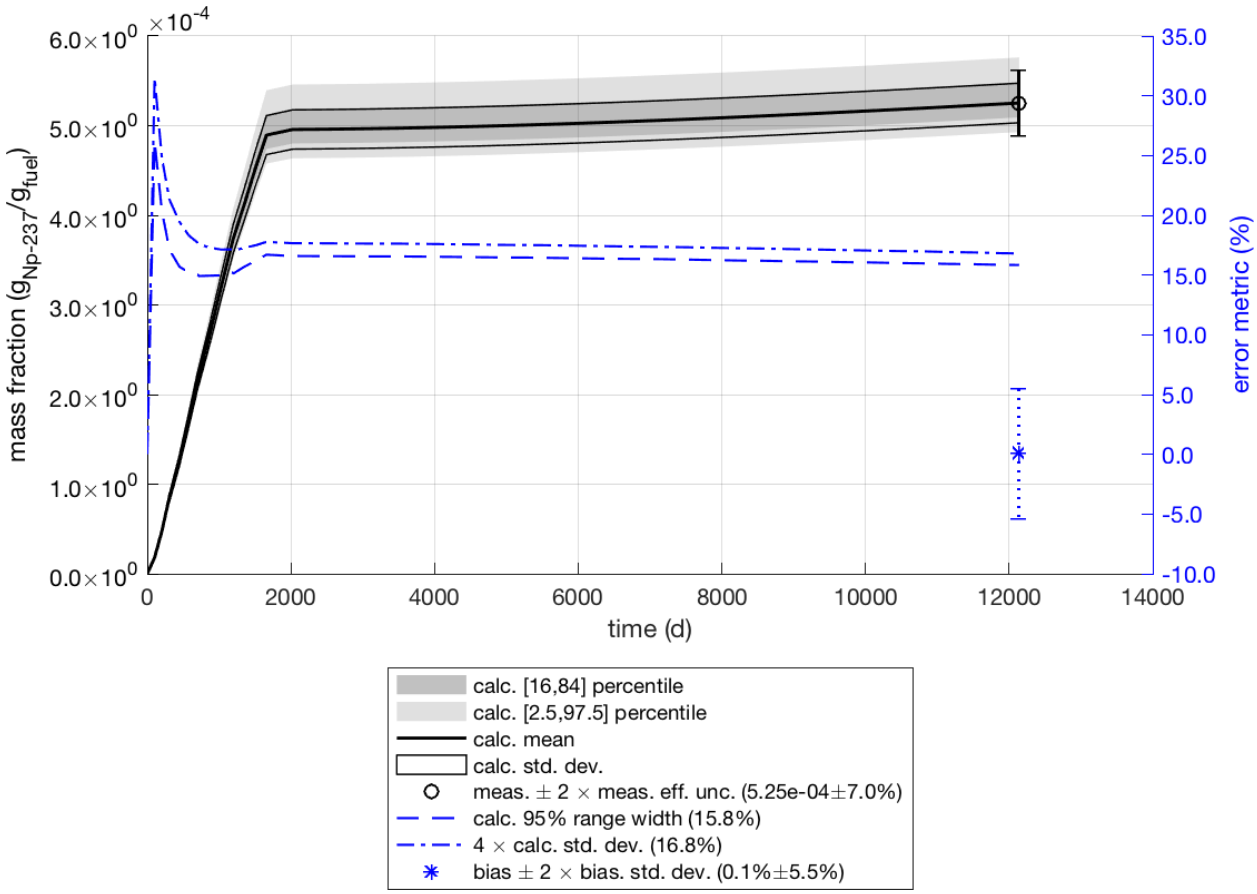

Figure 3-43 ^{237}Np Isotopic Uncertainty

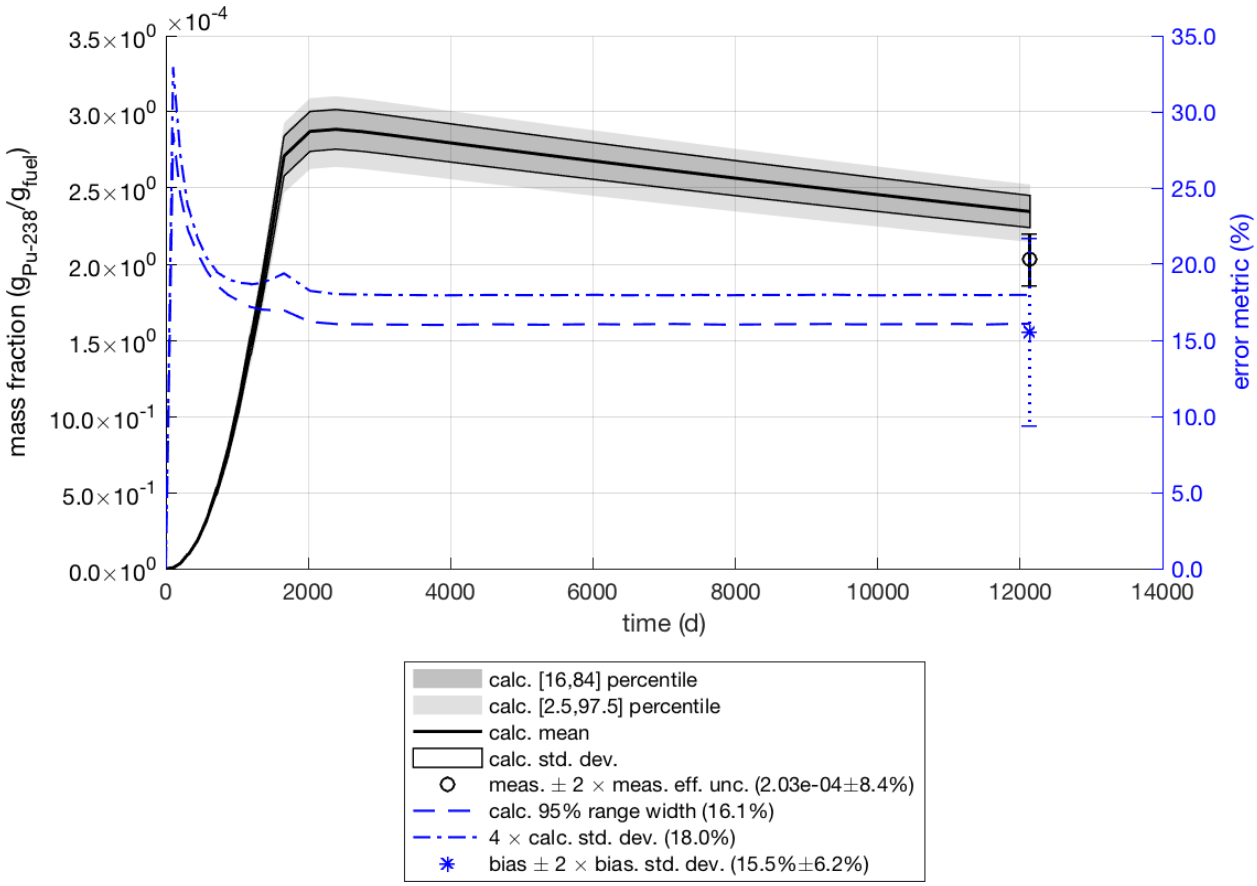

Figure 3-44 ^{238}Pu Isotopic Uncertainty

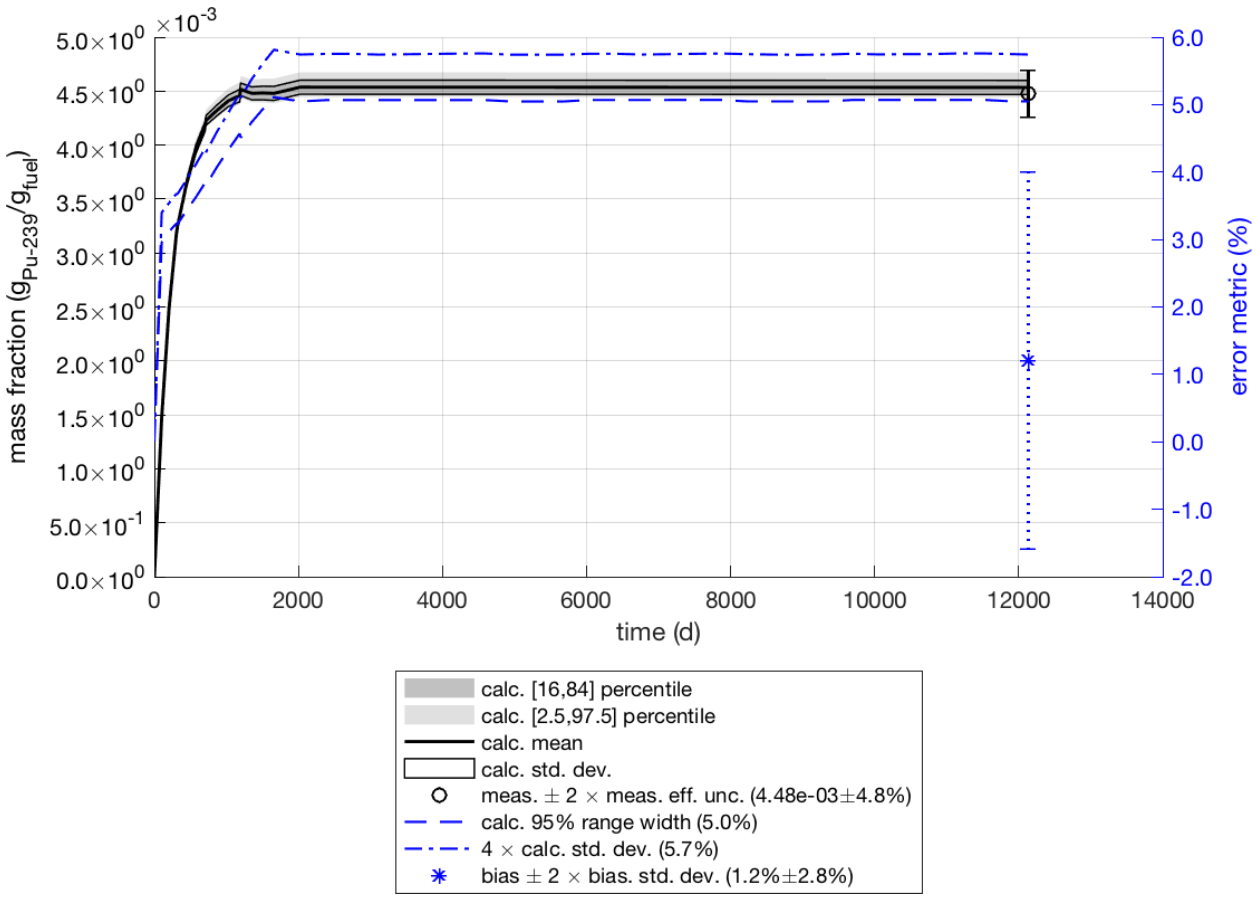

Figure 3-45 ^{239}Pu Isotopic Uncertainty

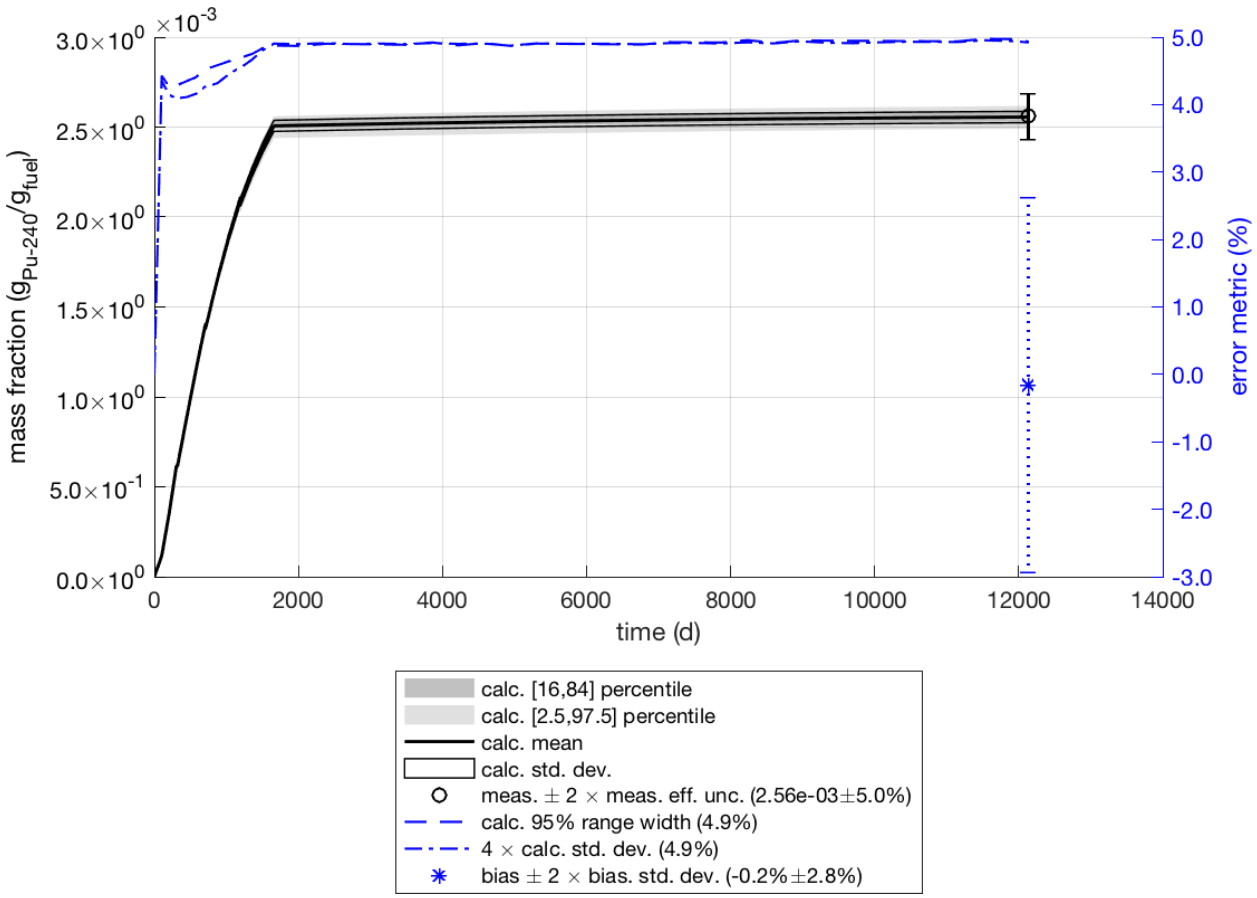

Figure 3-46 ^{240}Pu Isotopic Uncertainty

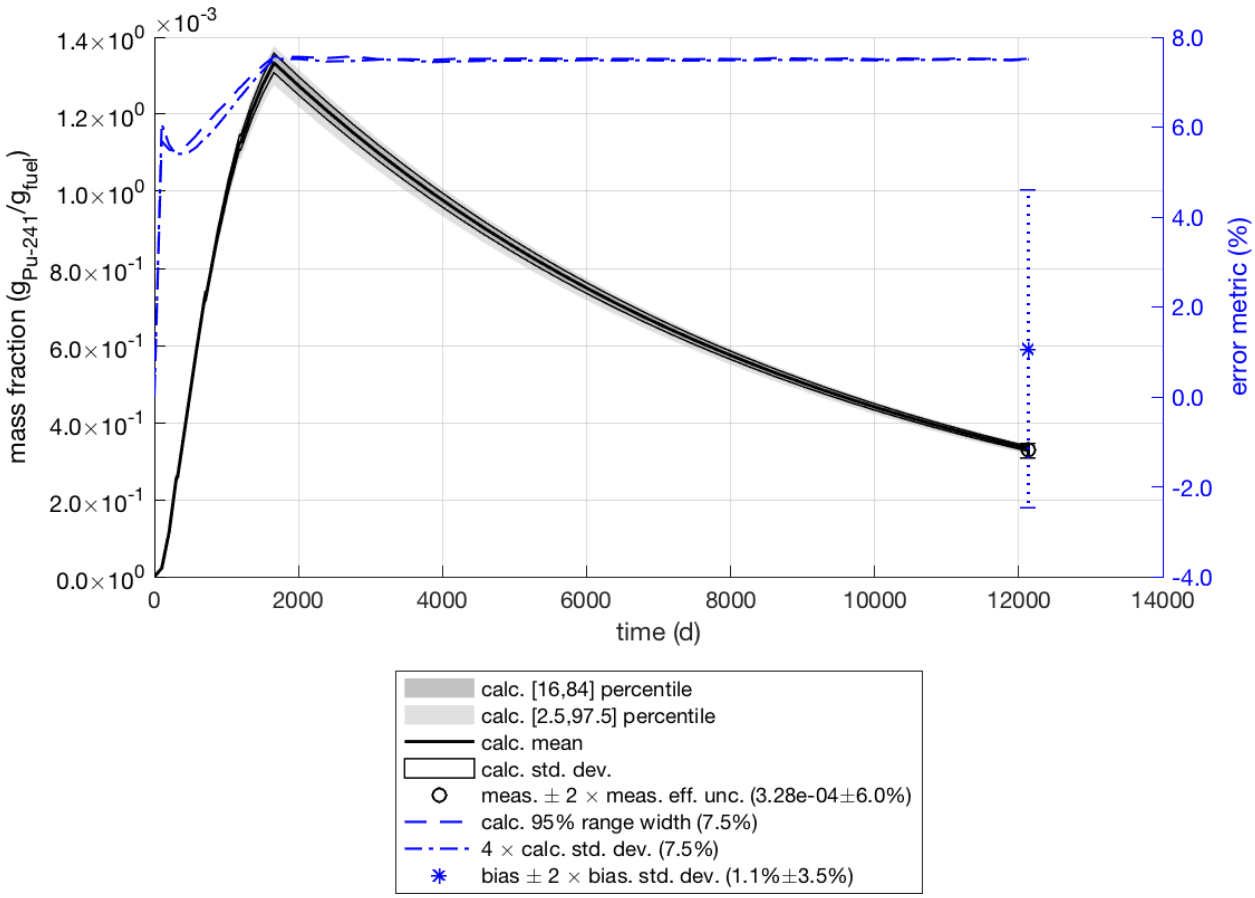

Figure 3-47 ^{241}P Isotopics Uncertainty

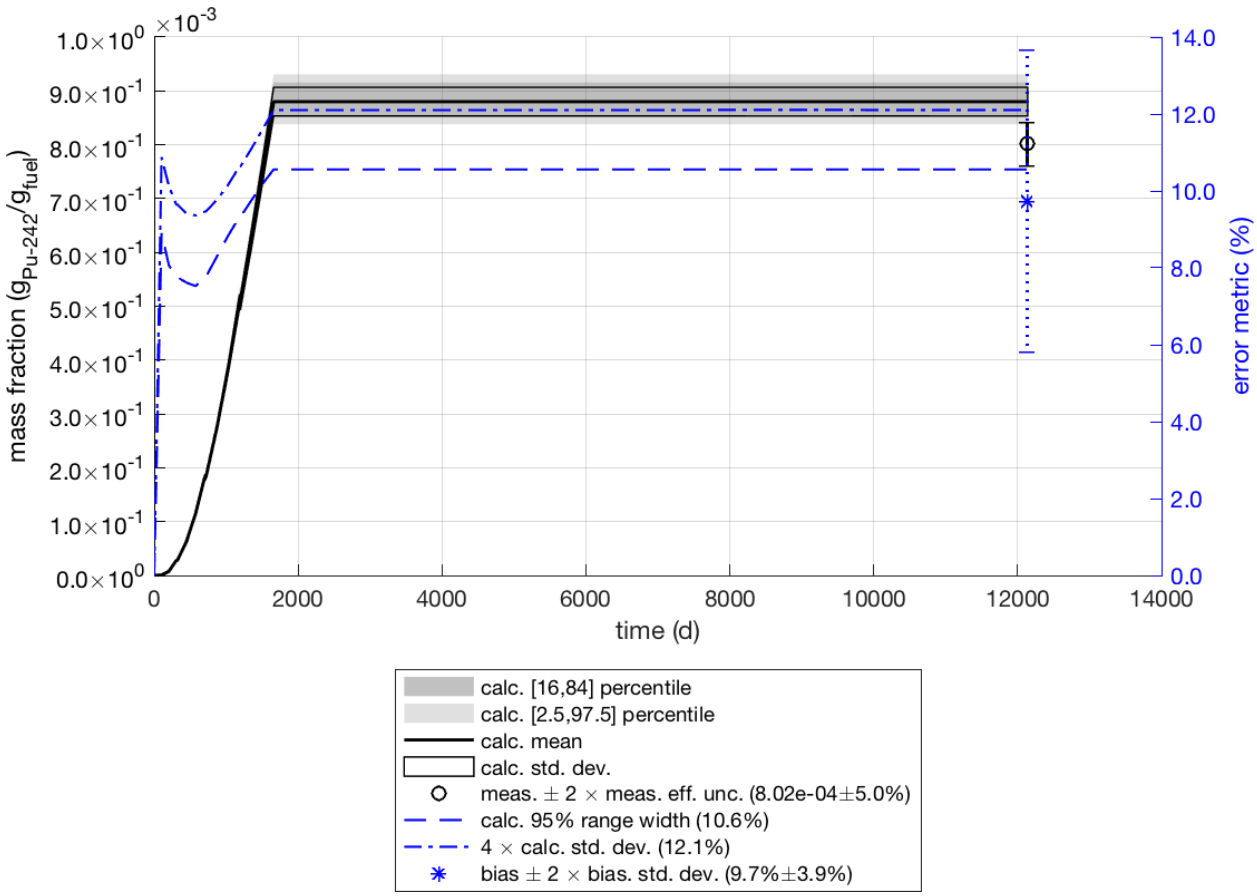

Figure 3-48 ^{242}Pu Isotopic Uncertainty

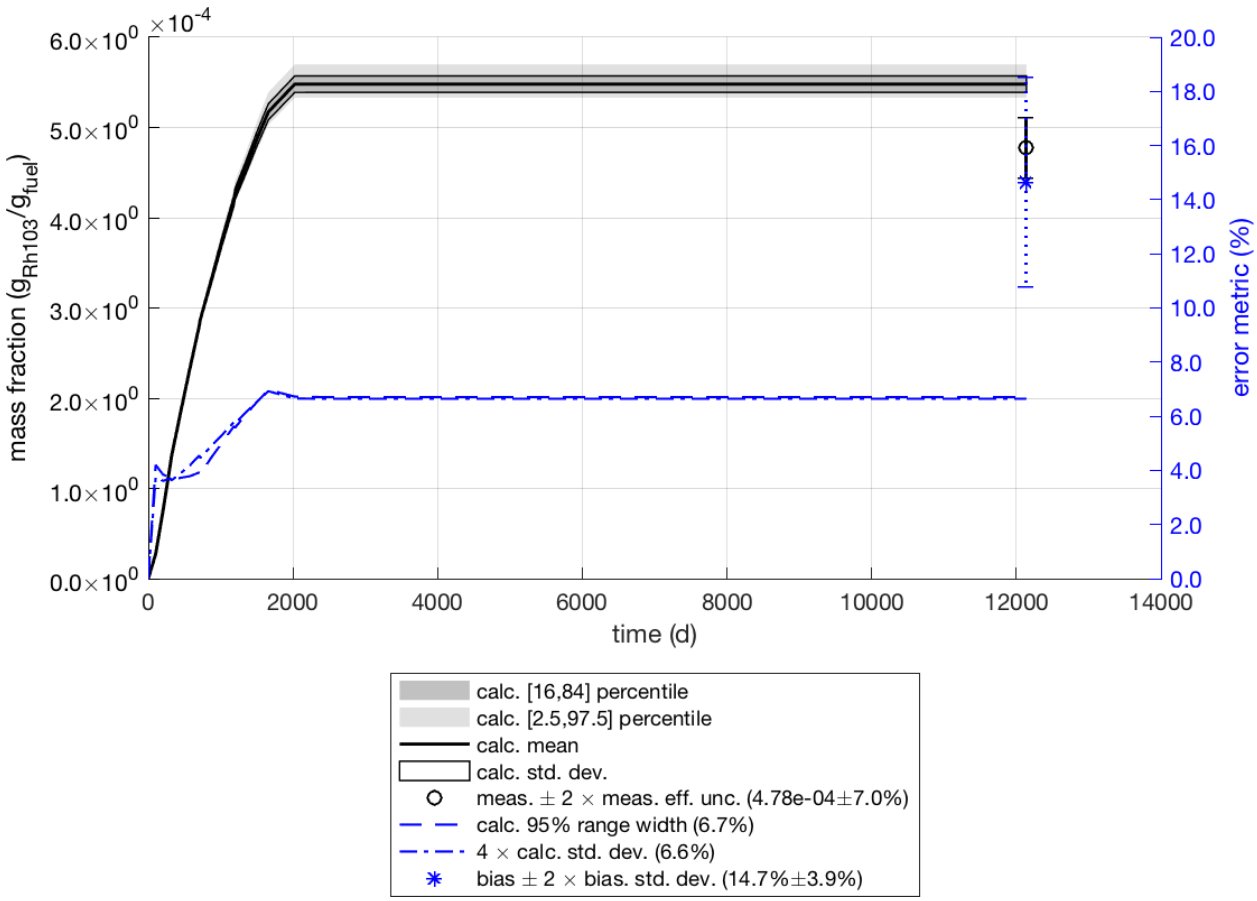

Figure 3-49 ^{103}Rh Isotopic Uncertainty

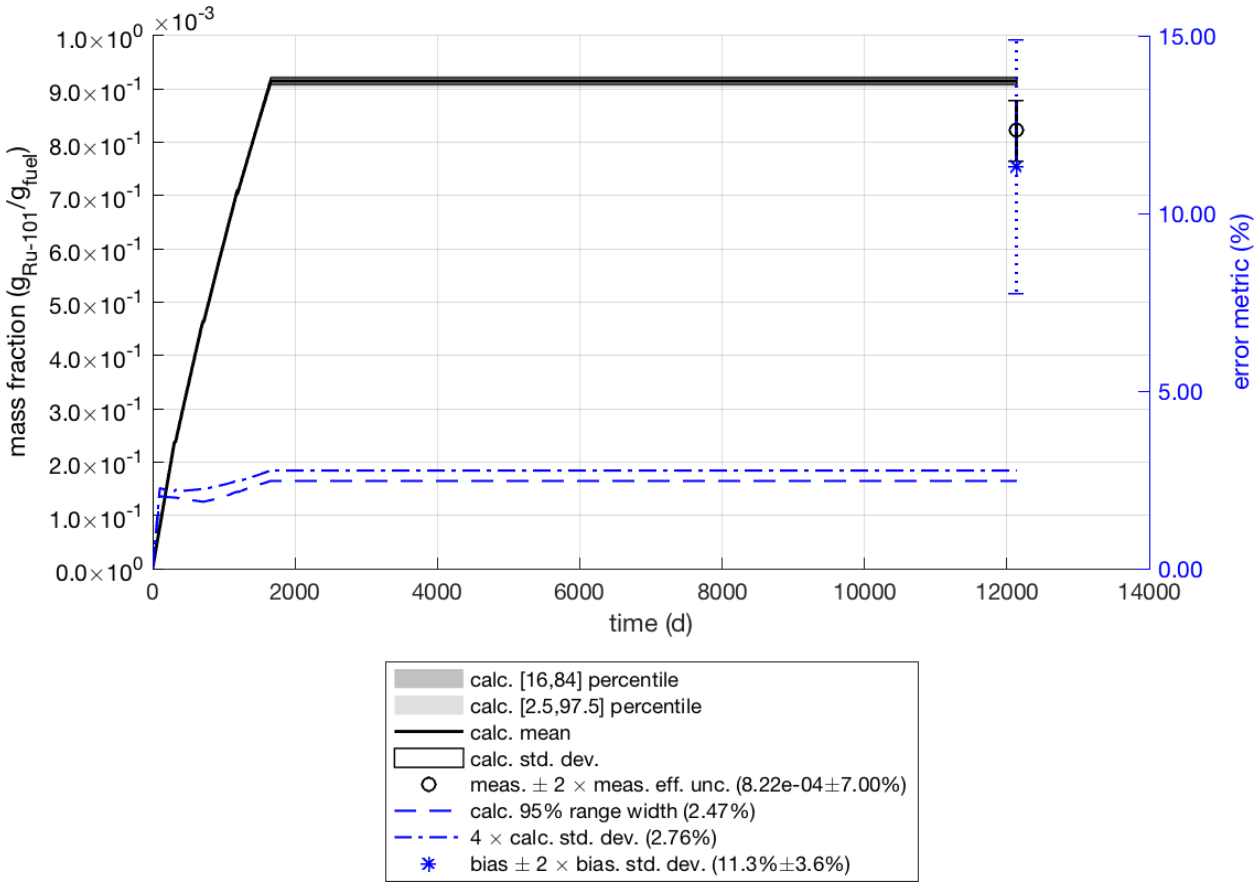

Figure 3-50 ^{101}Ru Isotopic Uncertainty

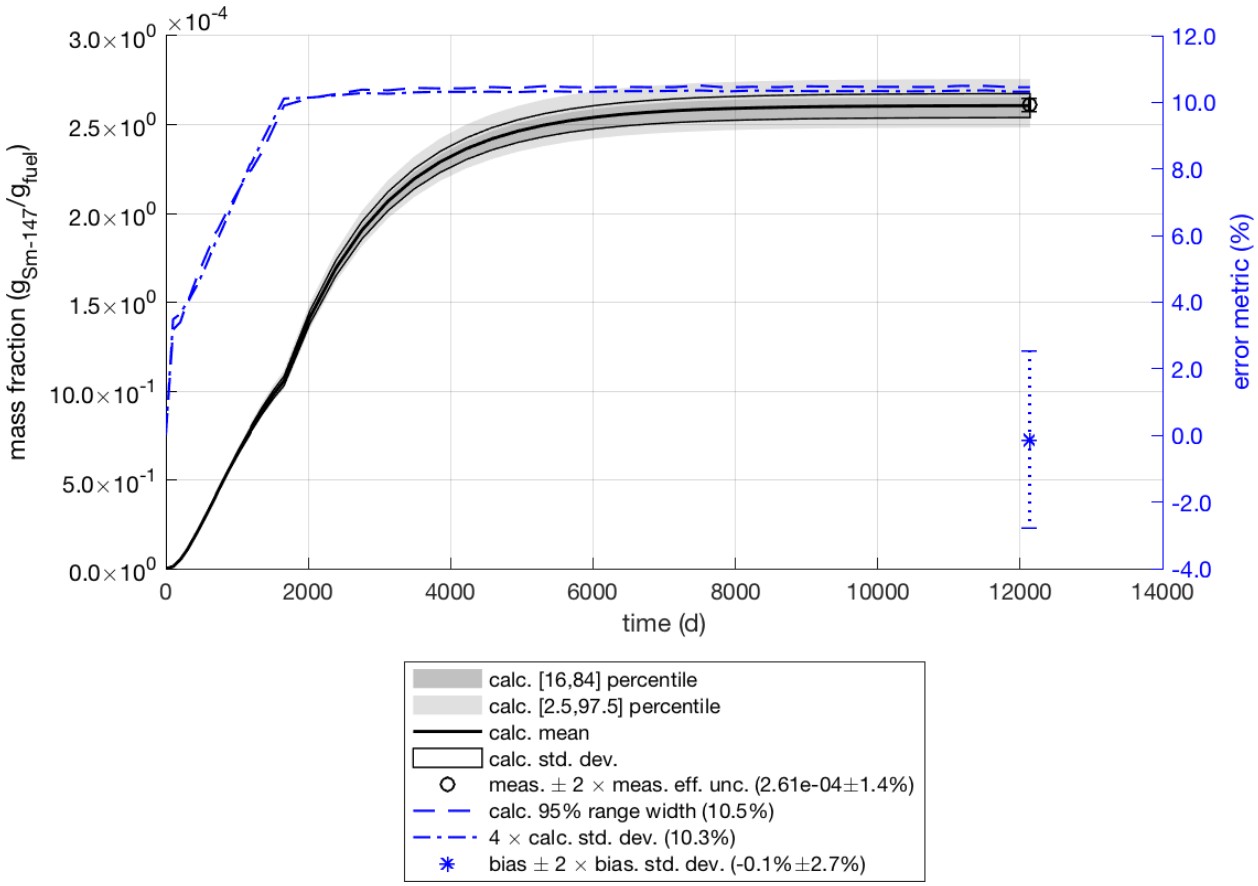

Figure 3-51 ^{147}Sm Isotopic Uncertainty

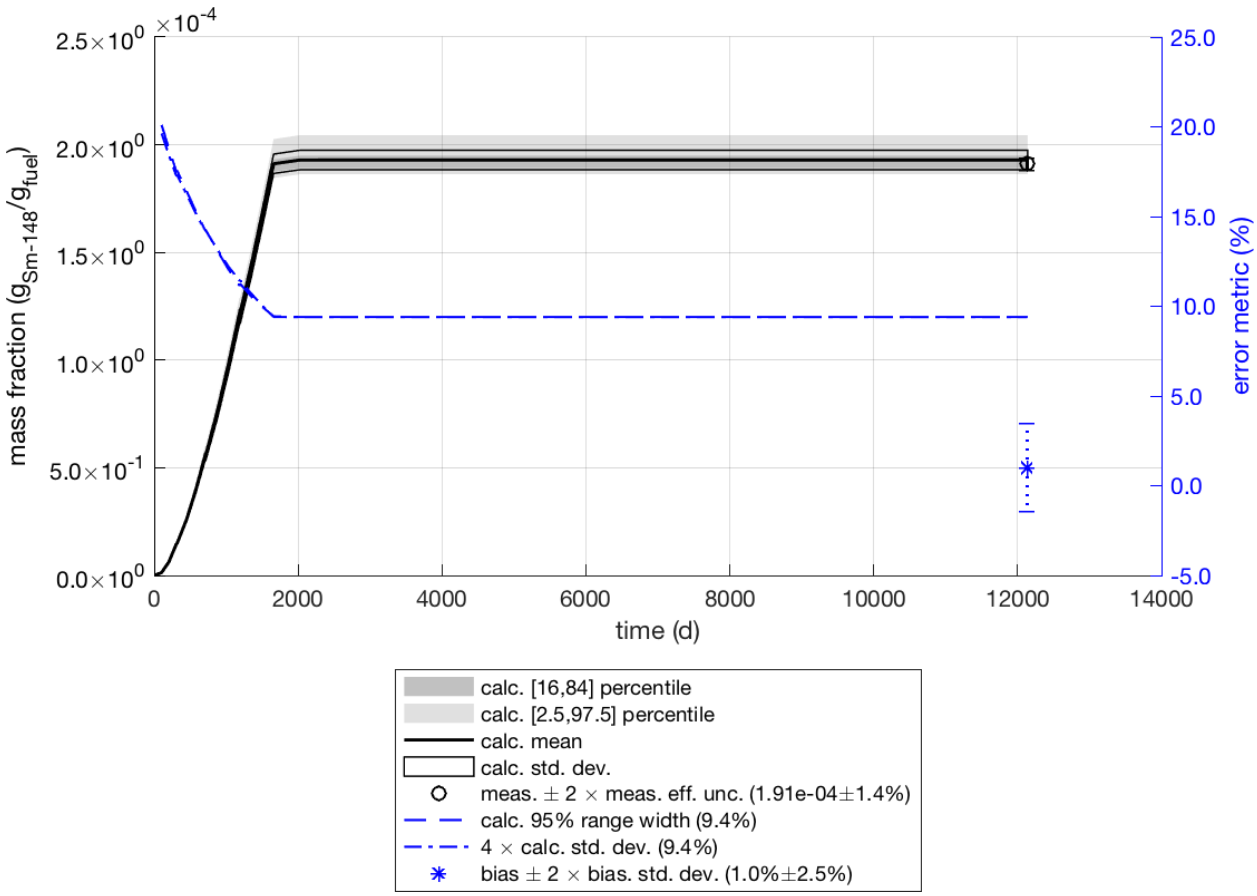

Figure 3-52 ^{148}Sm Isotopic Uncertainty

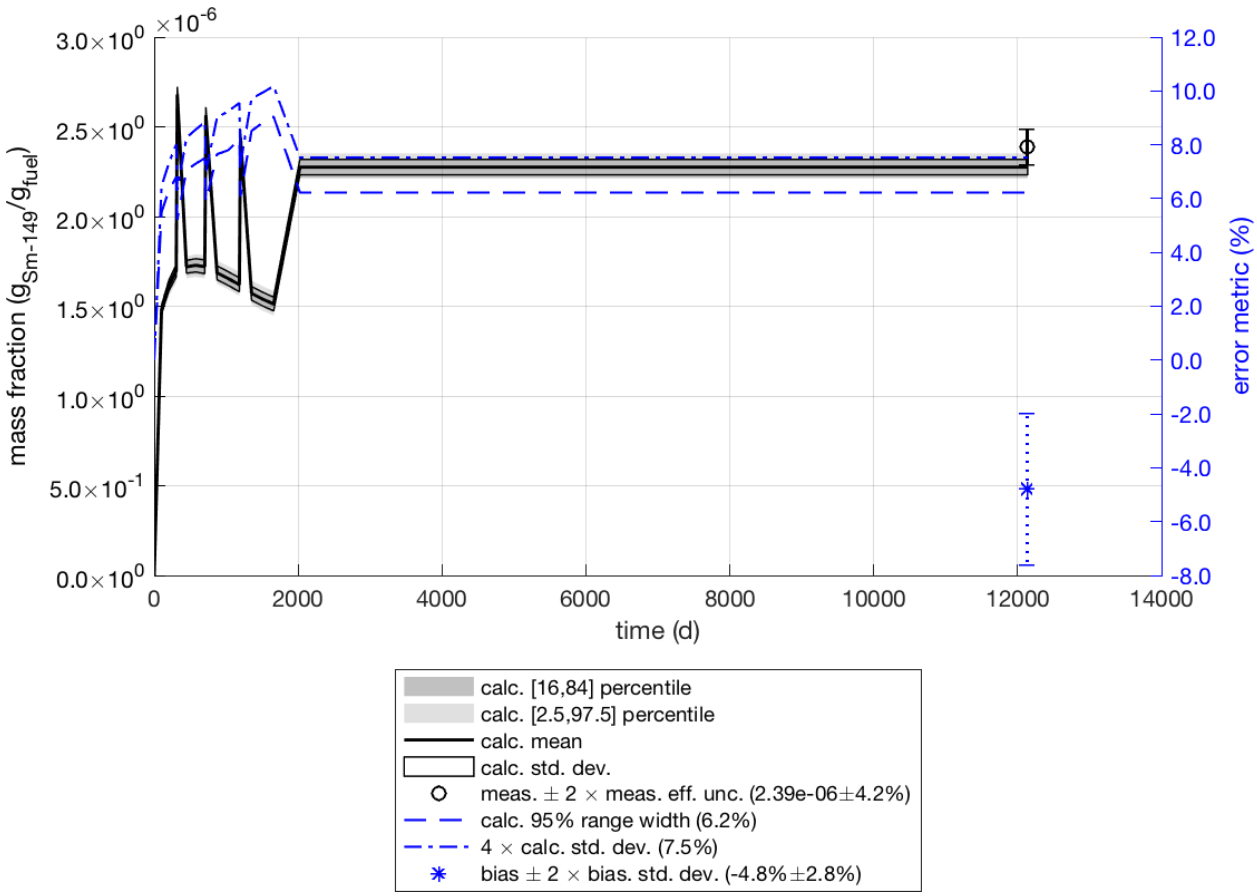

Figure 3-53 ^{149}Sm Isotopic Uncertainty

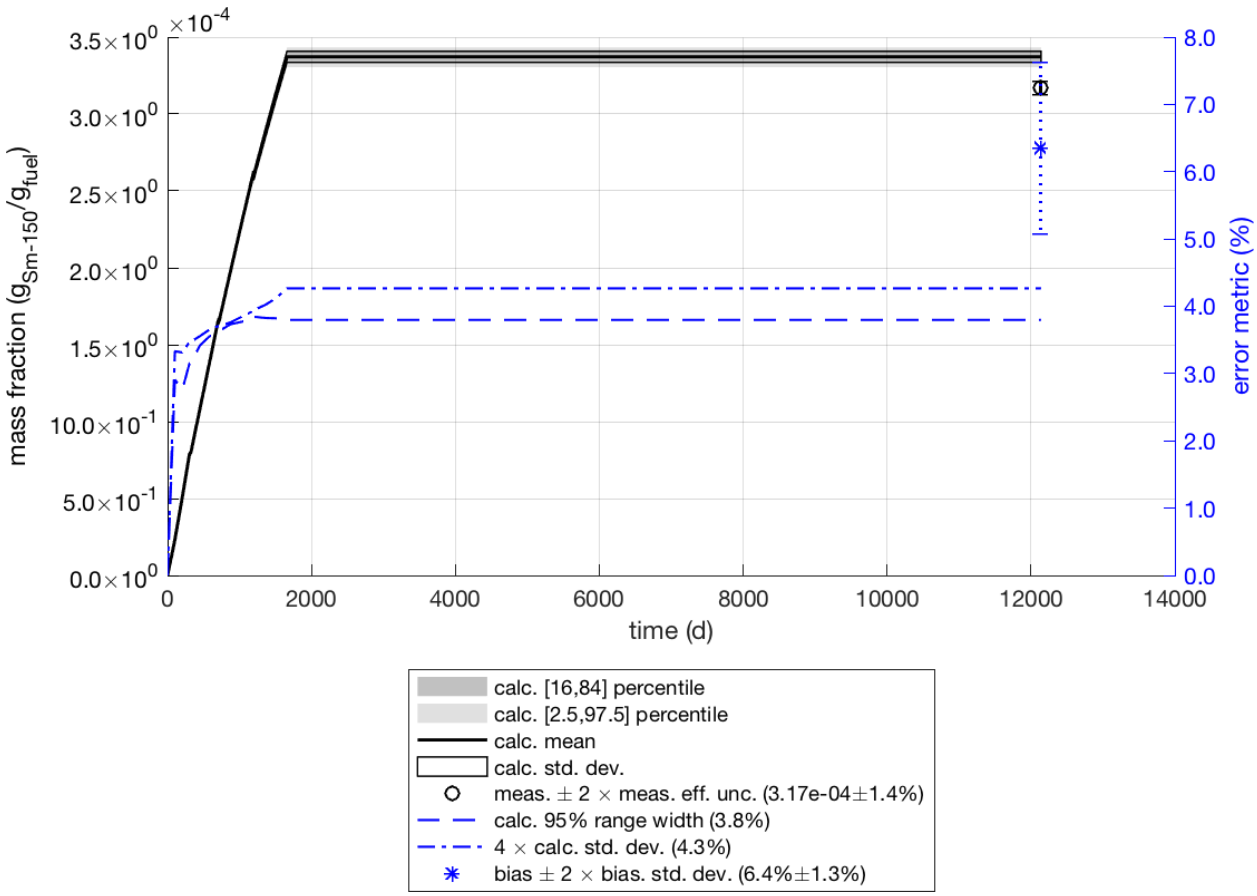

Figure 3-54 ^{150}Sm Isotopic Uncertainty

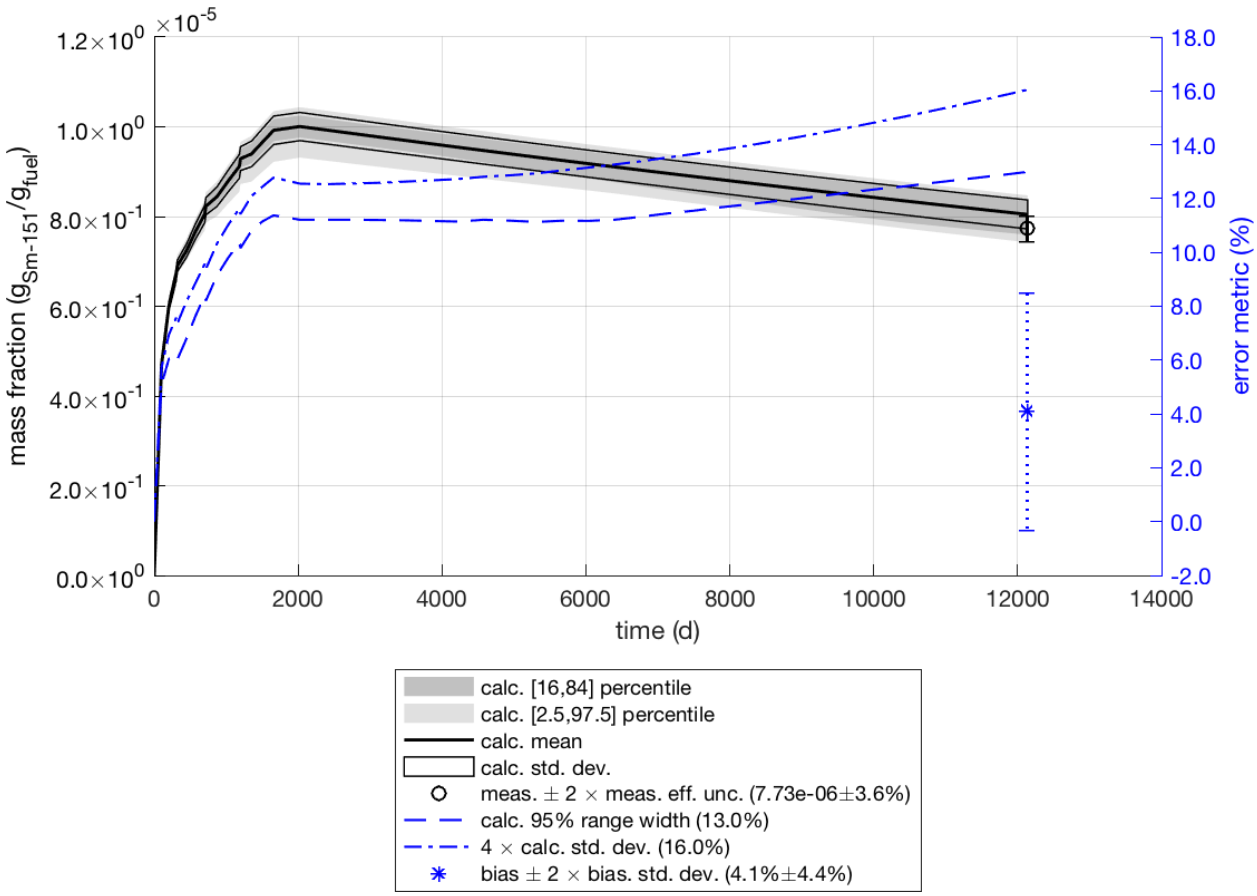

Figure 3-55 ^{151}Sm Isotopic Uncertainty

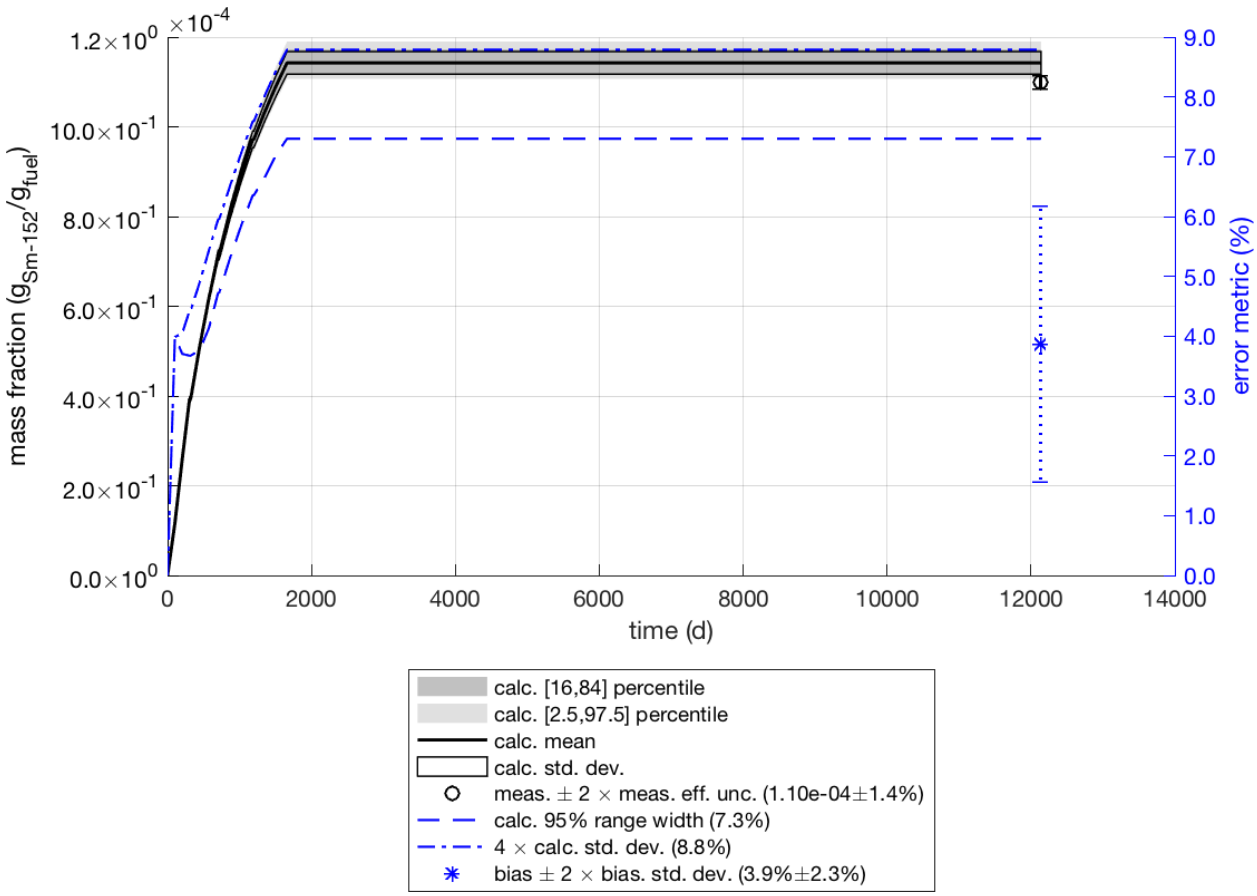

Figure 3-56 ^{152}Sm Isotopic Uncertainty

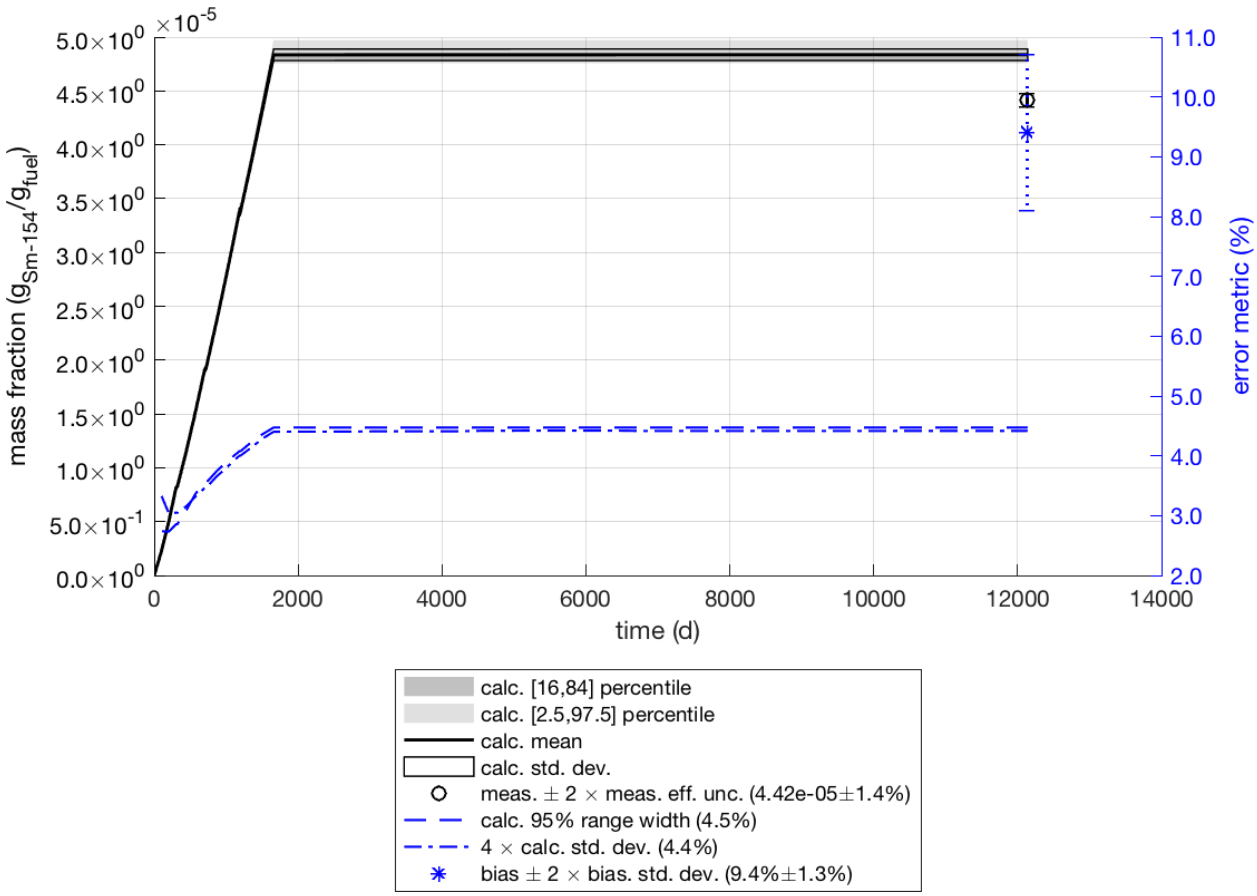

Figure 3-57 ^{154}Sm Isotopic Uncertainty

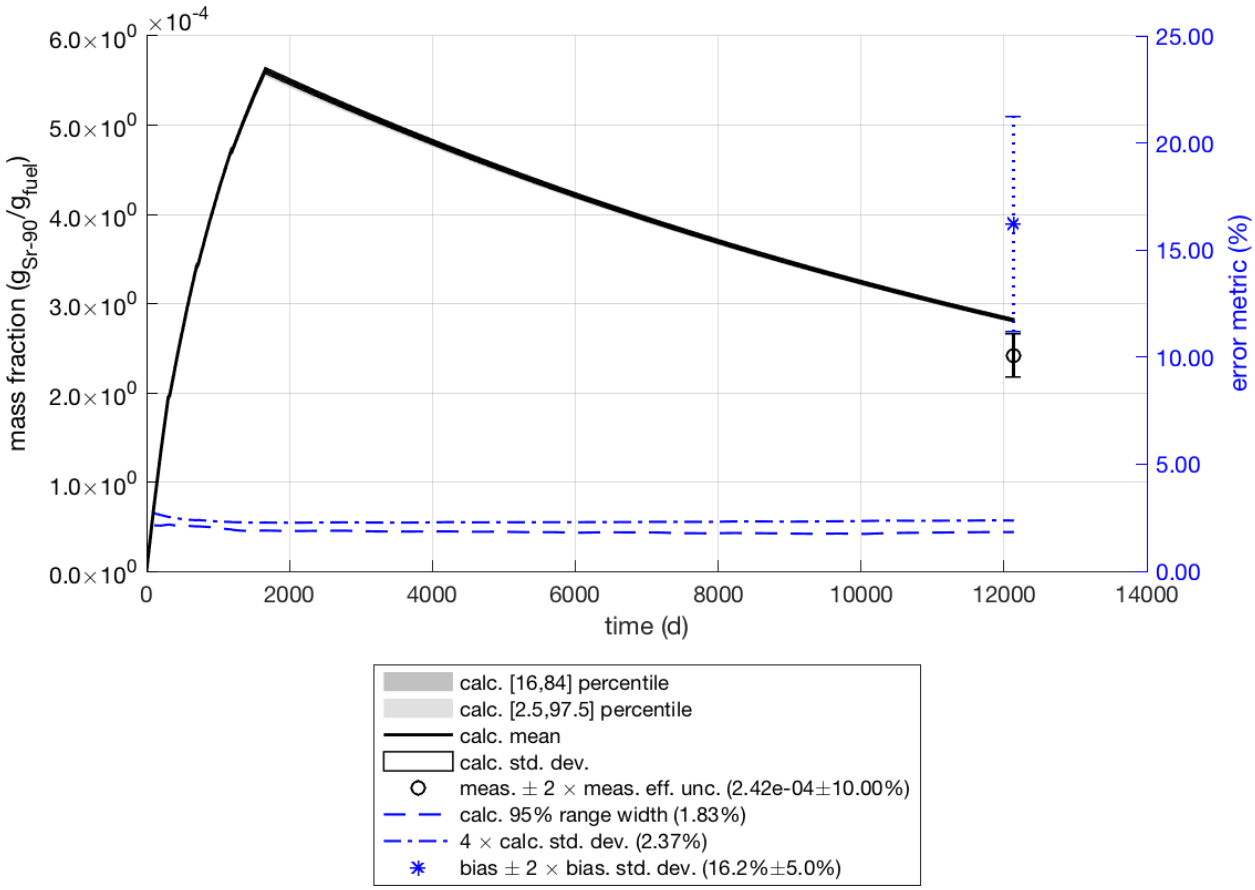

Figure 3-58 ^{90}Sr Isotopic Uncertainty

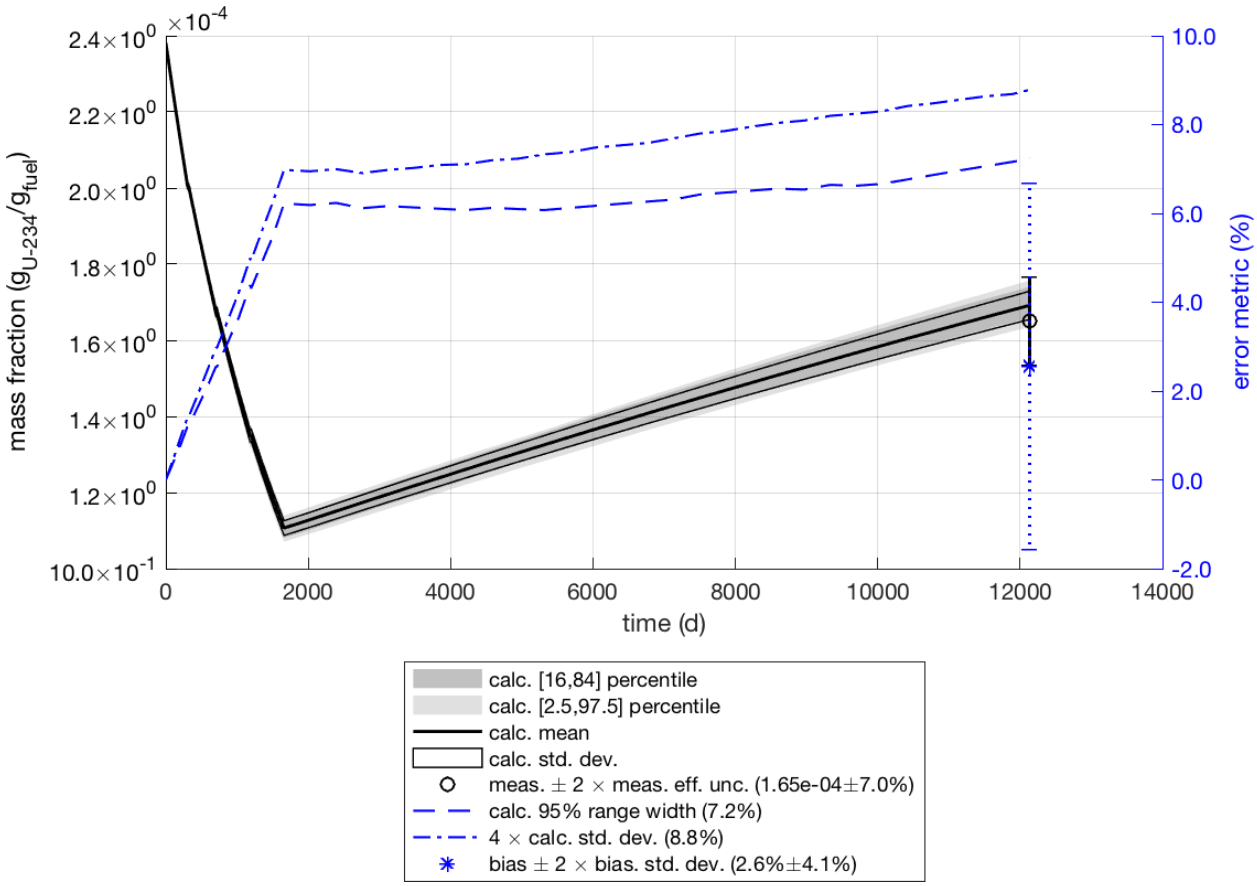

Figure 3-59 ^{234}U Isotopic Uncertainty

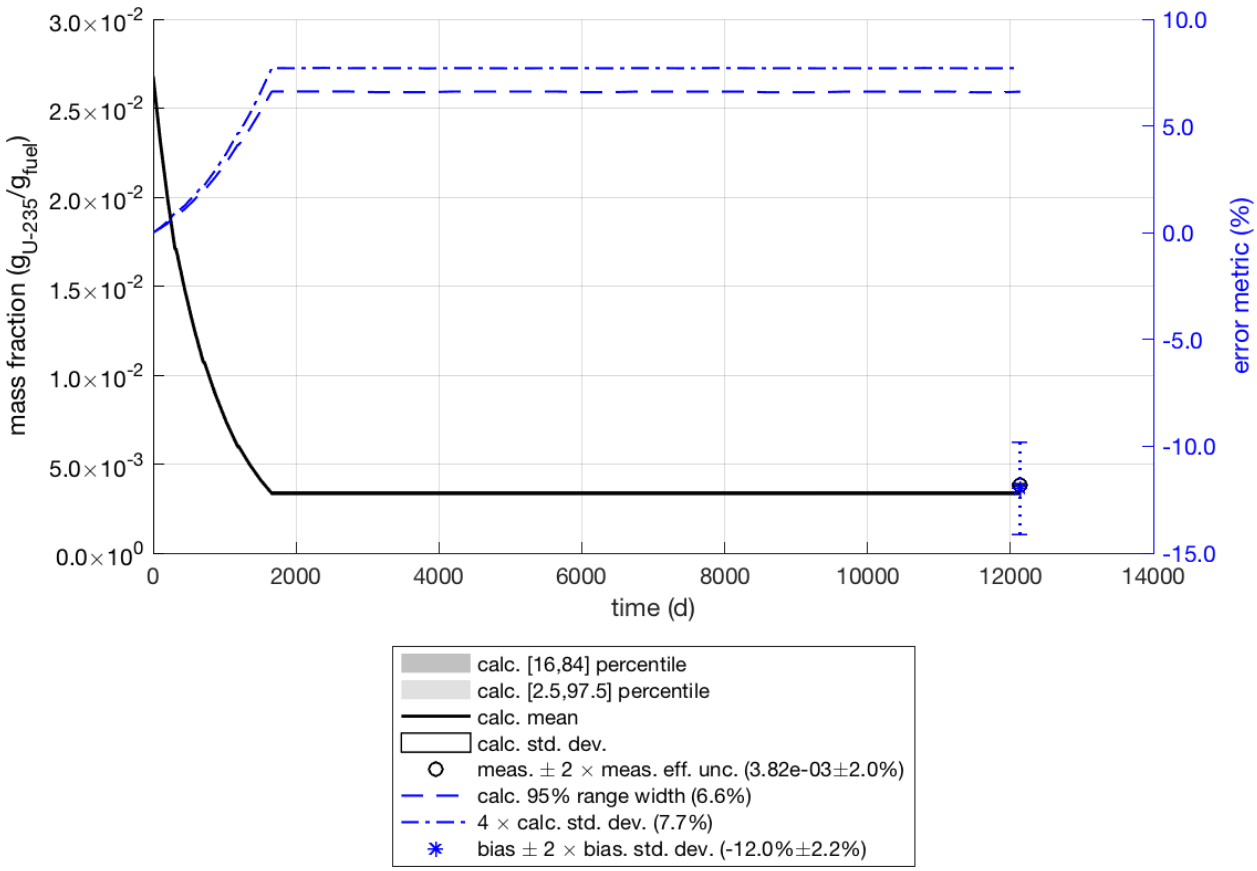

Figure 3-60 ^{235}U Isotopic Uncertainty

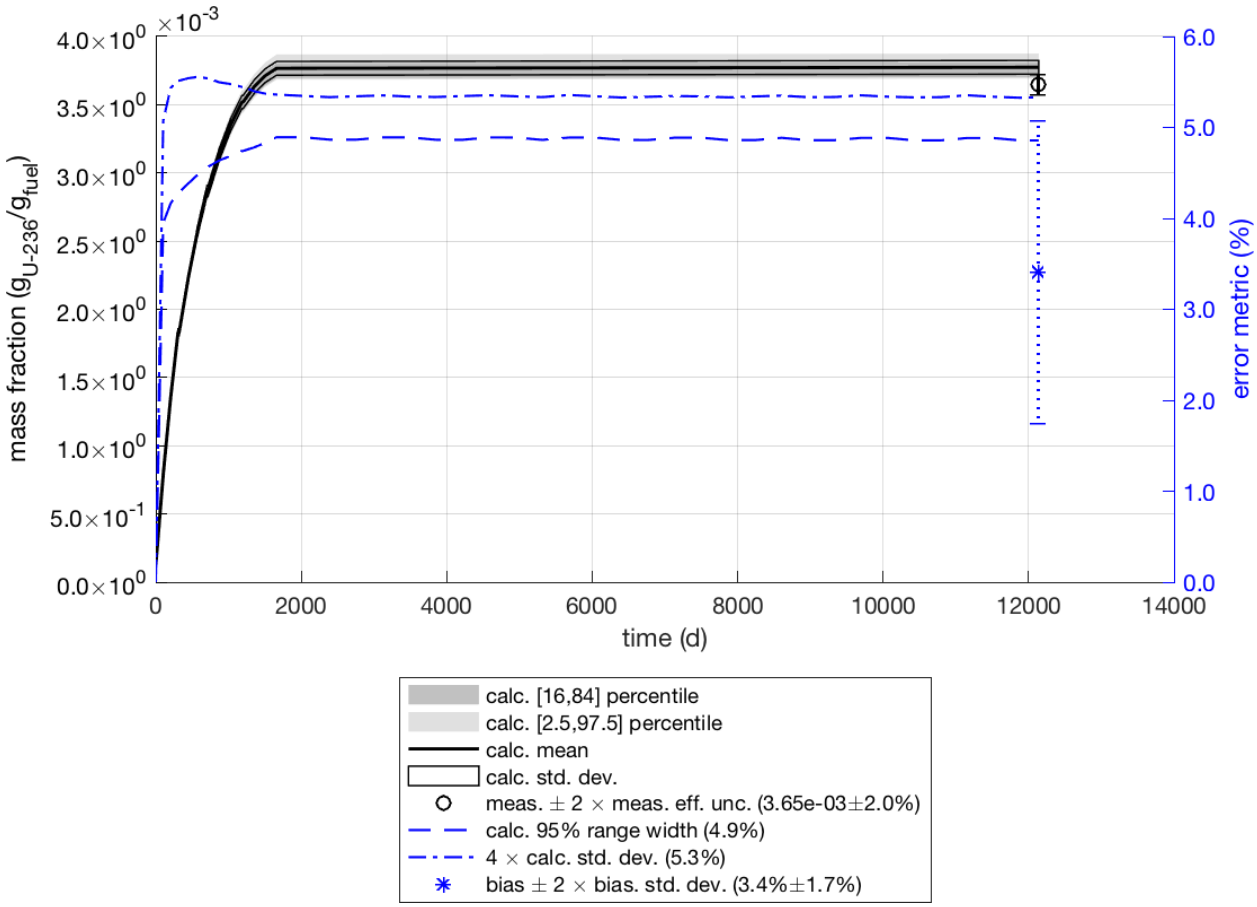

Figure 3-61 ^{236}U Isotopic Uncertainty

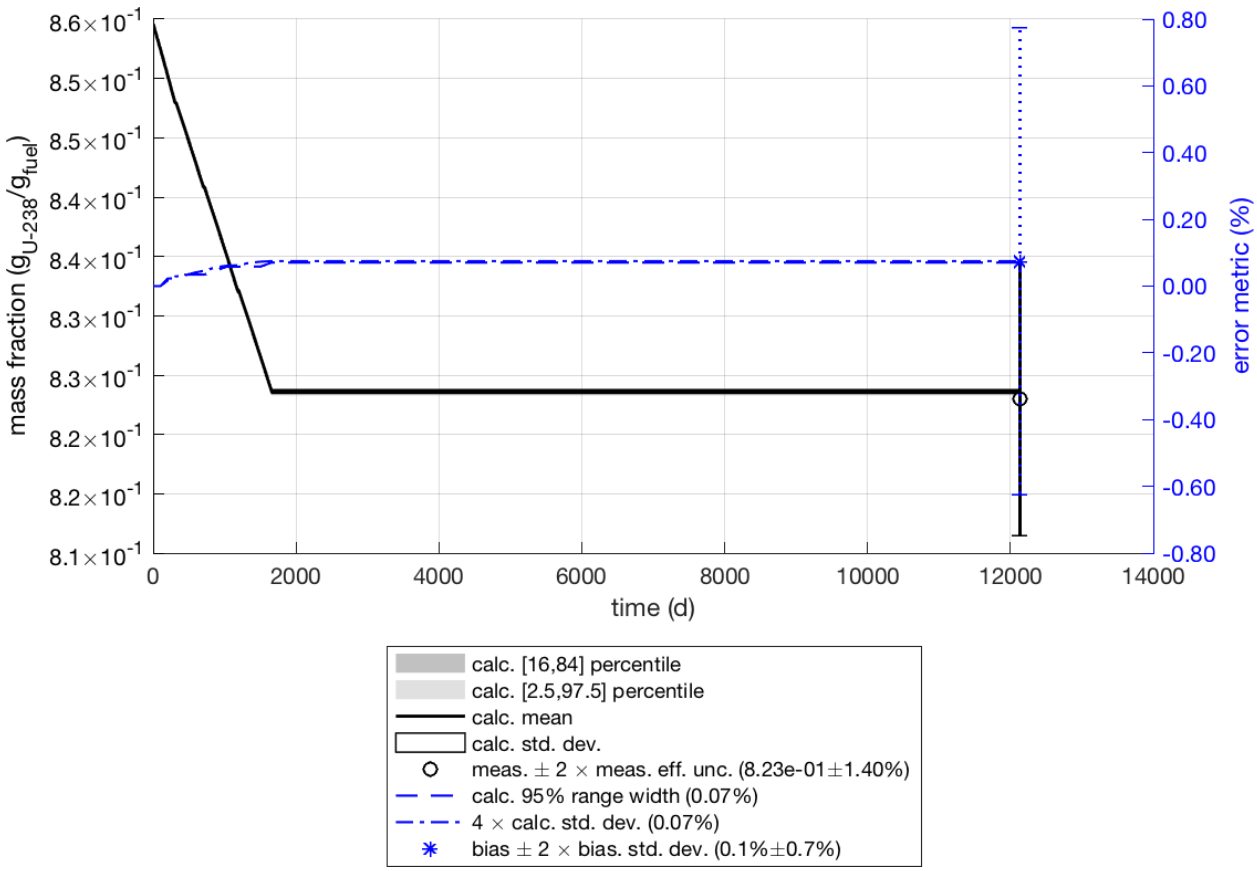

Figure 3-62 ^{238}U Isotopic Uncertainty

3.2.5 Source Terms

Figure 64 shows the decrease in total activity after discharge, with an initial uncertainty of 1.6%, decreasing gradually to 1.4% after decay. These uncertainties reflect those in the predicted nuclide concentrations at the time of discharge, as well as the uncertainties in the decay data after discharge.

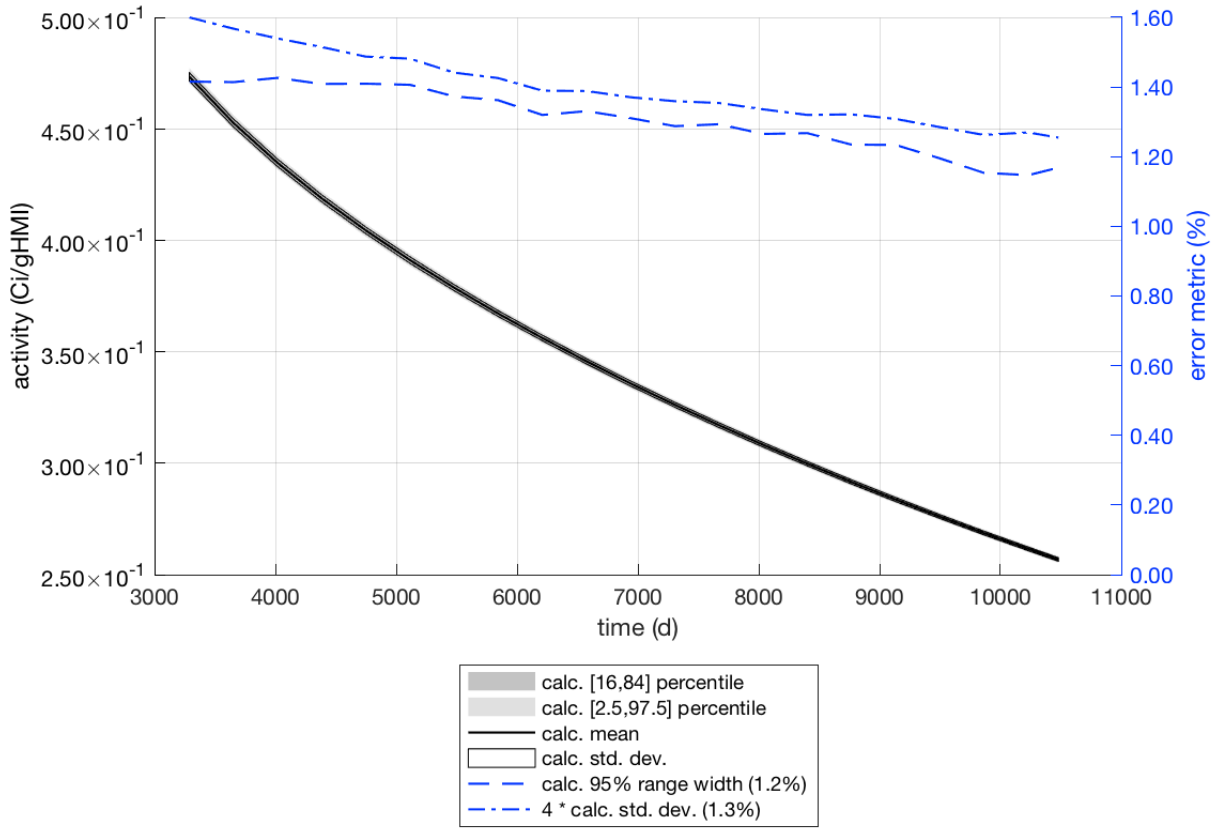

Figure 3-63 Activity Uncertainty

4 DISCUSSION

In the previous section, uncertainties in the various quantities of interest are presented for an example application modeling the MKP109 fuel rod Calvert Cliffs fuel assembly D047. The previous section highlights the comparisons to destructive assay measurements for two similar samples, S1 and S2, from adjacent axial positions of the same fuel rod.

This study used a simplified model as compared to the high fidelity model used for Calvert Cliffs assembly D047 described in Hu et al. [7]. Using the simplified model for this study reduced the run time by an order of magnitude. This study was only intended to investigate the various properties of the data uncertainty and how that uncertainty impacts calculations, while the Calvert Cliffs assembly was chosen for modeling because the available measurements facilitate discussion of the complex interrelationship and interpretation of calculation uncertainty, measurement uncertainty, and bias when using experimental data.

This section provides general guidance on interpreting calculation uncertainties.

4.1 Importance of Non-Data Error

Depending on the specific scenario being modeled, error from sources other than nuclear data may significantly impact the total error and cannot be neglected. Examples can include manufacturing tolerances, geometry variations in the fuel during irradiation caused by fuel swelling and other physical changes, associated changes in the fuel temperature, bowing of fuel rods, and uncertainties in the moderator temperature and void. On the experimental side, uncertainties in measurement dates and measured burnup can also contribute to overall uncertainty when comparing calculations to measurements.

Uncertainty propagation is not necessary when there is a strong validation suite for the application of interest. The distribution of biases from validation indicates the actual error. Uncertainty propagation methods described here only give an expectation for the error due to nuclear data. In the future, as data uncertainty becomes more routinely used and reliable, it will be useful to determine the minimum expected uncertainty present in quantities of interest for which validation data are not available. These methods can also be used to support the extrapolation of uncertainties beyond the validated range.

4.2 Calculation Uncertainty Is a Prediction

Uncertainty in calculated quantities, like calculated quantities themselves, must be regarded as a prediction. Confidence in each prediction is developed in different ways.

Non-data sources of uncertainty can be minimized so that isotopic comparisons to the measurements presented may be used to gain further confidence in calculated data uncertainty. For example, it is not certain that including data uncertainty provides a better understanding of the bias. For example, the ^{243}Am nuclide concentration has a bias of 7% compared to the experimental uncertainty of ~7% (2-sigma). However, the large data uncertainty of ~15% (2-sigma) provides some additional information indicating that a bias of 7% is well within expectations. In some cases, the calculation uncertainty may be much greater than the observed bias. Both the fundamental data and the data uncertainty should undergo constant revision and refinement to better match observations. This is discussed in the next section on data assimilation.

Just as calculation uncertainty is a prediction, so is measurement uncertainty. The measurement of CC-1 fuel was made with two nearly identical samples, S1 and S2. A measurement uncertainty was provided for each measurement, but it has been shown that when samples S1 and S2 are compared to provide a more robust estimate of the true error (more specifically the reproducibility component), the estimates do not hold for all samples. For example, for ^{152}Eu, 15% (1-sigma) uncertainty has been claimed, but when the two samples (2.64E-8 and 1.50E-7 g/gFuel) are compared, there is a standard deviation of 70% when using sample statistics with two samples. This is identified in the work by Hu et al. as a likely underestimate of measurement uncertainty caused by the extremely low isotopic concentration of this nuclide that is near the detection limit. With only two samples, the likelihood of one of the measurements being an outlier is non-negligible. However, because measurement uncertainty is a prediction, additional cross checks and independent multi-laboratory measurements are useful to gain confidence in these uncertainty estimates.

4.3 Data Assimilation

Data assimilation (or data adjustment) is the step in which the underlying data are adjusted within uncertainty to better agree with observations: in effect, to reduce bias. Propagating data uncertainty is necessary for this procedure. Data assimilation is a rigorous procedure to improve data quality using measurements of integral quantities. Although the techniques are well known [8], the process is complex, and the nuclear data libraries are large, so a necessarily automated solution continues to be beyond reach.

4.4 Significant Bias Identification

Data uncertainty propagation allows for the capability to separate biases from a comparison to measurement into two categories: expected and unexpected (or significant) biases. Large unexpected biases may be the result of a source of error that has not been taken into account. This can lead to the need to refine models by including extra uncertainty in some variables or providing feedback to the nuclear data community/measurement laboratory about potential issues with the data/measurement.

5 CONCLUSIONS

This report presents the current state of the art in SCALE for nuclear data uncertainty analysis capability, and it provides an overview of the uncertainty in multigroup cross sections, fission product yields, and decay data. The effect of nuclear data uncertainty is demonstrated for a typical LWR depletion analysis problem involving a Combustion Engineering 14 × 14 assembly irradiated in Calvert Cliffs Unit 1. A single fuel rod from assembly D047, designated MKP109, has been subjected to destructive radiochemical assay to measure the isotopic contents.

The 95% range width (difference between the 97.5th and 2.5th percentiles) is used in this study to assess the calculation uncertainty. This approach uses the actual distribution of the data and does not make any assumptions about the normality of the distributions. If the distribution were normal, then the 95% range width would correspond to 4-sigma range, i.e., +/- 2 sigma.

The calculation uncertainty determined in nuclide concentrations for the MKP109 rod range from a few percent to 50%. The power factor for this fuel rod shows a very low uncertainty of less than 0.5%. There is also a low uncertainty of less than 2% in activity.

Uncertainties in the macroscopic cross sections, reactivity, and power distributions are generally low in the few percent range. The effective delayed neutron fraction, β_{eff}, shows an unexpected high uncertainty of 20–100%.

The considered application of the MKP109 fuel rod enabled a bias estimation and comparisons of calculated uncertainty in the isotopic concentrations to measurements of samples S1 and S2. In this case, the relative bias range was calculated to include both the calculation and measurement uncertainty. A bias range (2.5th–97.5th percentile) that includes zero is within expectation, whereas a bias which does not include zero is unexpected. Identifying unexpected biases can lead to improvements in the model or in nuclear data.

6 FUTURE WORK

Numerous uncertainty-related improvements will be included in the SCALE 6.3 release. First, continuous energy perturbations will be available, which will allow the continuous energy Monte Carlo methods to be used with the Sampler code. Continuous perturbations are applied to the master library once at the beginning of a continuous energy calculation,

$$\sigma_{i,x}{}'(E) = p_{i,x}^{g}\ \sigma_{i,x}(E)\ \text{ for } E^{g} \leq E \leq E^{g-1}. \tag{36}$$

This introduces artificial discontinuities in the continuous energy cross sections at group boundaries. Future work will seek to limit this artifact. Additionally, the fission product uncertainty data have been expanded to include all available nuclides. Corrections to the decay heat uncertainty data (discussed in Section 2.3) are being implemented for distribution at the time that SCALE 6.2.3 is released. Other future work includes the following:

- Kinetics parameter uncertainty should be investigated, as it is of paramount importance to reactor transient and safety analysis.

- Cross section uncertainty should be extended to the so-called *activation cross section library* used by the ORIGEN depletion code. This multigroup cross section library is based on the JEFF/3.1-A activation library and is used to supplement reactions available in ENDF/B. The reactions available in ENDF/B have traditionally focused on neutron interactions relevant to neutron transport calculations, and they do not include such data as isomeric branching cross sections. Currently, zero uncertainty is assumed in all data originating from JEFF/3.1-A.

- Data uncertainty must be imposed consistently for any remaining data in SCALE. For example, alpha particle interaction probabilities are used in ORIGEN neutron emission models. These data effectively have no uncertainty.

- Additional tools and processes should be implemented to make data uncertainty a standard part of the analysis process. Necessary improvements will occur only when such data are routinely used and required to be reliable.

- Data assimilation should be pursued in a rigorous, automated framework based on validation results comparing calculation to measurement for a wide array of measurements.

7 REFERENCES

[1] M. B. Chadwick, M. Herman, P. Obložinský, M.E. Dunn, Y. Danon, A. C. Kahler, D. L. Smith, B. Pritychenko, G. Arbanas, R. Arcilla, R. Brewer, D. A. Brown, R. Capote, A. D. Carlson, Y. S. Cho, H. Derrien, K. Guber, G. M. Hale, S. Hoblit, S. Holloway, T. D. Johnson, T. Kawano, B. C. Kiedrowski, H. Kim, S. Kunieda, N. M. Larson, L. Leal, J. P. Lestone, R. C. Little, E. A. McCutchan, R. E. MacFarlane, M. MacInnes, C. M. Mattoon, R. D. McKnight, S. F. Mughabghab, G. P. A. Nobre, G. Palmiotti, A. Palumbo, M. T. Pigni, V. G. Pronyaev, R. O. Sayer, A. A. Sonzogni, N. C. Summers, P. Talou, I. J. Thompson, A. Trkov, R. L. Vogt, S. C. van der Marck, A. Wallner, M. C. White, D. Wiarda, and P. G. Young, "ENDF/B-VII.1 Nuclear Data for Science and Technology: Cross Sections, Covariances, Fission Product Yields and Decay Data," In *Nuclear Data Sheets*, Volume 112, Issue 12, 2011, Pages 2887–2996, ISSN 0090-3752, https://doi.org/10.1016/j.nds.2011.11.002.(http://www.sciencedirect.com/science/article/pii/S009037521100113X).

[2] *SCALE: A Comprehensive Modeling and Simulation Suite for Nuclear Safety Analysis and Design,* ORNL/TM-2005/39, Version 6.1, Oak Ridge National Laboratory, Oak Ridge, Tennessee, June, 2011. Available from Radiation Safety Information Computational Center at Oak Ridge National Laboratory as CCC-785.

[3] M. L. Williams, D. Wiarda, G. Ilas, W. J. Marshall, and B. T. Rearden, "Covariance Applications in Criticality Safety, Light Water Reactor Analysis, and Spent Fuel Characterization," *Nuclear Data Sheets*, Volume 123, January 2015, Pages 92–96, ISSN 0090-3752, https://doi.org/10.1016/j.nds.2014.12.016.

[4] M. L. Williams, G. Ilas, M. A. Jessee, B. T. Rearden, D. Wiarda, W. Zwermann, L. Gallner, M. Klein, B. Krzykacz-Hausmann, and A. Pautz, "A Statistical Sampling Method For Uncertainty Analysis With SCALE And XSUSA," *Nuclear Technology* 183,3, p515–527 (Sept. 2013).

[5] M.T. Pigni, M. W. Francis, and I. C. Gauld, "Investigation of Inconsistent ENDF/B-VII.1 Independent and Cumulative Fission Product Yields with Proposed Revisions," *Nuclear Data Sheets*, Volume 123, January 2015, Pages 231–236, ISSN 0090-3752, https://doi.org/10.1016/j.nds.2014.12.040.

[6] R. J. Guenther et al., *Characterization of LWR Spent Fuel MCC-Approved Testing Material ATM-104*, PNL-5109-104, 1991.

[7] J. Hu, J. M. Giaquinto, I. C. Gauld, G. Ilas, and T. J. Keever, "Analysis of new measurements of Calvert Cliffs spent fuel samples using SCALE 6.2," *Annals of Nuclear Energy*, Volume 106, August 2017, Pages 221–234, ISSN 0306-4549, https://doi.org/10.1016/j.anucene.2017.04.005.

[8] G. Palmiotti, M. Salvatores, and G. Aliberti, "A-priori and A-posteriori Covariance Data in Nuclear Cross Section Adjustments: Issues and Challenges," *Nuclear Data Sheets*, Volume 123, 2015, Pages 41–50, ISSN 0090-3752, https://doi.org/10.1016/j.nds.2014.12.008.

NRC FORM 335
(12-2010)
NRCMD 3.7

U.S. NUCLEAR REGULATORY COMMISSION

BIBLIOGRAPHIC DATA SHEET

(See instructions on the reverse)

1. REPORT NUMBER
(Assigned by NRC, Add Vol., Supp., Rev., and Addendum Numbers, if any.)

NUREG/CR-7249
ORNL/TM-2017/706

2. TITLE AND SUBTITLE

Overview of Nuclear Data Uncertainty in Scale and Application to Light Water Reactor Uncertainty Analysis

3. DATE REPORT PUBLISHED

MONTH	YEAR
December	**2018**

4. FIN OR GRANT NUMBER

NRC JCN V6449

5. AUTHOR(S)

William Wieselquist, Mark L. Williams, Dorothea Wiarda, Marco Pigni, Ugur Mertyurek

6. TYPE OF REPORT

Technical

7. PERIOD COVERED (Inclusive Dates)

8. PERFORMING ORGANIZATION - NAME AND ADDRESS (If NRC, provide Division, Office or Region, U. S. Nuclear Regulatory Commission, and mailing address; if contractor, provide name and mailing address.)

Oak Ridge National Laboratory
Managed by UT-Battelle, LLC
Oak Ridge, TN 37831-6170

9. SPONSORING ORGANIZATION - NAME AND ADDRESS (If NRC, type "Same as above", if contractor, provide NRC Division, Office or Region, U. S. Nuclear Regulatory Commission, and mailing address.)

Division of System Analysis and Regulatory Effectiveness
Office of Nuclear Regulatory Research
U. S. Nuclear Regulatory Commission
Washington, DC 20555–0001

10. SUPPLEMENTARY NOTES

11. ABSTRACT (200 words or less)

This report presents the current state of the art in SCALE for nuclear data uncertainty analysis capability, and it provides an overview of the uncertainty in multigroup cross sections, fission product yields, and decay data. The effect of nuclear data uncertainty is demonstrated for a typical LWR depletion analysis problem involving a Combustion Engineering assembly irradiated in Calvert Cliffs Unit 1. A single fuel rod from assembly D047 has been subjected to destructive radiochemical assay to measure the isotopic contents.

The 95% range width (difference between the 97.5th and 2.5th percentiles) is used in this study to assess the calculation uncertainty. This approach uses the actual distribution of the data and does not make any assumptions about the normality of the distributions. If the distribution were normal, then the 95% range width would correspond to 4-sigma range, i.e., +/- 2 sigma.

The calculation uncertainty determined in nuclide concentrations for the MKP109 rod range from a few percent to 50%. The power factor for this fuel rod shows a very low uncertainty of less than 0.5%.

Uncertainties in the macroscopic cross sections, reactivity, and power distributions are generally low in the few percent range. The effective delayed neutron fraction shows an unexpected high uncertainty of 20–100%.

12. KEY WORDS/DESCRIPTORS (List words or phrases that will assist researchers in locating the report.)

uncertainty quantification
calculation uncertainty
nuclear data
SCALE
spent nuclear fuel
validation

13. AVAILABILITY STATEMENT

unlimited

14. SECURITY CLASSIFICATION

(This Page)
unclassified

(This Report)
unclassified

15. NUMBER OF PAGES

16. PRICE

Printed
on recycled
paper

Federal Recycling Program

UNITED STATES
NUCLEAR REGULATORY COMMISSION
WASHINGTON, DC 20555-0001

OFFICIAL BUSINESS

@NRCgov

NUREG/CR-7249

Overview of Nuclear Data Uncertainty in SCALE and Application to Light Water Reactor Uncertainty Analysis

December 2018